U.S. DEPARTMENT OF COMMERCE
National Technical Information Service

PB-283 819

Investigation of Saturated Laser Fluorescence and CARS Spectroscopic Techniques for Combustion Diagnostics

United Technologies Research Center, East Hartford, Conn

Prepared for

Industrial Environmental Research Lab, Research Triangle Park, N C

Jun 78

TECHNICAL REPORT DATA
(Please read Instructions on the reverse before completing)

1. REPORT NO.	2.	3. RECIPIENT'S ACCESSION NO.
EPA-600/7-78-104		

4. TITLE AND SUBTITLE	5. REPORT DATE
Investigation of Saturated Laser Fluorescence and CARS Spectroscopic Techniques for Combustion Diagnostics	June 1978
	6. PERFORMING ORGANIZATION CODE
7. AUTHOR(S)	8. PERFORMING ORGANIZATION REPORT NO.
A. C. Eckbreth, P. A. Bonczyk, and J. A. Shirley	
9. PERFORMING ORGANIZATION NAME AND ADDRESS	10. PROGRAM ELEMENT NO.
United Technologies Research Center East Hartford, Connecticut 06108	EHE624
	11. CONTRACT/GRANT NO.
	68-02-2176
12. SPONSORING AGENCY NAME AND ADDRESS	13. TYPE OF REPORT AND PERIOD COVERED
EPA, Office of Research and Development Industrial Environmental Research Laboratory Research Triangle Park, NC 27711	Final; 10/76-1/78
	14. SPONSORING AGENCY CODE
	EPA/600/13

15. SUPPLEMENTARY NOTES IERL-RTP project officer is William B. Kuykendal, Mail Drop 62 919/541-2557.

16. ABSTRACT The report gives results of comparisons of saturated laser-excited molecular fluorescence measurements of CH and CN in atmospheric pressure acetylene flames with absorption measurements of these flame radicals. It was found possible to saturate the fluorescence intensity of both radicals with readily achieved levels of laser spectral intensity (100,000 to 1 million watts per square centimeter-reciprocal centimeter). Coherent Anti-Stokes Raman Spectroscopy (CARS) thermometry investigations were conducted on flame nitrogen in a variety of flames, including highly sooting propane diffusion flames. CARS species sensitivity was addressed in a study of CO detectability.

17. KEY WORDS AND DOCUMENT ANALYSIS

a. DESCRIPTORS		b. IDENTIFIERS/OPEN ENDED TERMS	c. COSATI Field/Group	
Pollution	Propane	Pollution Control	13B	07C
Combustion	Acetylene	Stationary Sources	21B	
Diagnosis	Nitrogen	CH	06E	07B
Raman Spectroscopy	Cyanogen	CARS	14B	
Fluoroscence	Carbon Monoxide	Anti-Stokes	20F	
Lasers	Stokes Law		20E	20D

18. DISTRIBUTION STATEMENT	19. SECURITY CLASS (This Report)	21. NO. OF PAGES
Unlimited	Unclassified	156
	20. SECURITY CLASS (This page)	22. PRICE
	Unclassified	PC A08/MF A01

EPA Form 2220-1 (9-73)

United States
Environmental Protection
Agency

Industrial Environmental Research
Laboratory
Research Triangle Park NC 27711

EPA-600/7-78-104
June 1978

PB 283 819

EPA

Investigation of Saturated Laser Fluorescence and CARS Spectroscopic Techniques for Combustion Diagnostics

interagency
Energy/Environment
R&D Program Report

REPRODUCED BY
NATIONAL TECHNICAL
INFORMATION SERVICE
U. S. DEPARTMENT OF COMMERCE
SPRINGFIELD, VA. 22161

136

RESEARCH REPORTING SERIES

Research reports of the Office of Research and Development, U.S. Environmental Protection Agency, have been grouped into nine series. These nine broad categories were established to facilitate further development and application of environmental technology. Elimination of traditional grouping was consciously planned to foster technology transfer and a maximum interface in related fields. The nine series are:

1. Environmental Health Effects Research
2. Environmental Protection Technology
3. Ecological Research
4. Environmental Monitoring
5. Socioeconomic Environmental Studies
6. Scientific and Technical Assessment Reports (STAR)
7. Interagency Energy-Environment Research and Development
8. "Special" Reports
9. Miscellaneous Reports

This report has been assigned to the ENVIRONMENTAL PROTECTION TECHNOLOGY series. This series describes research performed to develop and demonstrate instrumentation, equipment, and methodology to repair or prevent environmental degradation from point and non-point sources of pollution. This work provides the new or improved technology required for the control and treatment of pollution sources to meet environmental quality standards.

REVIEW NOTICE

This report has been reviewed by the U.S. Environmental Protection Agency, and approved for publication. Approval does not signify that the contents necessarily reflect the views and policy of the Agency, nor does mention of trade names or commercial products constitute endorsement or recommendation for use.

This document is available to the public through the National Technical Information Service, Springfield, Virginia 22161

EPA-600/7-78-104
June 1978

Investigation of Saturated Laser Fluorescence and CARS Spectroscopic Techniques for Combustion Diagnostics

by

A.C. Eckbreth, P.A. Bonczyk, and J.A. Shirley

United Technologies Research Center
East Hartford, Connecticut 06108

Contract No. 68-02-2176
Program Element No. EHE624

EPA Project Officer: William B. Kuykendal

Industrial Environmental Research Laboratory
Office of Energy, Minerals, and Industry
Research Triangle Park, NC 27711

Prepared for

U.S. ENVIRONMENTAL PROTECTION AGENCY
Office of Research and Development
Washington, DC 20460

1b

DISCLAIMER

This report has been reviewed by the Industrial Environmental Research Laboratory, U.S. Environmental Protection Agency, and approved for publication. Approval does not signify that the contents necessarily reflect the views and poli ies of the U.S. Environmental Protection Agency, nor does mention of trade names or commercial products constitute endorsement or recommendation for use.

FOREWORD

Under Contract 68-02-2176 sponsored by the Environmental Protection Agency, the United Technologies Research Center (UTRC) is conducting analytical and experimental investigation of non-perturbing, spatially precise, in-situ diagnostic techniques to measure species concentrations and temperature in flames. Under Task I, a comprehensive review (EPA-600/7-77-066) was conducted of potential techniques to measure chemical composition and temperature in flames with particular emphasis on instrumentally hostile environments such as research scale furnaces. In Task II, laboratory investigations of the most promising diagnostic techniques emerging from the Task I study have been conducted and are reported herein. The Task II experimental studies focussed upon two diagnostic approaches, saturated laser-excited molecular fluorescence and CARS (coherent anti-Stokes Raman spectroscopy).

ABSTRACT

The report gives results of comparisons of saturated laser-excited molecular fluorescence measurements of CH and CN in atmospheric pressure acetylene flames with absorption measurements of these flame radicals. It was found possible to saturate the fluorescence intensity of both CH and CN with readily achieved levels of laser spectral intensity (10^5 to 10^6 watts/cm^{2}cm^{-1}). Coherent anti-Stokes Raman Spectroscopy (CARS) thermometry investigations were conducted on flame nitrogen in a variety of flames, including highly sooting propane diffusion flames. CARS species sensitivity was addressed in a study of CO detectability limits.

TABLE OF CONTENTS

Section		Page
	SUMMARY	1
	INTRODUCTION	5
I	SATURATED LASER FLUORESCENCE INVESTIGATIONS OF CH AND CN SPECIES DETECTION	9
	Introduction	9
	Experimental Apparatus	14
	Absorption Measurements of CH and CN Radicals in Flames	20
	Fluorescence Measurements	34
	Experimental Results	47
	Discussion	49
II	CARS INVESTIGATIONS IN FLAMES	57
	Introduction	57
	Experimental Approach	60
	BOXCARS: Crossed-Beam Phase Matching	68
	Flat Flame Thermometry	80
	Sooting Flame Temperature Measurements	89
	CO Species Concentration Measurements	97
III	CONCLUSIONS AND RECOMMENDATIONS	107
	Saturated Laser Fluorescence Investigations	107
	CARS Investigations in Flames	109
IV	REFERENCES	113
	APPENDIX I - CARS Spectra of Combustion Gases	I-1

LIST OF FIGURES

Figure		Page
1	CH and CN Energy Level Diagrams	13
2	Schematic of Laser Induced Fluorescence Apparatus	15
3	Saturated Laser Fluorescence Experiment	16
4	Slot Burner and Optical Geometry	21
5	Flame Absorption Measurements Schematic	23
6	Absorption Spectrum of CH in Oxy-Acetylene Slot Burner	25
7	Absorption Spectrum of CN in Nitrous Oxide-Acetylene Slot Burner	27
8	Rotational Temperature Plot for CH ($X^2\Pi$) $v'' = 0$	28
9	Rotational Temperature Plot for CN ($X^2\Sigma^+$) $v'' = 0$	30
10	CH Emission Spectrum	35
11	CN Emission Spectrum	36
12	OMA Measurement of Dye Laser Spectral Output	38
13	Laser and CH Fluorescence Pulses	39
14	Laser Excited CH Flame Fluorescence	40
15	Laser Excited Anti-Stokes CH Flame Fluorescence	42
16	Laser Excited CN Flame Fluorescence	43
17	Laser Excited CH Fluorescence Spectrum	46
18	CH Concentration Data Reduction	50
19	CN Concentration Data Reduction	51
20	CARS - Coherent Anti-Stokes Raman Spectroscopy	58

LIST OF FIGURES (Cont'd)

Figure		Page
21	UTRC CARS Experimental Arrangement.	62
22	CARS Experimental Apparatus	63
23	CARS Generation From Air at 4733Å	66
24	Broadband Dye Laser Spectral Stability.	67
25	CARS Phase-Matching Approaches.	69
26	Collinear CARS Curves of Growth	71
27	BOXCARS Experimental Arrangement.	75
28	BOXCARS Intensity Variation With Angular Detuning	77
29	BOXCARS Spatial Resolution.	78
30	Computer Generated CARS Spectra	82
31	Experimental BOXCARS Spectrum of Flame N_2	84
32	Computed CARS Spectrum for Flame N_2	86
33	Single Pulse CARS Spectrum of Flame N_2.	88
34	Low Resolution CARS Spectra	90
35	BOXCARS Spectrum From Laminar, C_3H_8 Diffusion Flame	92
36	Laser Induced Soot Emissions.	94
37	BOXCARS Spectrum of N_2 in a Highly Sooting Laminar Propane Diffusion Flame	96
38	Computed Flame CO Spectra	99
39	Crossed Beam, Phase Mismatched CARS Spatial Resolution.	103
40	Crossed Beam, Phase Mismatched, CARS Spectrum of Flame CO	104
41	CARS Spectrum of CO in CH_4 Rich Flame	106

LIST OF TABLES

Table		Page
I	Summary of Absorption Data.	33
II	Numerical Values Used in Sample Calculation of N_1, N and Q for CH.	52
III	Summary of Results of Fluorescence Measurements for CH and CN	52
IV	Collinear Phase-Matched CARS Probing Volume	70
V	BOXCARS Phase-Matching Angles	73

SUMMARY

Under Contract 68-02-2176 sponsored by the Environmental Protection Agency, the United Technologies Research Center (UTRC) is conducting analytical and experimental investigations of non-perturbing, spatially precise, in-situ diagnostic techniques to measure species concentrations and temperature in flames. Under Task I, a comprehensive review (EPA-600/7-77-066) was conducted of potential techniques to measure chemical composition and temperature in flames with particular emphasis on instrumentally hostile environments such as research scale furnaces. In Task II, laboratory investigations of the most promising diagnostic techniques emerging from the Task I study have been conducted and are reported herein. The Task II experimental studies focussed upon two diagnostic approaches, saturated laser-excited molecular fluorescence and CARS (coherent anti-Stokes Raman spectroscopy).

Saturated laser-excited molecular fluorescence measurements, using a tunable, flashlamp-pumped dye laser, were performed on CH and CN in atmospheric pressure, acetylene flames. The fluorescence was observed from the $A^2\Delta$ of CH at 4315Å and the $B^2\Sigma$ state of CN at 3880Å. The fluorescence intensity dependence on laser intensity was observed to depart markedly from linearity at high laser spectral intensities for both CH and CN indicative of saturation. Quite importantly, saturation occurred at readily achieved laser spectral intensities in the range of 10^5 to 10^6 Watts/cm^2cm^{-1} for both CH and CN. These are the first observations of saturated fluorescence from these important flame radicals. The saturated fluorescence data permitted evaluation of the species concentration and total excited-state foreign species quenching rate for both CH and CN. In order to test the validity of the saturated fluorescence results, absorption measurements of these flame radicals were made to independently determine the concentrations. The absorption measurements were per-

formed in a single pass on a specially constructed slot burner operating at atmospheric pressure. Absorption indicated a CH concentration of about 60 ppm in an oxy-acetylene flame and approximately 150 ppm of CN in a nitrous oxide-acetylene flame. The concentrations measured by absorption were larger by about a factor of two for CH and four for CN than the values determined by saturated fluorescence. Various potential sources of error are analyzed. It is believed that the saturated laser fluorescence measurements are low, most probably due to overestimating the fluorescence sample volume due to the sharp spatial gradients of concentration probably present in these small, high pressure flames. This is not a fundamental limitation however. These experiments have demonstrated the viability of saturated laser fluorescence for trace species detection of important molecular radicals in flames. Although problem areas remain, it is believed that saturated laser excited fluorescence will become an important diagnostic in combustion applications.

CARS offers very promising potential for the temperature and species probing of practical combustion environments due to its large signal conversion efficiencies and coherent signal nature. Although CARS thermometry received the major emphasis in the investigations reported herein, CO species sensitivity was also examined. The CARS spectra are produced by mixing a 10 pps, frequency-doubled neodymium "pump" laser with a spectrally broadband, laser-pumped "Stokes" dye laser. In this approach which avoids the requirement to frequency scan the dye laser, the entire CARS spectrum is generated in a single pulse permitting "instantaneous" measurements of medium properties.

A new crossed-beam phase-matching technique, termed BOXCARS, has been demonstrated for the first time and is described. This approach, which will be extremely useful in studies of stratified flames, leads to greatly enhanced and unambiguous spatial resolution in contrast to the conventional collinear phase-matching approaches. Using this technique, moderate resolution (~ 1.25 cm^{-1}) CARS spectra from hot N_2, obtained by scanning the spectrum in premixed laminar flames, show excellent agreement with computer generated model predictions. Lower resolution (~ 2.7 cm^{-1}) collinear phase-matched CARS spectra of flame N_2 have been obtained in a single

10 nanosecond pulse using an optical multichannel analyzer. These single pulse spectra also display good agreement with predicted spectra and demonstrate the feasibility of single pulse thermometry. Measurements in a highly sooting, laminar propane diffusion flame revealed the existence of a coherent spectral interference arising from electronically, resonantly-enhanced CARS generation from C_2. The C_2 is produced by the laser vaporization of soot which occurs even on a ten nanosecond time scale as illustrated by a study of the incoherent C_2 Swan emissions. The CARS from C_2 occurs within the N_2 spectrum which is generally employed for thermometry. Reduction of the Stokes laser bandwidth and use of polarization filters permitted low distortion N_2 CARS spectra to be obtained. These spectra, when computer fitted, permitted determination of the temperature in the highly sooting flame marking the first measurement in such flames by a remote, spatially precise diagnostic technique. These sooting flame measurements are highly indicative that CARS will be applicable to the probing of practical combustion environments.

The species sensitivity of CARS was examined in an investigation of CO detectability levels. Very good agreement between CARS CO spectra and computer modelling was obtained at the 4 percent CO level in studies over a premixed flat flame. These spectra display very interesting features such as the appearance of destructive interferences not normally observed in linear spectroscopic processes. With the fluctuations in the experimental apparatus it was difficult to detect the presence of CO below the 1-2 percent level. The computer calculations indicate that CO would be barely detectable to about 0.5 percent practically using conventional CARS approaches.

In Section I the laser excited saturated molecular fluorescence investigations of CN and CH are described together with the absorption measurements of these flame radicals. Section II details the CARS investigations. Section III contains the conclusions of these investigations and recommendations for future research and development efforts in these areas. References are contained in Section IV. Appendix I contains a description of the CARS computer code.

MONITOR: EPA/600/2-76/096

ABSTRACT: AN EXPERIMENTAL PROGRAM HAS BEEN CONDUCTED TO MEASURE AND COMPARE THE EFFICIENCY OF TWO STACK SAMPLING SYSTEMS TO COLLECT VANADIUM-BEARING PARTICULATE EMISSIONS IN FLUE GAS. ONE SAMPLING SYSTEM WAS EPA'S METHOD 5. THE OTHER WAS DEVELOPED BY EXXON RESEARCH AND ENGINEERING COMPANY FOR SPECIALIZED IN-HOUSE STUDIES. TO EVALUATE COLLECTION EFFICIENCY, AN EXTENSIVE FACTORIAL STUDY WAS CARRIED OUT IN A 50 HP FOUR-PASS FIRETUBE BOILER BURNING TYPICAL RESIDUAL FUEL OILS. IN EACH TEST THE SAMPLING SYSTEMS WERE OPERATED SIMULTANEOUSLY IN THE STACK TO COLLECT THE VANADIUM-BEARING PARTICULATE EMISSIONS. THREE RESIDUAL FUEL ENTER-

-MORE-

OILS WERE TESTED: TWO VENEZUELAN (359 AND 149 PPM V) AND ONE ARABIAN (39 PPM V). A VANADIUM BALANCE WAS ESTABLISHED FOR EACH EXPERIMENT BY INVENTORYING BOTH THE PARTICULATE EMISSIONS AND THE PARTICULATES REMAINING IN THE BOILER. TEST VARIABLES, IN ADDITION TO THE SAMPLING SYSTEMS AND FUEL OILS, ALSO INCLUDED TWO COMBUSTION RESIDENCE TIMES AND TWO SAMPLING PROBE LOCATIONS. THE RESULTS OF THE STUDY SHOW THAT VANADIUM COLLECTION EFFICIENCY DEPENDS ON TWO VARIABLES: COMBUSTION RESIDENCE TIME AND SAMPLING SYSTEM. FOR BOTH SYSTEMS EFFICIENCY DECREASES AS COMBUSTIONRESIDENCE TIME INCREASES, WHICH RESULTS IN A PARTICULATE SIZE DISTRIBUTION SHIFT TO THE SUBMICRON RANGE. WHERE PARTICULATE EMISSIONS ARE IN THE COARSE SIZE RANGE, COLLECTION EFFICIENCY IN BOTH SAMPLING SYSTEMS IS ALMOST QUANTITATIVE. THE OXIDATION STATES OF VANADIUM IN FUEL OIL EMISSIONS ARE BRIEFLY DISCUSSED.

DESCRIPTORS: *VANADIUM, *SAMPLING, *PARTICLES, *AIR POLLUTION, *FLUE GASES, COMBUSTION PRODUCTS, FINES, INDUSTRIAL WASTES, GAS ANALYSIS, RESIDUAL OILS, BOILERS, EFFICIENCY, TOXICITY, EXPERIMENTAL DESIGN, CHIMNEYS, SULFURIC ACID, OXIDATION, ASH CONTENTS, CONCENTRATION(COMPOSITION), SULFATES, COLLECTING METHODS, BIBLIOGRAPHIES, EMISSION SPECTRUM, ATOMIC SPECTROSCOPY

IDENTIFIERS: IN PLANT PROCESSES, *AIR POLLUTION DETECTION, NTISEPAORD

ENTER-

-MORE-

INTRODUCTION

With the advent of laser light sources, light scattering spectroscopic diagnostic techniques are assuming an ever-increasing role in a broad spectrum of physical investigations. Of particular importance is the potential application of laser spectroscopy to the hostile, yet sensitive, environments characteristic of those in which combustion occurs. Laser spectroscopic diagnostics should facilitate greatly improved understanding of a variety of combustion processes which, in turn, should lead to enhanced efficiencies and cleanliness in energy, propulsion and waste disposal systems.

Under Contract 68-02-2176 sponsored by the Environmental Protection Agency, the United Technologies Research Center (UTRC) is conducting analytical and experimental investigations aimed at developing non-perturbing, spatially precise, in situ diagnostic techniques to measure species concentrations and temperature in flames. The contract is divided into two tasks. Under Task I, a comprehensive review (Ref. 1) has been conducted of potential unobtrusive, in-situ techniques to measure chemical composition and temperature in flames with particular emphasis on hostile environments such as research scale furnaces. In Task II, laboratory development of the most promising diagnostic techniques emerging from the Task I studies has been investigated and these investigations are reported herein.

The Task I technical report entitled "Review of Laser Raman and Fluorescence Techniques for Practical Combustion Diagnostics" (Refs. 1, 2) focussed upon four general laser diagnostic techniques, namely: spontaneous and near-resonant Raman scattering, laser fluorescence and coherent anti-Stokes Raman spectroscopy (CARS). For diagnosis of highly luminous, particle laden flames, spontaneous and near-resonant Raman scattering appeared to possess a low probability of successful application even with advanced state-of-the-art laser sources. For diagnosis of clean flames, i.e., low to moderate particle loadings. spontaneous Raman scattering is the diagnostic of first resort because of its simplicity, high level of theoretical and experimental understanding and advanced state of development. Laser

fluorescence appeared capable of measuring species concentrations to tens of ppm in practical flames, and tenths of ppm in clean flames for selected molecules whose absorptions can be saturated. In this approach, depending on the degree of saturation, fluorescence magnitudes do not depend upon or can be corrected experimentally for quenching effects. The technique applies to a half dozen or so molecules of intense combustion interest such as NO, OH, CH, CN, C_2 and NH. CARS was perceived capable of successful thermometry and major species measurements in practical environments, although some potential jeopardies such as soot interaction effects had yet to be addressed. CARS sensitivity for most molecules is limited to about 0.1 to 1 percent although sophisticated variants of CARS may lower the sensitivity limit by one to two orders of magnitude.

For the Task II experimental investigations, two specific avenues of study were of interest in view of the foregoing perspective, namely, saturated laser fluorescence and CARS. For combustion applications, saturated laser fluorescence is still in a very early stage of development. The success of the technique will reside in the ability to achieve laser spectral intensities high enough to saturate the molecular absorption transitions. Calculations of saturation intensities are often questionable due to the lack of or impreciseness of the fundamental rates required for such computations. The capability to minimize the effects of or to correct for quenching in saturated fluorescence depends on the applicability of simple, two level models. For the Task II experimental program, saturated laser fluorescence was investigated via an examination of its feasibility to the measurement of the molecules CH and CN which are of great interest in regard to NO formation. These radicals can be probed directly with flashlamp-pumped dye lasers without the requirement to frequency double the dye laser and can be partially saturated with such lasers. These two molecules are also of interest in regard to the physics of saturated laser fluorescence, since CH is anticipated to exhibit two level behavior while CN may display potential three level character. Although CARS is further advanced at this stage than saturated fluorescence, questions remain in regard to its ultimate capabilities and limitations. To probe these questions

further, various CARS investigations were carried out. Major emphasis in these studies was placed on the utility of CARS for thermometry in a variety of flames including highly sooting diffusion flames. Species sensitivity was also addressed in a study of CO detectability limits.

Section I of this report, which follows, details the saturated laser fluorescence investigations of CH and CN. Also described are concentration measurements of these radicals via absorption which serve as a basis of comparison for the fluorescence measurements. Section II details the CARS investigations in flames conducted during the Task II program. Section III contains the conclusions reached during these investigations and recommendations for future studies which are a logical extension of the investigations presented herein. The references are compiled in Section IV.

SECTION I

SATURATED LASER FLUORESCENCE INVESTIGATIONS OF CH AND CN SPECIES DETECTION

Introduction

Saturated laser-excited molecular fluorescence is a promising technique for the measurement of ppm level species concentrations in combustion environments. The importance of saturated fluorescence to species determination was first realized by Piepmeier (Ref. 3). Further theoretical developments were made by Daily (Ref. 4), and successful application of the technique to C_2 measurement in a laboratory flame has been made by Baronavski and McDonald (Ref. 5). The technique has several important and distinguishing characteristics. One is that concentration may be determined with high spatial resolution. The laser output is focused to a small cross-sectional area, and appropriate optics collect emitted fluorescence from a sample volume of order 1 mm^3 or less. Saturated fluorescence, which occurs only in the presence of high laser spectral intensity, permits determination of concentration without explicit knowledge of the details of fluorescence quenching due to foreign species present. This latter feature is very important. In conventional non-saturated fluorescence, the rate of quenching, including its temperature dependence, must be known beforehand. This information is generally not available for all foreign species present. This is particularly true of combustion applications, and consequently, has the effect of precluding concentration measurement in such environments.

The way in which saturation eliminates complications arising from fluorescence quenching may be explained within the framework of a simple two level quantum mechanical system. From rate equations for a two-level system, and in the steady-state approximation, it may be shown that the number density in the upper level, N_2, is related to that in the lower level, N_1, by

$$N_2 = N_1 B_{12} \left[\frac{Q_{21} + A_{21}}{I_{L\nu}} + (B_{12} + B_{21}) \right]^{-1}. \qquad (1)$$

where B_{12} and B_{21} are the Einstein coefficients for, respectively, stimulated absorption and emission of radiation; $I_{L\nu}$, the laser spectral intensity in units of Watts/cm^{2}cm^{-1}; Q_{21}, the total rate of quenching of level 2; and A_{21}, the spontaneous radiative decay rate of level 2. The fluorescence power, S_F, is proportional to N_2, and is given in general by

$$S_F = (hc/\lambda_F)(A_{21}/4\pi)\Omega_c V_c (N_2/N_1) N_1. \qquad (2)$$

where h is Planck's constant; c, the speed of light; λ_F, the fluorescence wavelength; Ω_c and V_c, light collection solid angle and sample volume size, respectively. In the limit of small laser spectral intensity where $I_{L\nu}\ (B_{12} + B_{21})/(Q_{21} + A_{21}) \ll 1$, it follows from Eqs. (1) and (2) that

$$S_F^{(1)} = (hc/\lambda_F)(B_{12}/4\pi)\Omega_c V_c [A_{21}/(Q_{21}+A_{21})] I_{L\nu}\ N_1. \qquad (3)$$

In Eq. (3), it is evident that the fluorescence power depends on quenching through the Stern-Vollmer factor $[A_{21}/(Q_{21}+A_{21})]$ (Ref. 6), and that S_F depends linearly on $I_{L\nu}$. On the other hand, if the laser spectral intensity is large so that $I_{L\nu}\ (B_{12}+B_{21})/(Q_{21}+A_{21}) \gg 1$, it follows also from Eqs. (1) and (2) that

$$S_F^{(2)} = (hc/\lambda_F)(A_{21}/4\pi)\Omega_c V_c [1 + (g_1/g_2)]^{-1}\ N_1, \qquad (4)$$

where use has been made of $B_{21}/B_{12} = g_1/g_2$, in which g_1 and g_2 are level degeneracies. The power $S_F^{(2)}$ corresponds to saturated fluorescence emission; it is independent of $I_{L\nu}$ and Q_{21}. This defines saturation for a two-level system. From the latter inequality, saturation occurs when the rate for stimulated emission of radiation significantly exceeds the combined rates for electronic quenching and radiative decay. In practice, it may be very difficult to saturate fully since the rate of quenching is generally large in a flame. However, in this case as well, provided that partial saturation is achieved, it has been shown by Baronavski and McDonald (Ref. 5) that species concentration can be determined without reference to

separately determined quenching data, and indeed that the total quenching rate is determined together with the concentration. This case of partial saturation is pertinent to the work reported herein; the related theory is somewhat more complex than that above and is deferred to a later section of this report.

The saturation fluorescence technique is not applicable to all molecular species. There are specific criteria which must be met. The molecule must first of all have a known emission spectrum. This is not always the case since a molecule upon optical excitation to a higher energy state may, in fact, dissociate prior to emission, which precludes application of the technique. Secondly, the molecular absorption wavelength must be accessible to a tunable laser source. In effect, this means that the absorption wavelength must occur in the interval 2000Å to 1.5 microns. Thirdly, the rate of radiative decay of the emitting level must be known. This is evident from Eq. (3) above. Finally, a means is required for handling the uncertainties introduced by foreign gas quenching of the fluorescence intensity. As indicated above, one way to achieve this end is to use a laser source with high spectral intensity in order to saturate the absorbing transition. Upon application of the above criteria only certain molecules are amenable to saturated fluorescence detection. These are listed in Table VII of the Task I report (Ref. 1) and include C_2, CH, CN, CS, NH, NO, OH, CH_2O, HCN, NH_3, and SO_2. The five molecules selected for closer scrutiny in the Task I review were: CH, CN, NH, OH and NO. The latter three molecules were not considered in the Task II experimental investigations due primarily to wavelength considerations. NH, OH and NO have absorption wavelengths of 3360, 3064 and 2074Å, respectively. To achieve these wavelengths with the available flashlamp-pumped, tunable dye laser requires frequency doubling of the laser output. Although this may be done in principle, there results in practice a reduction in laser intensity, which makes it more difficult to saturate the molecular transition. Since it was anticipated beforehand that saturation might be difficult to achieve, and hence, that maximum available laser spectral intensity would be required, losses due to frequency doubling would be limiting and serious. Moreover, the reduction is particularly significant for a flashlamp-pumped dye laser

with its relatively poor output beam quality. Since CH and CN have absorption wavelengths at 4315 and 3883Å, respectively, and these wavelengths may be achieved without frequency doubling, they were selected as candidates for detailed study. There is an additional reason for selecting CN and CH. The developed theory of saturated fluorescence is appropriate to a two-level system. The molecule CH, apart from its rotational structure, is a two-level system with respect to electronic excitation as seen in Fig. 1 (Ref. 7). The CN molecule, on the other hand, has in addition to its blue-violet $B^2\Sigma^+ \rightarrow X^2\Sigma^+$ emission, strong red emission which corresponds to the transition $A^2\Pi \rightarrow X^2\Sigma^+$. The state $B^2\Sigma^+$ lies above $A^2\Pi$ in energy as shown in Fig. 1 and $B^2\Sigma^+ \rightarrow A^2\Pi$ emission also occurs. Since $B^2\Sigma^+$ may de-excite by these two channels, CN approximates a three-level system with regard to electronic excitation, and thereby distinguishes itself from CH in an important way. By studying both CH and CN then, a test of the applicability of the two-level theory to more complex systems is possible.

Since saturated fluorescence is a new technique with its related theory not yet fully developed, it is important to have at hand a second, independent and reliable reference technique. For this reason, it was decided to supplement the fluorescence studies with absorption measurements. For absorption, the theory and interpretation of spectra are well understood. Accordingly, comparison of the two serves as a useful test of the accuracy of fluorescence measurements; hence, CH and CN concentrations are determined in this work from fluorescence and from absorption as well. There is an important difference between fluorescence and absorption which must not be overlooked. Fluorescence is a point measurement technique, while absorption is a line-of-sight measurement. Accordingly, only if the flame is spatially homogeneous with respect to concentration is it expected that fluorescence and absorption results would be the same and, indeed, that absorption results have any useful meaning. This, then, underscores the importance of fluorescence in that the technique is applicable to inhomogeneous media while absorption is not. In this work, a homogeneous flame was created for the explicit purpose of making meaningful comparisons of absorption and fluorescence results.

FIG. 1

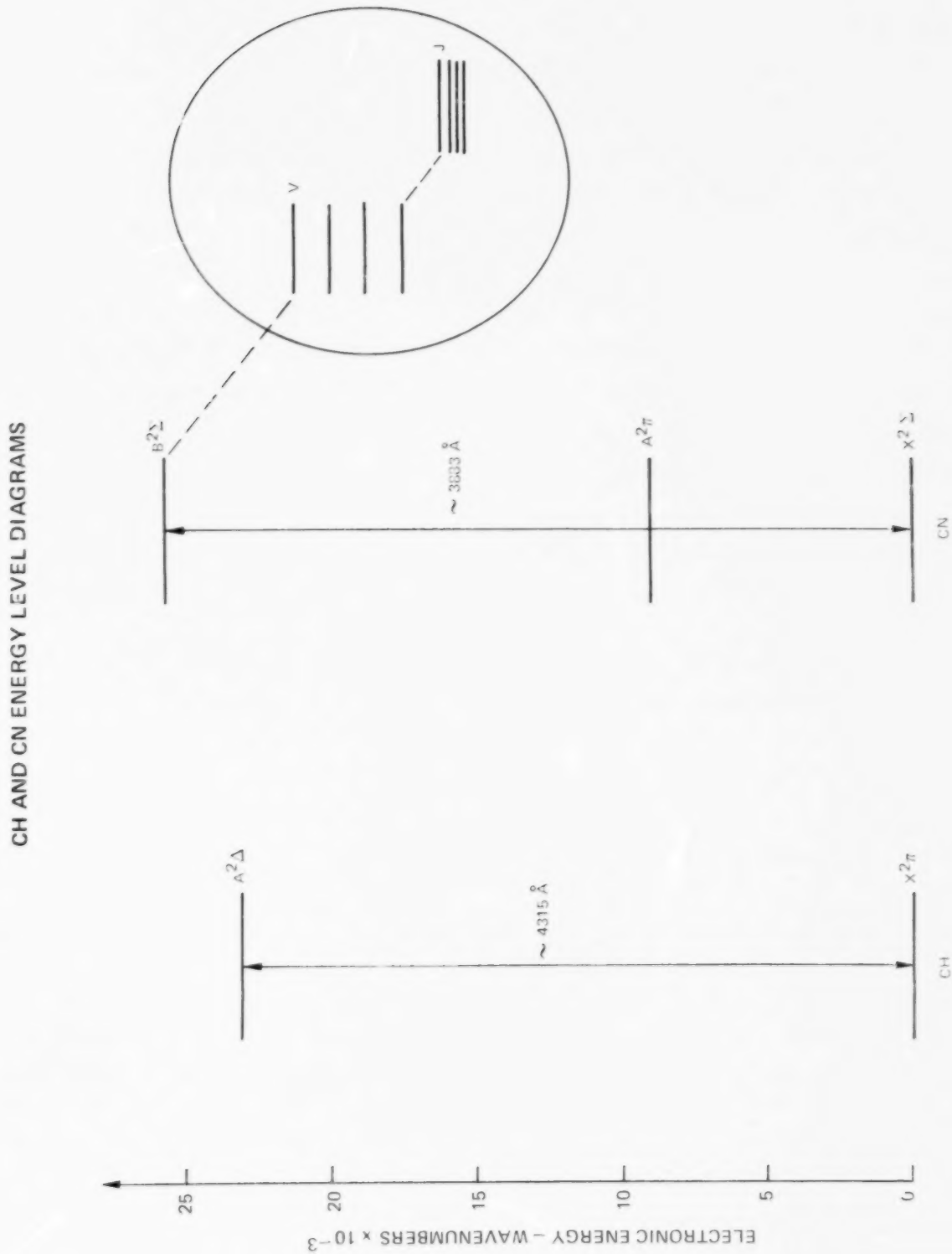

78-02-189-1

The description of the experimental apparatus employed in the saturated fluorescence investigations is given immediately below. This is followed by a self-contained discussion of the absorption measurements of CH and CN. The fluorescence measurements, which include the observation of saturation for both CH and CN, are then summarized. Finally, species concentration and quenching rates are evaluated and the results discussed.

Experimental Apparatus

The saturated laser fluorescence experimental layout is shown schematically in Fig. 2 and photographically in Fig. 3. A wavelength-tunable pulsed dye laser provides the exciting radiation which is focused by a lens into a small laboratory flame which serves as the source of CH or CN. Appropriately placed lenses collect the fluorescence at 90° to the exciting laser direction and focus it onto the slit of a spectrometer to isolate the species fluorescence from other unwanted radiations.

Laser

The source of exciting radiation in these experiments is a Phase-R model 2100C flashlamp-pumped dye laser employing a coaxial optical pumping configuration. A xenon gas discharge lamp provides the pumping radiation. The lamp is capable of absorbing about 160J of electrical energy. Although in principle the laser may be repetitively pulsed, in practice it performs best on a single-shot basis. A Fabry-Perot optical cavity is employed consisting of a flat output mirror and a grating to spectrally condense and tune the emitted radiation. Laser energy is coupled out of the cavity through the flat mirror which has a reflectance at the laser wavelength of typically 25-50 percent. Depending on the operating wavelength, and the degree to which the flashlamp is driven, the laser delivers (20-60) mJ of spectrally narrow, tunable energy in a pulse length of 150-300 nsec with a laser beam diameter of 11 mm.

For the CH measurements, the laser was made to operate near 4315Å which corresponds to $A^2\Delta \rightarrow X^2\Pi$, $v = 0 \rightarrow v' = 0$ emission. The laser oscillated near this

FIG. 2

SCHEMATIC OF LASER INDUCED FLUORESCENCE APPARATUS

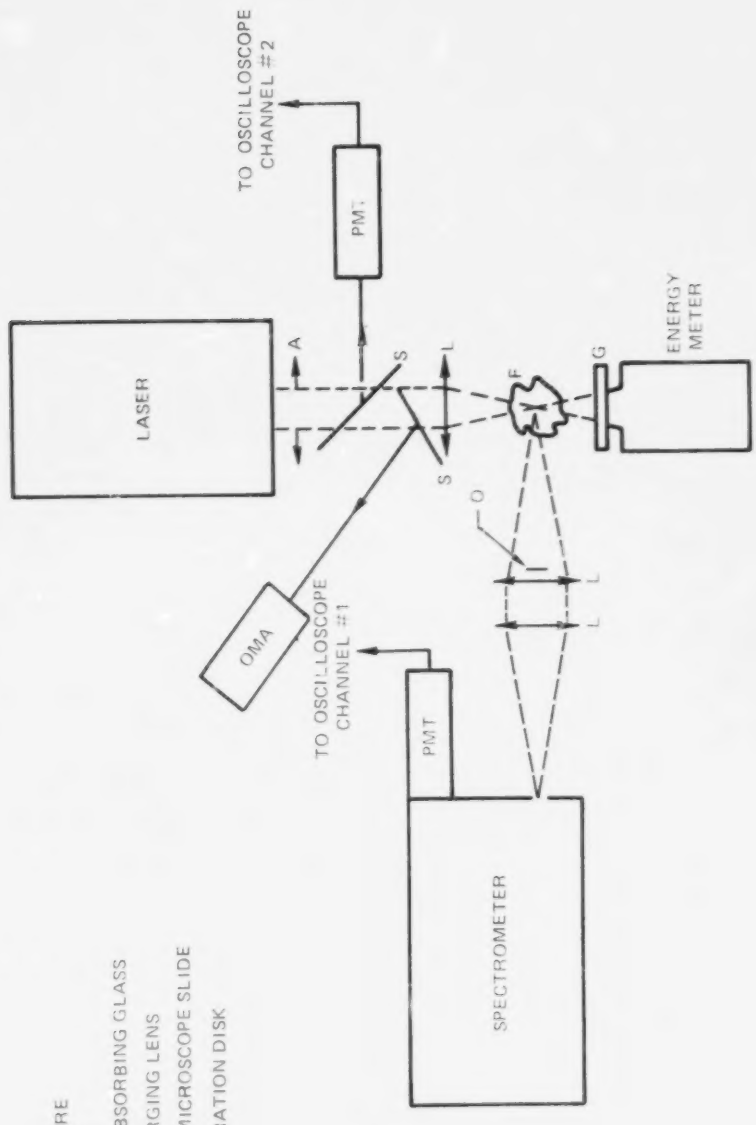

A, APERTURE
F, FLAME
G, HEAT ABSORBING GLASS
L, CONVERGING LENS
S, GLASS MICROSCOPE SLIDE
O, OBSCURATION DISK

78-02-130-1

FIG. 3

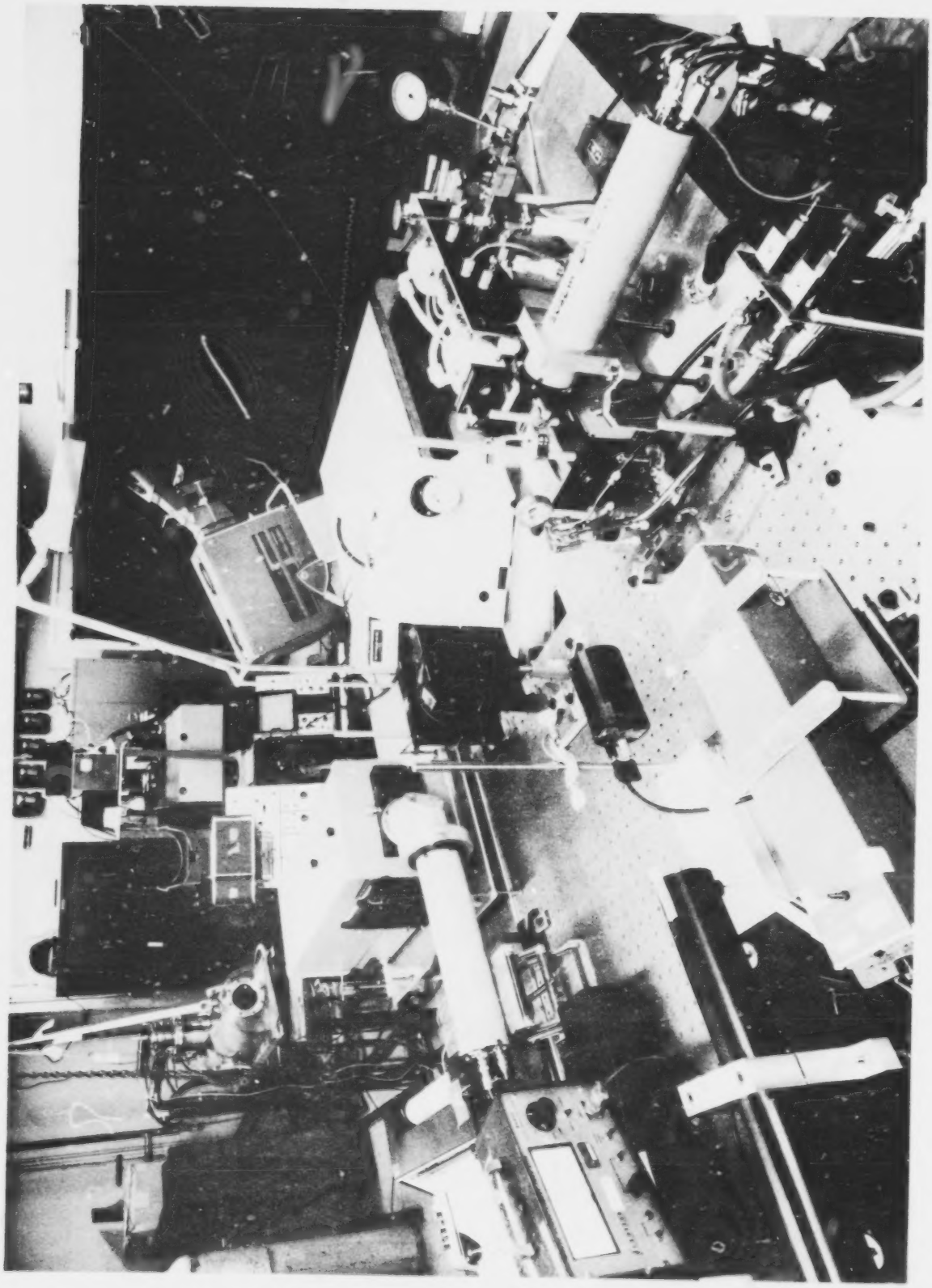

SATURATED LASER FLUORESCENCE EXPERIMENT

78-65-D

78-02-189-3

wavelength with Exciton LD423 laser-grade dye dissolved in methanol. Typical dye concentrations were 0.2 gm dissolved in 6 liters of methanol (1.3×10^{-4} molar). When the laser cavity consisted of a 100 percent reflecting flat mirror and a 50 percent reflecting, flat output mirror, the laser energy was 200-300 mJ. In order to narrow and tune the laser spectral output, the 100 percent reflecting mirror was replaced by a PTR Optics TF-R2 echelle-type diffraction grating. This grating has high dispersion since it is designed to operate in high order (n = 8-10) at a relatively large angle of incidence, 50-60°. With insertion of the grating into the cavity, the laser energy dropped to 50-60 mJ maximum. The energy measurements were made with a Scientech model, S-3620, power meter positioned as shown in Figs. 2 and 3. Also shown in Figs. 2 and 3 is a Princeton Applied Research optical multi-channel analyzer (OMA). This instrument was used in order to determine the wavelength, spectral width and reproducibility of the laser emission. In this way, it was determined that laser output could be obtained in the interval 4210-4330Å by angle-tuning the echelle grating, and that the spectral width of the laser output over this entire range was 2Å. Peak laser emission occurred near 4270Å. Accordingly, this wavelength was used to excite CH since the energy associated with it was high, and the wavelength given coincides with an R-branch rotational transition in the $A^2\Delta \rightarrow X^2\Pi$, $v = 0 \rightarrow v' = 0$ spectrum.

It was not possible to use the same dye solvent combination for CN measurements as for CH. For CN emission corresponding to $B^2\Sigma^+ \rightarrow X^2\Sigma^+$, $v = 0 \rightarrow v' = 0$, laser oscillation near 3883Å s required. Exciton BBQ laser-grade dye dissolved in 6 liters of solvent (3.0×10^{-4} molar) gave optimum energy. In this latter case, it was not possible to achieve energies near 3883Å as high as were achieved near 4315Å. With two flat mirrors comprising the laser cavity, the energy was typically 60-100 mJ for a 50 percent output coupling mirror. This represents a reduction in energy by a factor of three from that associated with LD423/methanol lasing. Not surprisingly, then, the energy with the grating in the cavity was only 12-20 mJ. There was a further acute difficulty with the BBQ/p-dioxane combination. After only 100 shots or so, the laser performance, as regards energy, degraded significantly. Consequently,

in order to avoid operation at even further reduced energies, very frequent dye/solvent changes were required. Th problem was present for LD423/methanol as well, but in this case the higher, nominal pulse energies made losses somewhat more tolerable. The OMA measurements in the CN case displayed spectral condensation similar to that above. The laser energy peaked near 3840Å, and this, as above, served to dictate an R-branch line in the CN spectrum as the exciting line for fluorescence measurements.

Burners

For the CH measurements, two different types of burners were used. The first of these was a small, portable oxy-acetylene welding torch. For this flame, the oxygen and acetylene were premixed. Although this torch proved to be perfectly adequate for fluorescence measurements, it was not possible to use it successfully to make absorption measurements due to the relatively short absorption path length associated with it. Accordingly, a similar slot-type burner with a considerably longer active path length was constructed and used. A description of this burner is given below as part of the discussion of absorption measurements. The slot burner is evident in the apparatus photograph, Fig. 3. CN absorption and fluorescence measurements were made with the slot burner alone. To go from CH to CN with the slot burner, it was merely necessary to replace oxygen by nitrous oxide as a premixed component of the flame. The presence of CH and CN in the flames of these torches was verified by viewing the corresponding emissions with a spectrometer and identifying characteristic band spectra.

Optics

As may be seen in Figs. 2 and 3, a single lens was used to focus the output of the laser into the flame. The lens is plano-convex and anti-reflection coated, and has a 50 mm focal length. Since the beam quality of the laser was poor, it was found useful to aperture the output beam prior to its incidence upon the lens. The size of the focused spot for the CH/CN measurements was typically 1-2 mm dia. Further

reduction of spot size by increased aperturing of the beam resulted in intolerable energy reduction.

As shown in Fig. 2, the fluorescence intensity was viewed at right angles to the direction of laser propagation. The light was collected by an imaging system which consisted of two lenses and a 0.5 meter Jarrell-Ash spectrometer with 16Å/mm linear exit slit dispersion. The lenses and their spatial positioning were such that the optics were f/8 and the magnification of the source at the entrance slit of the spectrometer was near unity. The f/8 optics were selected to match those of the spectrometer. The lens nearest the flame has an obscuration disk in front of it. This disk sets a limit to the effective depth-of-field of the light collecting optics (Ref. 8). The combination of lenses and spectrometer were made light-tight to prevent stray light incursion.

Pulse Recording Instrumentation

The apparatus in Figs. 2 and 3 includes two RCA model 8575B photomultiplier tubes. One is used to monitor the laser pulse energy, and the other, which is attached to the spectrometer, records the fluorescence pulses. The 8575B photomultiplier has near peak spectral sensitivity at the CH and CN wavelengths of interest, and has a 3 nsec response time. The laser and fluorescence pulses are observed simultaneously by using a fast-responding, 400 MHz, Tektronix model 7844 dual-beam oscilloscope. For each firing of the laser, a photograph is taken of the oscilloscope trace, which is then used for data analysis and processing. The laser photomultiplier serves two purposes. It gives a shot-to-shot record of the laser pulse amplitude and length. Secondly, it measured laser pulse energies below a few mJ or so since this latter energy represents the lower limit of reliable measurement of the Scientech energy meter. That is, at laser energies near a few mJ, the photomultiplier is calibrated against the Scientech, and then the photomultiplier is used exclusively for measurement of progressively smaller energies.

Absorption Measurements of CH and CN Radicals in Flames

In order to check the accuracy of the fluorescence measurements, the concentration of CH and CN species has been determined by absorption in atmospheric pressure flames. Measurements were made sequentially by absorption and fluorescence techniques using the same burner operating under identical gas flow conditions.

Measurements have been made previously of absorption by CH and CN radical species in flames. Results have been reported for CH in pre-mixed oxy-acetylene flames by several investigators (Refs. 9-13). In contrast only one previous determination (Ref. 14) of CN by absorption in a flame is known. That study differed from the present one in that CN was produced by the combustion of C_2N_2, O_2 and H_2 by Bulewicz et. al. whereas the combustion of C_2H_2 in N_2O was observed in the present investigation. Exemplary of the CH investigations is the work of Bulewicz et. al. (Ref. 13) and Bleekrode (Ref. 11). In these studies absorption was observed in low pressure ($\sim$ 5 Torr) slot burner flames using a multipath cell. Up to 30 traversals of a 20 cm wide burner have been used. The results of the present study will be compared to these studies later in this section.

It was desired to make the measurements with an atmospheric pressure burner to minimize problems of adapting the fluorescence apparatus to the burner system. This imposes a limitation on the accuracy of the absorption measurement because of the short lifetime of the radical species. For example, Bulewicz has measured CH concentration profiles above a low pressure (5 Torr) oxy-acetylene slot burner and has determined under certain conditions that the concentration reaches a maximum 1 cm from the burner and that the concentration is 50 percent of maximum value at 1/4 cm and again at approximately 3 cm. At atmospheric pressure it is expected that the CH species will be confined to a smaller region near the flame zone in inverse proportion to the ratio of the pressures. The effect of nonuniform flame properties can be understood from Fig. 4. Figure 4 illustrates the high aspect ratio slot burner used in the present experiments. Premixed fuel and oxidizer exit from a narrow slot and burn in a stable flame attached to the burner surface. An optical probe beam propagating parallel to the horizontal burner surface and the slot

FIG. 4

SLOT BURNER AND OPTICAL GEOMETRY

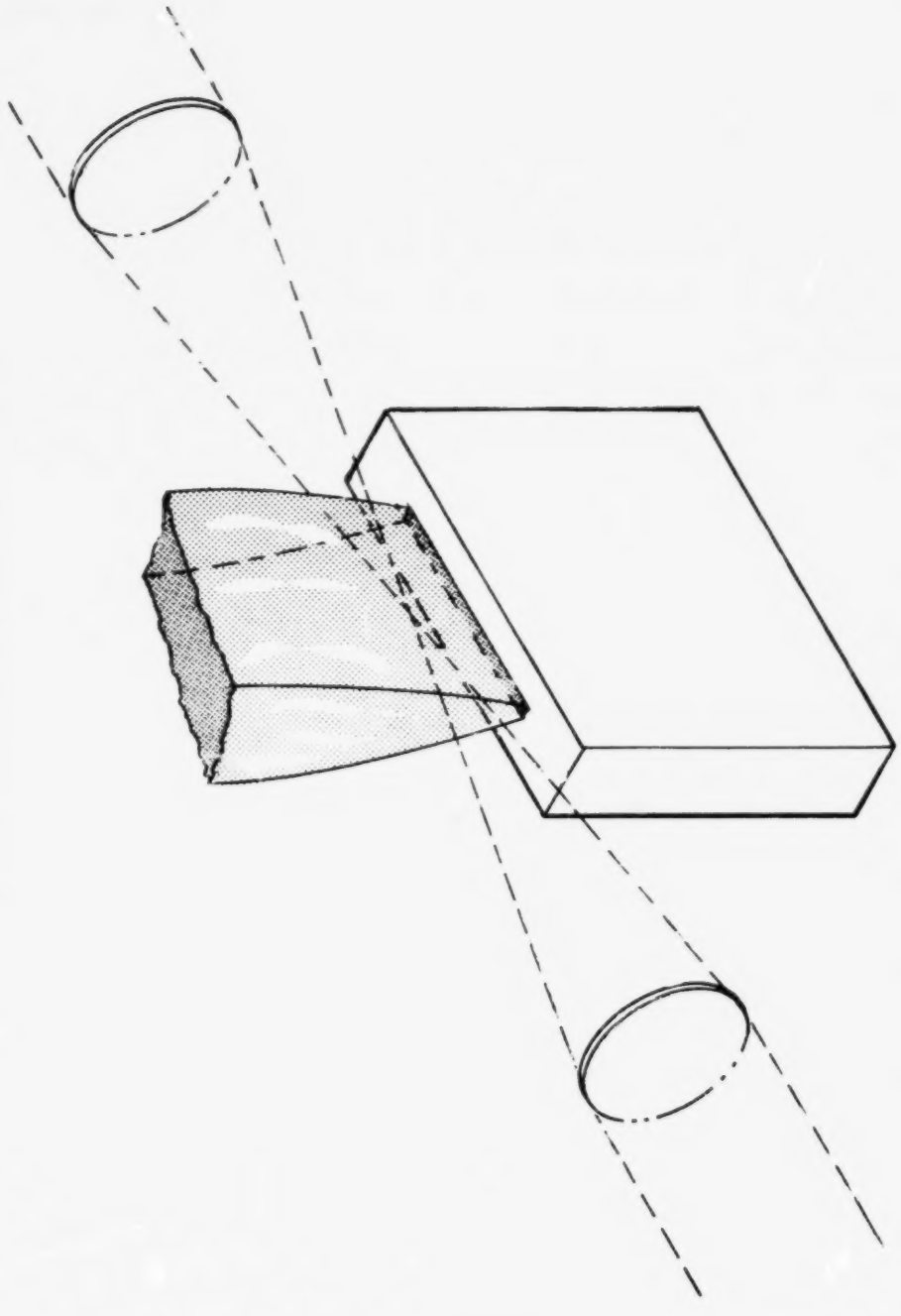

78-02-170-1

is brought to a focus at a point in the center of the burner. Details of the burner are presented later in this section. The optical path depth varies from ray to ray in the probe beam light pencil because the concentration in general varies along the pencil. The probe beam aperture has been kept small to minimize this effect. In the data reduction the optical path depth is assumed to be equal to the width of the flame. The concentrations determined in this manner must be interpreted to be minimum values.

The apparatus used for the absorption measurements is shown schematically in Fig. 5. Light from a high pressure xenon arc lamp is collimated and brought to a focus above the slot burner. The light is recollimated and focused onto the entrance slit of a 0.5 m monochromator. Radiation is detected at the exit slit by a photomultiplier tube. In the absorption mode of operation a chopper between the first focusing lens L2 and the flame modulates the xenon lamp radiation, thereby providing discrimination against the emission from CH species excited in the flame. In the emission mode the chopper is located between L4 and the monochromator and the xenon lamp is turned off or blocked. In the measurements reported here a point 1.5 mm from the burner exit is imaged onto the entrance slit. The entrance slit height is 1 mm in all cases and the slit width is approximately 20 μm. The focal length of lenses L3 and L4 are nearly equal so that the magnification is nearly unity.

The largest source of error in these experiments is the instability of the arc source. The light output stability was 3 percent peak-to-peak. Some effort was expended to improve this since some absorptions are expected to be near this level. A Hg-Xe lamp was found to have the same stability performance, and the light of one Hg-Xe lamp was found to drift 10 percent after warm-up. A tungsten strip lamp had much better stability; however, the signal intensity was an order of magnitude lower. This caused problems because the low ratio of lamp signal to the emission signal (in the bandpass of the tuned amplifier) caused an overload condition in the tuned amplifier. With the xenon lamp there were no problems with the emission from the flame.

FIG. 5

FLAME ABSORPTION MEASUREMENTS SCHEMATIC

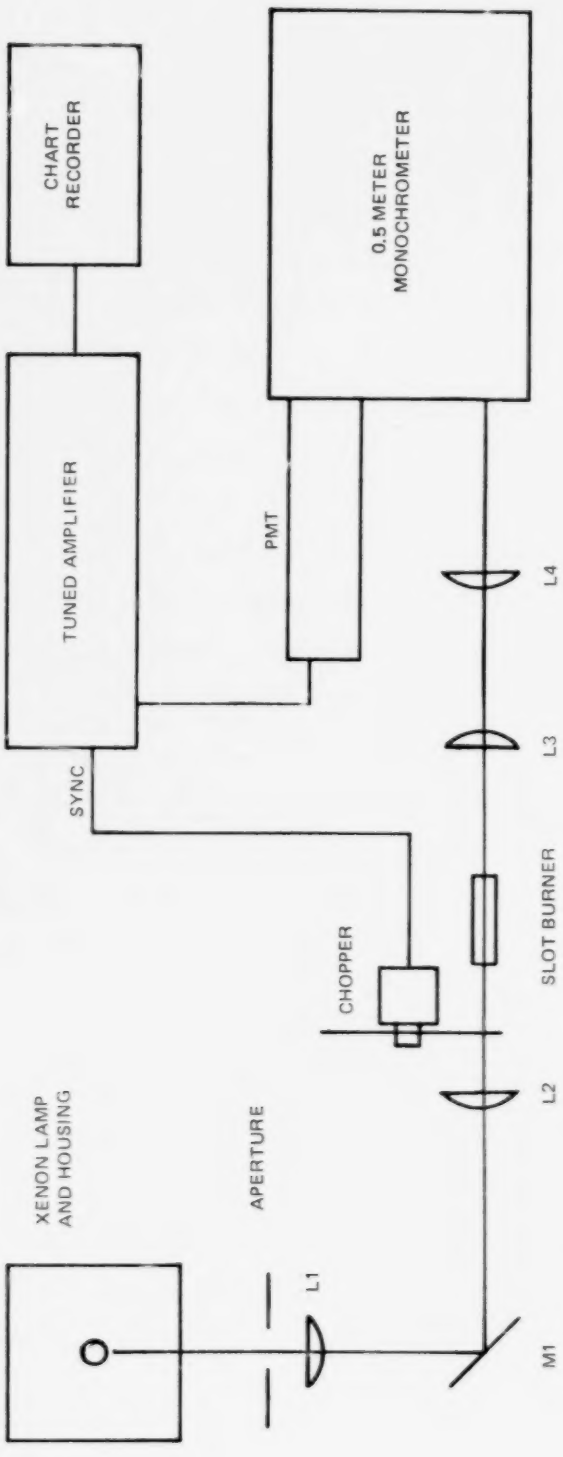

78-02-165-1

Another effect which is a potential problem is beam steering by the strong thermal gradients in the flame. The magnitude of beam steering was checked by tuning away from the absorption region of the spectrum and observing the effect of the presence of the flame. Beam steering effects were found to be small probably because in the geometry of these experiments the light propagated perpendicular to the temperature gradients.

The burner consists of two water-cooled, copper blocks which are joined to a standard welding torch to eliminate flashback. The copper blocks are separated by a piece of brass shim stock which determines the thickness of the gap between the copper blocks. A shim thickness of 0.2 mm was used here. The flame length was 2.4 cm. The flame was found to be stable and very uniform after the gap had been cleaned. The oxy-acetylene flame was adjusted to eliminate the "feather." The N_2O-C_2H_2 flame was adjusted to have a small zone of CN red emission. Flowmeters were used on the gas supplies to aid in resetting the flow rates.

A sample spectral scan of an oxy-acetylene flame in the CH ($X^2\Pi \rightarrow A^2\Delta$) region is shown in Fig. 6. Emission and absorption spectra are superimposed on the same plot. The emission spectra baseline has been displaced but the zero for the absorption spectra is as shown. The vertical scale for the emission spectra represents the PMT signal voltage with the lamp off and the chopper positioned just before the monochromator. Amplifier gain was a factor of 25 higher for the emission data. The positions of several R and Q branch lines in the $v' = 0 \leftarrow v'' = 0$ band have been marked. The P branch is weaker and has not been used in this study. The presence of absorption features is readily apparent. The peak absorption $[(I_o-I)/I_o]_{peak}$, where I is the lamp intensity at the signal minimum, and I_o is the unabsorbed intensity corresponding to that wavelength, is obtained from this spectrum and from a spectral scan of the lamp with the flame off. In practice little difference has been observed between the flame off scan and signal level in the absorption scan in regions of the spectrum where there is no absorption. Therefore, I_o in practice is obtained from an I_o line fitted to the absorption scan.

ABSORPTION SPECTRUM OF CH IN OXY-ACETYLENE SLOT BURNER

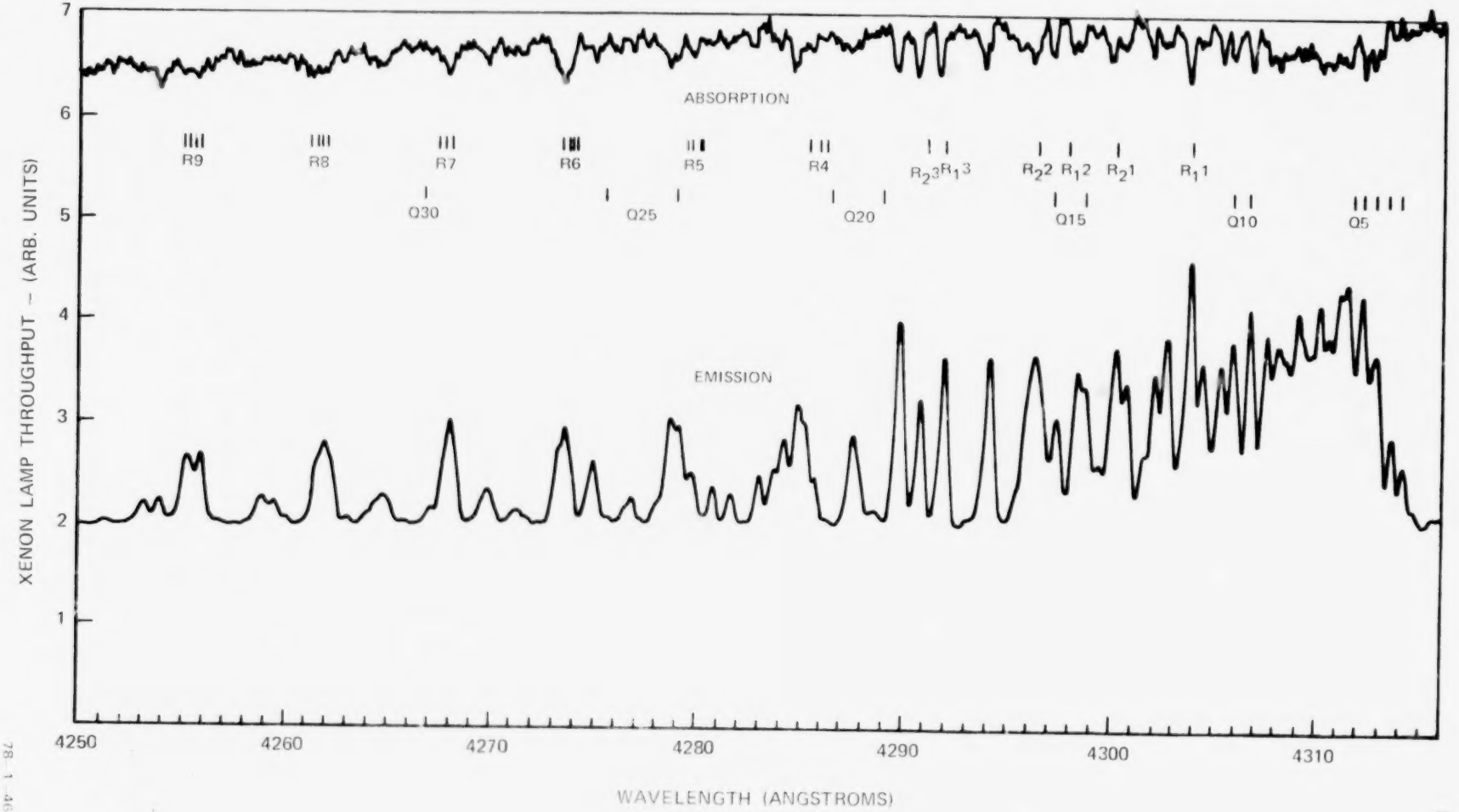

FIG. 6

The maximum absorption in the CH band is 6 percent. The resolution is insufficient to fully resolve all the components of the lines. In CH spin-orbit splitting is large at low K and decreases as K increases, where K is the nuclear rotational quantum number. Alternately, splitting due to λ doubling is small at small K and increases with K. The lowest spin-orbit components are resolved but overlapped with the Q branch. At the highest K values measured in these investigations λ doubling is almost resolved.

Figure 7 shows the absorption and emission spectra of the CN violet band ($X^2\Sigma^+ \rightarrow B^2\Sigma^+$) of a nitrous oxide-acetylene flame. Again the true zero is shown only for the absorption spectrum. Several $\Delta v=0$ transitions are overlapped with the strongest $v' = 0 \rightarrow v'' = 0$ transition. The Q branch is very weak and the P branch forms a head. The piling up in the P branch of the upper $\Delta v=0$ transitions is great enough to produce sizable absorptions which are superimposed on the absorption of the R branch of the (0,0) band. The resolution (~ 2 cm^{-1}) is insufficient to resolve any of the spin splitting of the lines. The maximum absorption is 16 percent, but absorptions are generally less than 8 percent.

The rotational temperature T_R can be obtained by an appropriate normalization of the data, accordingly

$$I_{abs} = \text{const } S_{K'K''} \nu \exp(-E_{K''}/kT_{R''}) \qquad (5)$$

where $S_{K'K''}$ is the rotational linestrength, ν is the transition frequency expressed in wavenumbers (cm^{-1}), $E_{K''}$ is the energy level of the Kth state and k is the Boltzmann constant. Figure 8 shows a semi-log plot of the CH absorption data normalized by $\bar{S}_{K'K''}$, where $\bar{S}_{K'K''}$ is the average rotational linestrength for the two R_1 and R_2 components. Rotational linestrengths have been taken from Beenakker et. al. (Ref. 15). The ν factor has been neglected in this plot as only a small (1 percent) error is involved. The straight line shown has been least squares fit to the data. P branch lines which are strongly overlapped with the Q branch have been neglected in this fitting. The best fit line corresponds to 2600°K. Several runs under identical conditions have been plotted on the figure.

FIG. 7

ABSORPTION SPECTRUM OF CN IN NITROUS OXIDE–ACETYLENE SLOT BURNER

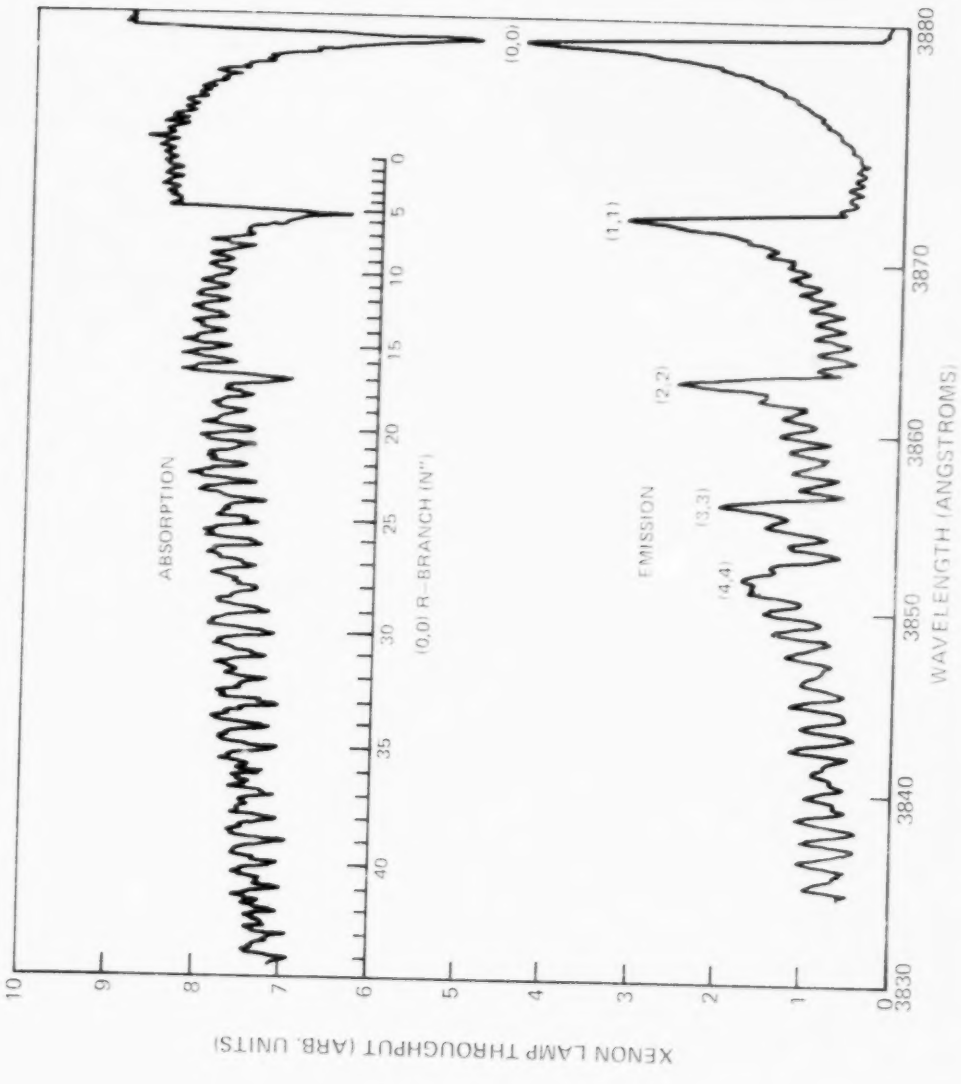

ROTATIONAL TEMPERATURE PLOT FOR CH ($X^2\Pi$) V'' = 0

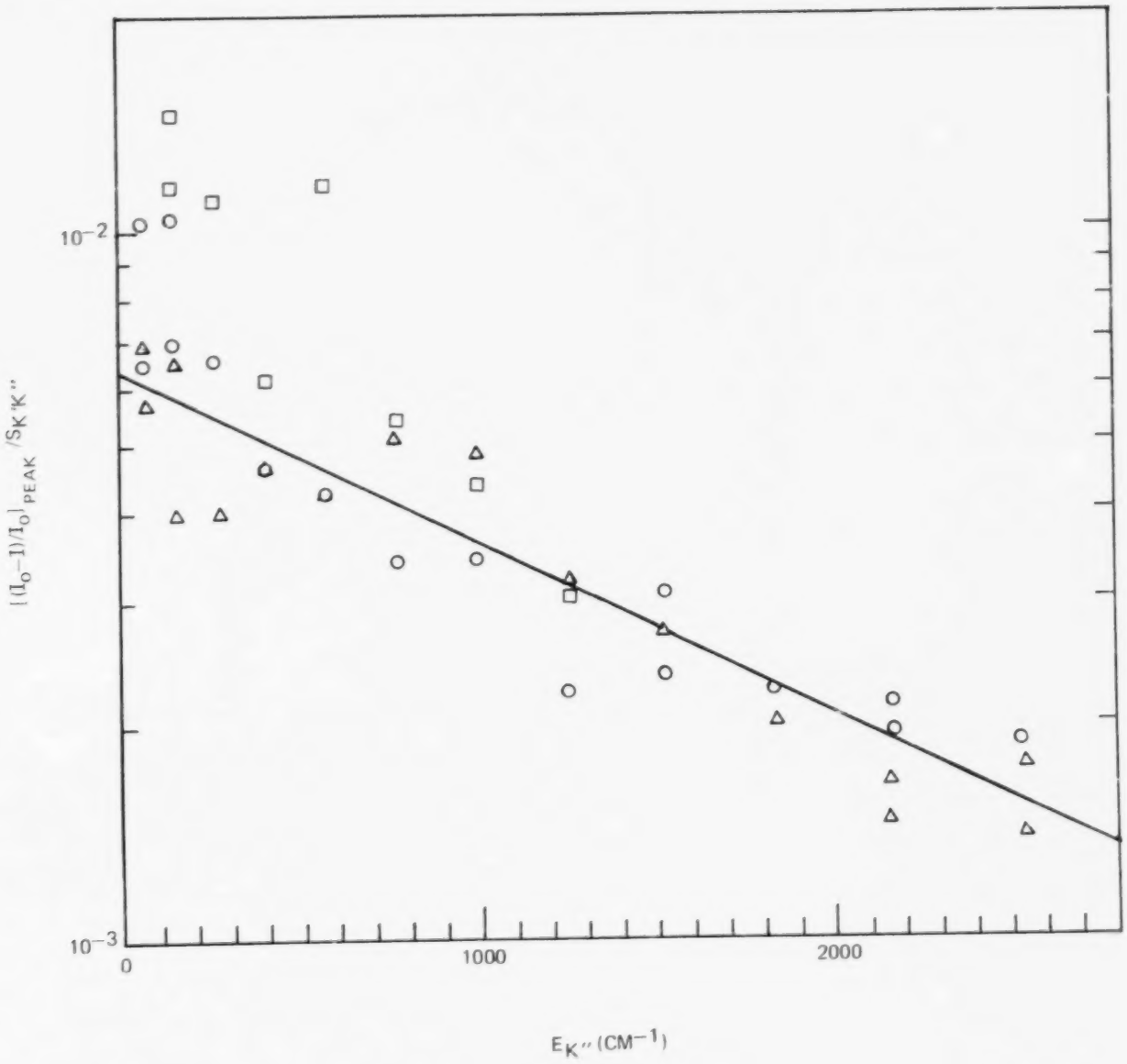

78-02-165-3

Figure 9 shows a rotational temperature plot of the CN (0,0) band data. Interferences due to overlapping with (1,1), (2,2), (3,3) P branches are clearly visible. A complete treatment of this data would fit the absorption spectra with computer generated simulated spectra which account for the overlapping with the higher $\Delta v=0$ P branches. This is beyond the scope of the present investigation. A straight line has been faired through the data in such a way as to attempt to compensate for the overlap effects. This straight line corresponds to 2900°K. It may be noted that the one previous investigation didn't mention these difficulties. This may be due to the lower temperature observed in that study.

The integrated absorption coefficient corresponding to a single transition n", v", J' (or K") → n', v', J' (or K') is given by

$$\int k_\nu d_\nu = (8\pi\nu^2 c)^{-1} \frac{g_{n'}}{g_{n''}} A_{n'n''} A_{v'v''} \frac{S_{J'J''}}{2J''+1} N_{n''v''J''} \qquad (6)$$

where $g_{n'}$ and $g_{n''}$ are the degeneracies of the upper and lower electronic states respectively, $A_{n'n''}$ is the electronic transition probability, $A_{v'v''}$ is the Franck-Condon factor, and the other quantities have their usual meanings. The population density of the state denoted by n", v", J" is given by

$$N_{nvJ} = \frac{N}{Q} (2-\delta_{0,\Lambda})(2J+1) \exp\left[-(T_n + G_v + F_J)\, hc/kT\right] \qquad (7)$$

where the partition function Q is given by

$$Q = Q_e Q_v Q_R = \sum_{n\Lambda s} (2-\delta_{0\Lambda'})(2S'+1) \exp\left(-hcT_n/kT\right) \cdot Q_v \cdot \frac{kT}{hcB_r} \qquad (8)$$

and

$$Q_v = \sum_{v=0} \exp\left[-G_0(v)hc/kT\right]. \qquad (9)$$

The factor $(2-\delta_{0,\Lambda'})$ accounts for Λ-type doubling wherein the electron spin (magnitude S) couples with the magnetic field produced by the electron angular momentum Λ and splits the spin components.

FIG. 9

ROTATIONAL TEMPERATURE PLOT FOR CN ($X^2\Sigma^+$) V″=0

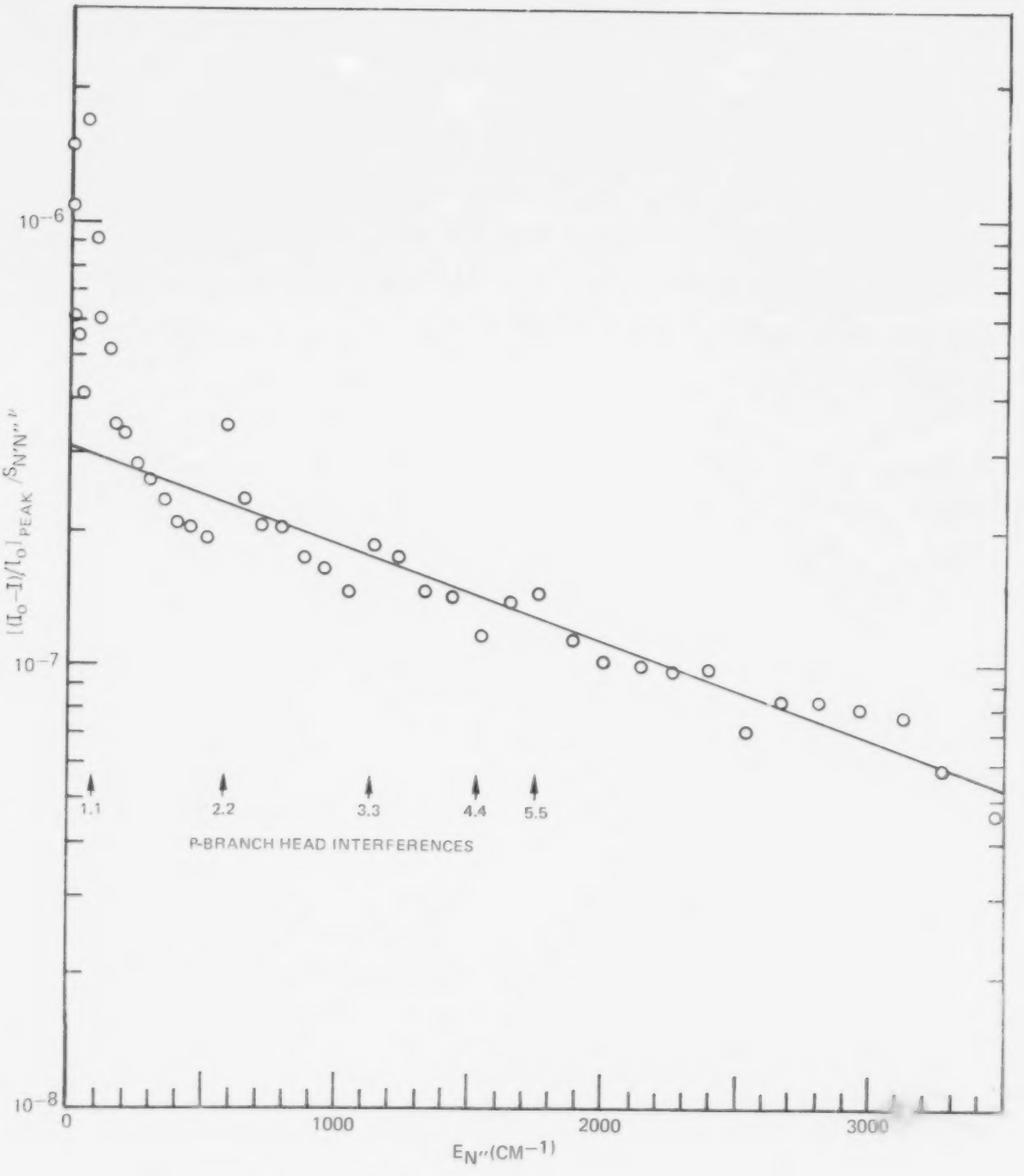

78-02-165-4

$$\delta_{0,\Lambda'} = 1 \text{ if } \Lambda' = 0$$
$$= 0 \text{ if } \Lambda' \neq 0. \tag{10}$$

T_n, G_v and F_J are the electronic, vibrational and rotational term values. For the temperatures of interest here $hcT_n/kT \gg 1$ and

$$Q_e \approx (2-\delta_{0,\Lambda})(2S'+1). \tag{11}$$

Combining these equations the integrated absorption for a single line is given by

$$\int_{\text{line}} k_\nu d_\nu = (8\pi\nu^2 c)^{-1} \frac{g_{n'}}{g_{n''}} A_{n'n''} A_{v'v''} \frac{S_{J'J''}}{2J''+1} \frac{N}{Q_v} \frac{hcB}{kT} \tag{12}$$
$$\cdot \exp\left[-(T_n + G_v - F_J)\, hc/kT\right]$$

When the absorption is small and the probe radiation bandwidth is greater than the absorption line, the integrated absorption is related to the measured intensities by

$$\int k_\nu d_\nu = \left(\frac{I_o - I}{I_o}\right)_{\text{peak}} \frac{\Delta\nu}{\ell} \tag{13}$$

where $\Delta\nu$ is the spectral slitwidth (cm^{-1}) and ℓ is the absorbing path length. The measured absorption depends on the resolution. The resolution in the present investigations is moderate. Observations were made in first order with slits approximately 20 μm. The resolution determined from pairs of just resolved lines in the CH spectrum is 2.1 ± 0.3 cm^{-1}. This resolution is not sufficient to resolve the spin split components of either radical. Since Equation (13) applies to a single transition the data reduction must be suitably modified.

The integrated absorption for two spin components, R_1 and R_2 of CH, for example, is

$$\int_{R_1+R_2} k_\nu d_\nu = (8\pi\nu^2 c)^{-1} \frac{g_{n'}}{g_{n''}} A_{n'n''} A_{v'v''} \frac{(S^{R_1}_{J'J''} + S^{R_2}_{J'J''})}{(2S'' + 1)} \frac{N}{Q_v} \frac{hcB}{kT} \tag{14}$$
$$\cdot \exp\left[-(T_n + G_v + F_J)\, hc/kT\right]$$

If the two lines were exactly coincident, the measured absorption would be given by

$$\left(\frac{I_o-I}{I_o}\right)_{peak} = \frac{\ell}{\Delta\nu}\int_{R_1+R_2} k_\nu d_\nu \qquad (15)$$

The data has been analyzed in this manner to account for the moderate resolution. For CH $(2S''+1) = 2$, therefore, $(S^{R_1}_{J'J''} + S^{R_2}_{J'J''})/(2S''+1) = \bar{S}_{J'J''}$.

Equations (14) and (15) can be solved for the radical number density

$$N = \left(\frac{I_o-I}{I_o}\right)_{peak} \frac{\Delta\nu}{\ell} \frac{8\pi\nu^2 c}{A_{n'n''}A_{v'v''}} \frac{1}{\bar{S}_{J'J''}} \frac{Q_v kT}{kcB} \cdot \exp\left[(T_n + G_v + F_J)\, hc/kT\right] \qquad (16)$$

The data for the (0,0) transition with the lower state being the electronic ground state has been analyzed for CH ($A^2\Delta \rightarrow X^2\Pi$) and CN ($B^2\Sigma^+ \rightarrow X^2\Sigma^+$), therefore, $T_n = G_v = 0$ and equation (16) reduces to

$$N = \left(\frac{I_o-I}{I_o}\right) \frac{\Delta\nu}{\ell} \frac{1}{\bar{S}_{J'J''}} C' \frac{Q_v kT}{hcB} \exp\left[F_J hc/kT\right]. \qquad (17)$$

where $C' = 8\pi\nu^2 c(A_{n'n''}A_{v'v''})$. Therefore, except for the ν factor the radical density is given by the intercept of the rotational temperature plot.

The data obtained here and the constant C' are summarized in Table I. The uncertainties arising from several possible sources have been estimated. The largest source of uncertainty is associated with data scatter which is typically ± 30 percent. The spectral bandwidth is undertain to approximately ± 15 percent. As discussed previously, the uncertainty in assigning the optical path length may be considerable. Although the visible extent of the flame is measurable to ± 5 percent, the actual optical path accounting for the extent of the radical species in the flame and the finite probe beam aperture is impossible to reliably assess. As pointed out before, however, the actual optical path depth is only likely to be less than the physical flame dimension taken here. Therefore, the radical densities determined from the absorption studies must be interpreted as minimum values.

The uncertainties assigned in Table I don't include uncertainties in the constant C', which would be principally due to errors in the radiative lifetime measurement. Historically the lifetime values have changed 33 percent, however, the current uncertainties in this number are not likely to be so high. The uncertainties assigned in Table I also don't include the uncertainty due to beam steering effects. It is estimated from the shift in the baseline of the xenon lamp intensity with the flame on and off that the maximum beam steering effect is to reduce the measured radical density 15 percent for CN and 25 percent for CH.

TABLE I

Summary of Absorption Data

Species	Intercept	Temp (°K)	C' (cm^{-1})	N (cm^{-3})
CH	$(6.3\pm1.2) \times 10^{-3}$	2600	5.08×10^{16}	$(1.6\pm0.5) \times 10^{14}$
CN	$(3\pm0.5) \times 10^{-7}$	2800±200	3.39×10^{13}	$(3.8\pm1.0) \times 10^{14}$

For CH the electronic transition probability has been taken from Hesser and Lutz (Ref. 16) who found a radiative lifetime of 470 ns. The Franck-Condon factor (=0.993) was taken from Liszt and Smith (Refs. 17). Transition frequencies from the Moore and Broida (Ref. 18) compilation were used.

For CN the electronic transition probability was taken from Luk and Bersohn (Ref. 19), who found the radiative lifetime to be 60.8 nsec. The Franck-Condon factor computed by Nicholls (Ref. 20) ($A_{vv} = .909$) was used. Transition frequencies were taken from Jevons (Ref. 21) or computed from spectroscopic constants found in Suchard (Ref. 22) using formulae from Jevons (Ref. 23).

The results shown in Table I for CH correspond to $57 \begin{smallmatrix} + 18 \\ - 23 \end{smallmatrix}$ ppm which includes the uncertainty due to beam steering. This result agrees quite well with other investigators. Bulewicz et. al. (Ref. 13) measured 47 ppm and a rotational temperature of 2250°K. Bleekrode determined the radical concentration to be 46 ppm and $T_R = 2200°K$. These measurements used higher spectral resolution than the present

study and low pressure multipath optics. Both these measurements used earlier radiative lifetime measurements (Ref. 24) corresponding to 560 nsec. Using the more recent data used in the present study would decrease the previously measured radical concentrations by 16 percent.

The results shown in Table I for CN correspond to $150 \begin{smallmatrix} + 39 \\ - 45 \end{smallmatrix}$ ppm. Again beam steering is reflected in the uncertainty but the finite aperture effect is not taken into account.

There is no previous data with which to directly compare the CN data. Bulewicz et. al. (Ref. 14) used different reactants. Her results correspond to 30 ppm and 2000°K. Again slightly different constants were used. The only known data for the flame used here is in Gaydon (Ref. 25). There he reports that Gaydon and Wolfhard measured the effective rotational temperatures of NH in emission in several compositions of a C_2H_2/N_2O flame. They found T_R = 3100-3800°K depending on the stoichiometry.

Fluorescence Measurements

Flame and Fluorescence Spectra

The flame spectra of both CH and CN were observed first without the presence of the exciting laser radiation. Recording these spectra was important since this served as a guide in selecting the particular transition to excite with the laser and, equally important, the wavelength at which to observe the emitted fluorescence. In this regard, it is important to point out that the measurements reported here are not resonance fluorescence measurements. The wavelength of the exciting laser radiation did not coincide with the fluorescence wavelength. This was done deliberately in order to preclude the potential interference of flame particulate Mie scattering and Rayleigh scattering with fluorescence, which may occur when the laser and fluorescence wavelengths coincide. Flame spectra of both CH and CN are presented in Figs. 10 and 11, respectively, There are several distinct differences to be noted. In the case of CH, the (0,0) band is relatively well displaced from other vibrational bands of the $A^2\Delta \rightarrow X^2\Pi$ spectrum; accordingly, it is the only band

FIG. 10

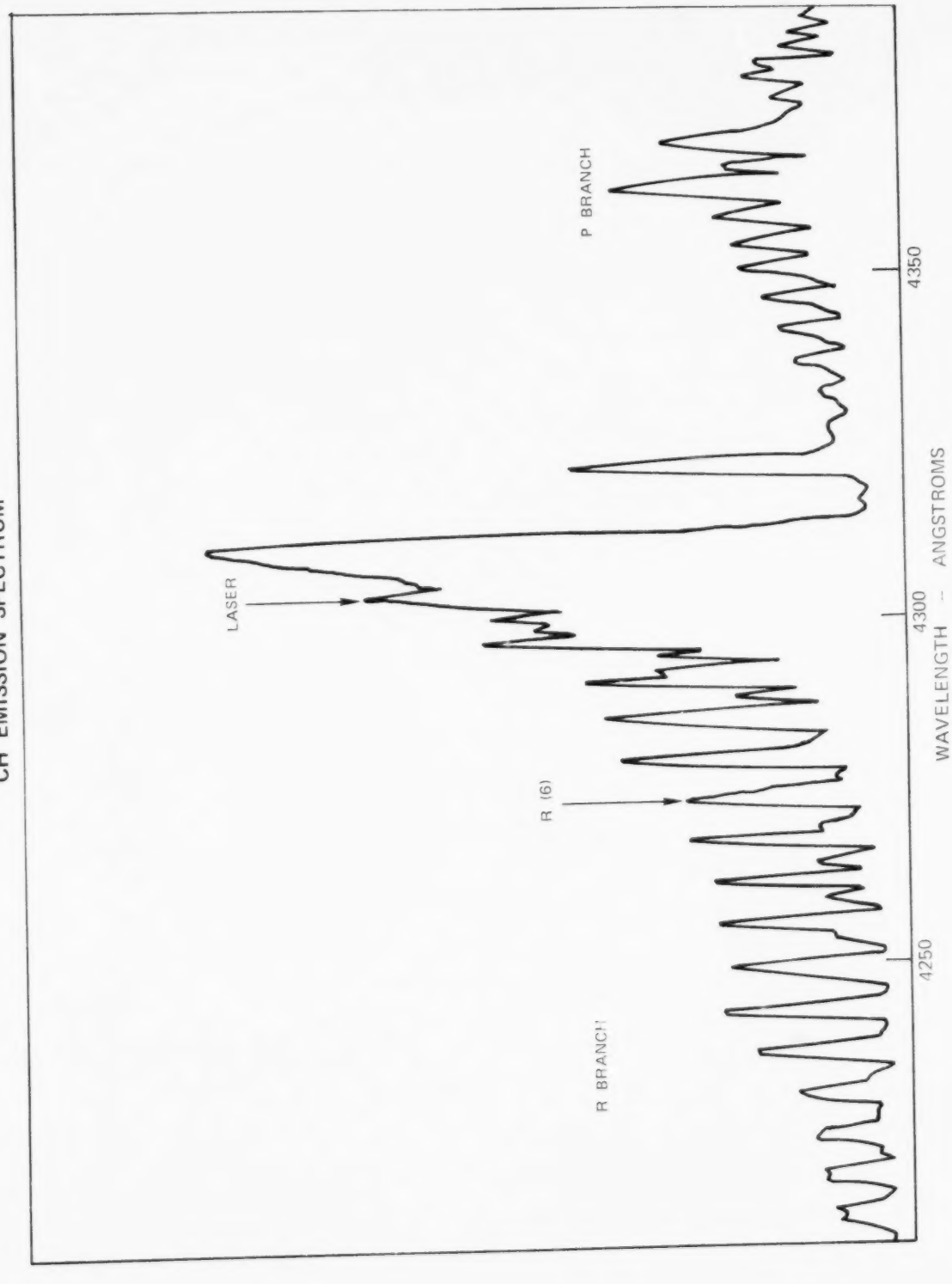

77-12-56-2

FIG. 11

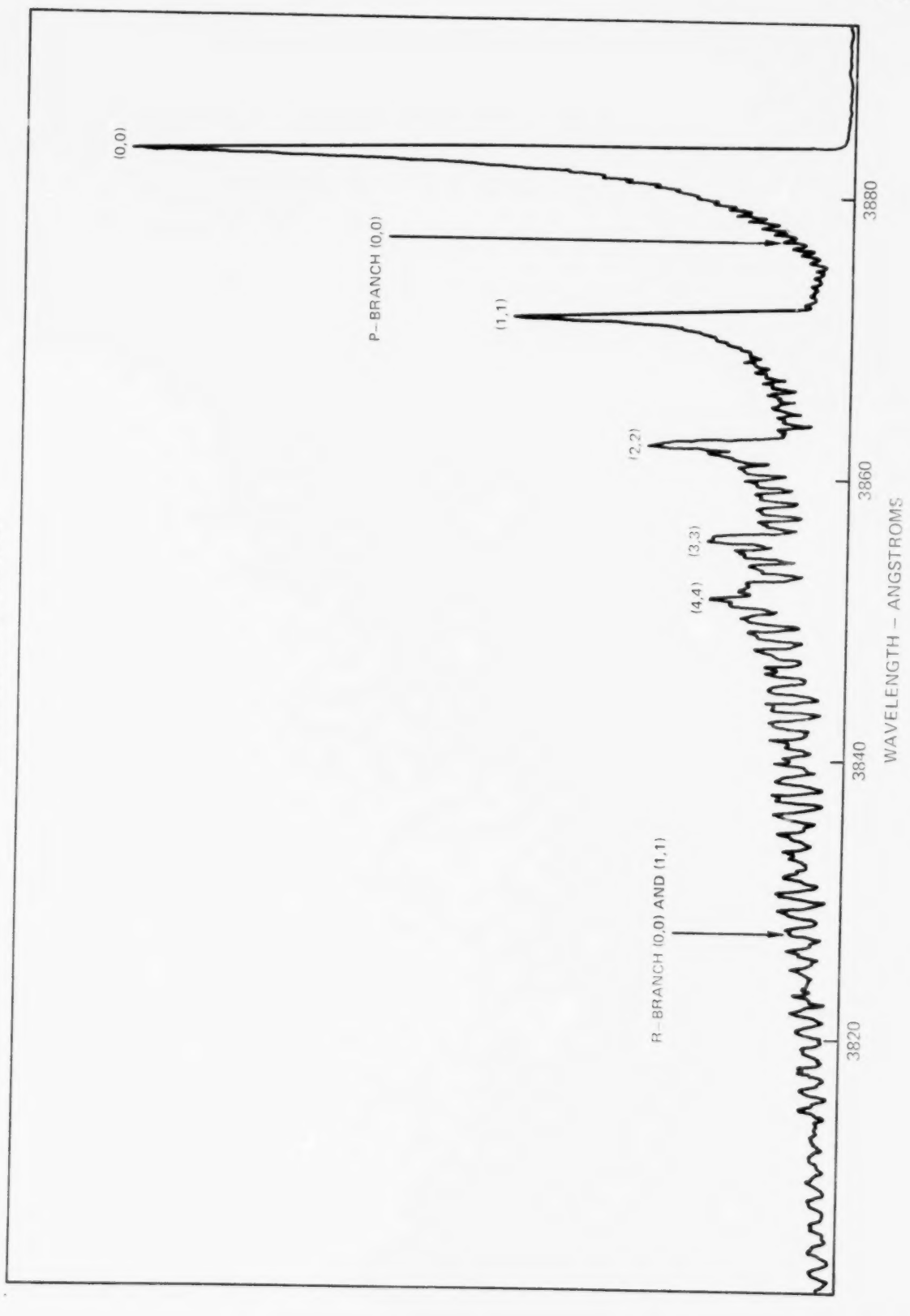

78-02-130-2

shown in Fig. 10. In the case of CN there is a clustering of the bands (0,0), (1,1), (2,2), etc., within a relatively narrow wavelength region with considerable overlap among them. In both cases, the (0,0) band is of prime interest. The presence of other bands complicates the identification of individual rotational lines in the (0,0) band. This identification is important since it is necessary to know precisely which transition (or transitions) the laser excites in order to determine the total number density of ground state molecules. A second difference between CH and CN, which is evident, is that the rotational structure in the case of CN is not resolved, whereas it is for CH. This occurs since the rotational constant of CN is about a factor of seven smaller than it is for CH. The significance of this difference is that it is easier to excite more than a single rotational line in the CN case than it is for CH. This latter possibility depends, of course, on the relation between the spectral width of the laser and the spacing between individual rotational lines.

The laser spectral widths corresponding to both the CH and CN measurements as measured with the OMA are given in Fig. 12. As seen the laser spectral width in both cases is about 2Å. Representative traces of the laser and fluorescence pulses are given in Fig. 13. The pulse lengths are both about 200 nsec. This temporal similarity indicates that the quenched lifetime of the fluorescence is at least as short as the duration of the laser pulse. Since the R-branch rotational lines in CH are separated by about 10Å near 4273Å, the laser excites a single rotational line. For CH, the line is split by both lambda and spin doubling. These splittings, however, are much smaller in magnitude than the spectral width of the laser pulse; in effect then, one excites all the molecules which correspond to the given state of rotation.

Laser-excited fluorescence data for CH are shown in Fig. 14. These data were taken with the oxy-acetylene welding torch. Each data point in Fig. 14 corresponds to a single laser shot. The laser was tuned to 4273Å since, at this wavelength, R-branch spectra are resolved, resulting in the excitation of a single rotational line, and equally important, at 4273Å the laser energy was near maximum. Fluorescence

FIG. 12

OMA MEASUREMENT OF DYE LASER SPECTRAL OUTPUT

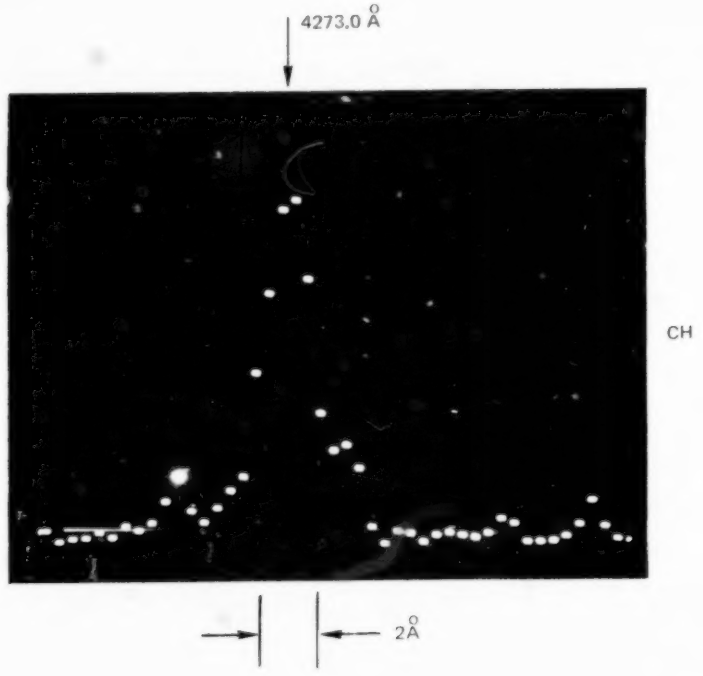

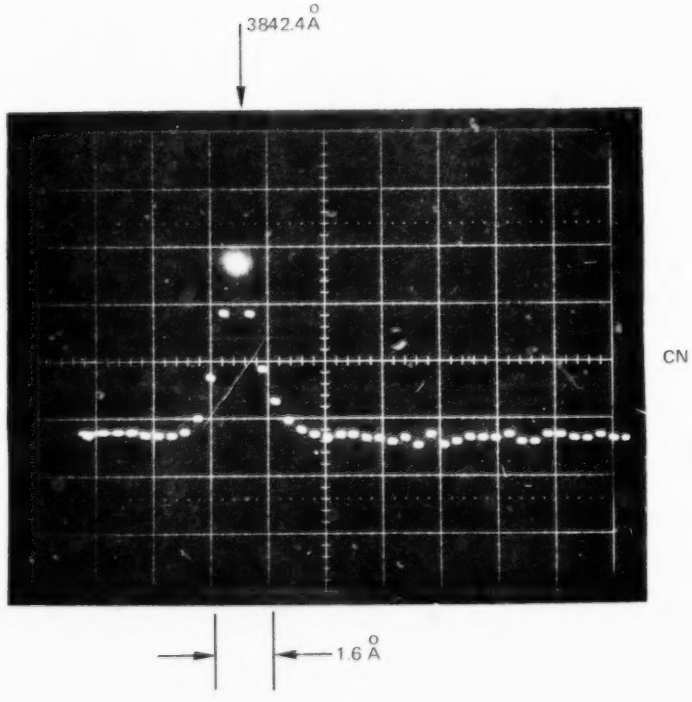

78-02-130-6

FIG. 13

LASER AND CH FLUORESCENCE PULSES

$\lambda_L \simeq 4273\mathring{A}$

$\lambda_F \simeq 4315\mathring{A}$

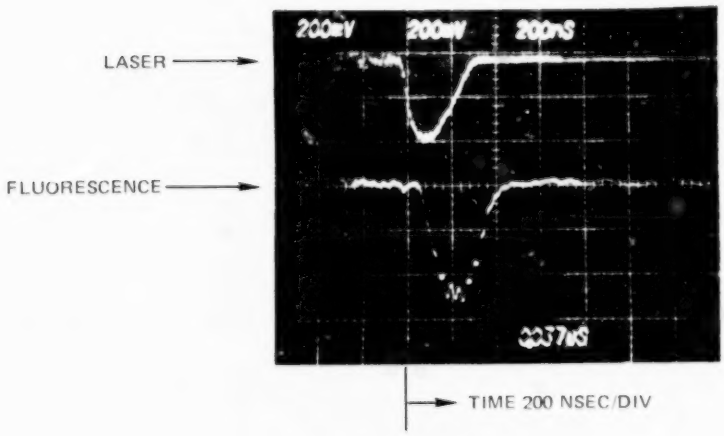

78-02-130-5

LASER EXCITED CH FLAME FLUORESCENCE

$$\lambda_{EXC} \cong 4273\ \text{Å}\left[{}^2\Pi\,(V=0) \longrightarrow {}^2\Delta\,(V=0)\right]$$

$$\lambda_{OBS} \cong 4315\ \text{Å}$$

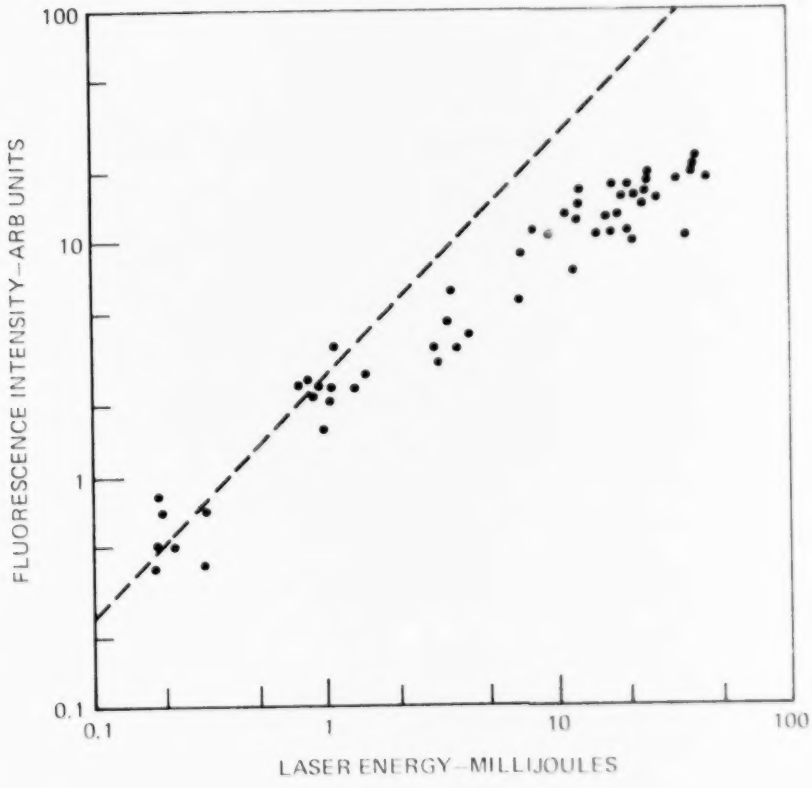

78-02-36-3

was observed at 4315Å since this wavelength was sufficiently removed from 4273Å in order to preclude Mie and Rayleigh scattering interferences, and the overlap of Q-branch lines near 4315Å enhanced the fluorescence intensity. The dependence of the fluorescence on laser energy clearly departs from linearity in Fig. 14 and indicates the onset of saturation. This makes it possible to determine the CH concentration without prior knowledge of quenching. This is the first demonstration of saturated CH fluorescence.

Data for laser excited anti-Stokes CH flame fluorescence are given in Fig. 15. Again, the fluorescence departure from linearity is apparent. In this case, the laser wavelength occurs in a region of the CH spectrum where there are many overlapping, predominantly Q-branch lines. This makes it more difficult to know the fractional population excited by the laser, but is not a limiting factor in principle. For the present, only the more straightforward Stokes-type data in Fig. 14 are used.

Data for CN are given in Fig. 16. Much of the commentary given for CH above applies to CN as well. The observation of saturation for CN, as for CH, has not been reported previously. A photograph of the OMA spectral width measurement of the laser pulse used to excite the CN spectra is given in Fig. 12. Since the rotational spacing near the 3842.2Å laser wavelength is of order 1Å and the laser spectral width was 2Å, it was not possible to excite a single CN rotational line, whereas this presented no difficulty in the case of CH.

Calibration Measurements

For species determination, it is necessary to know the absolute magnitude of the fluorescence power. Accordingly, calibration of the photomultiplier which records the fluorescence signals is required. The light source used to calibrate the RCA 8575B photomultiplier was a heated tungsten filament. The brightness temperature of this filament was measured with an optical pyrometer. Since the emissivity of the filament was known, the true temperature was calculated from the emissivity and the measured brightness temperature. By using an optical filter at

FIG. 15

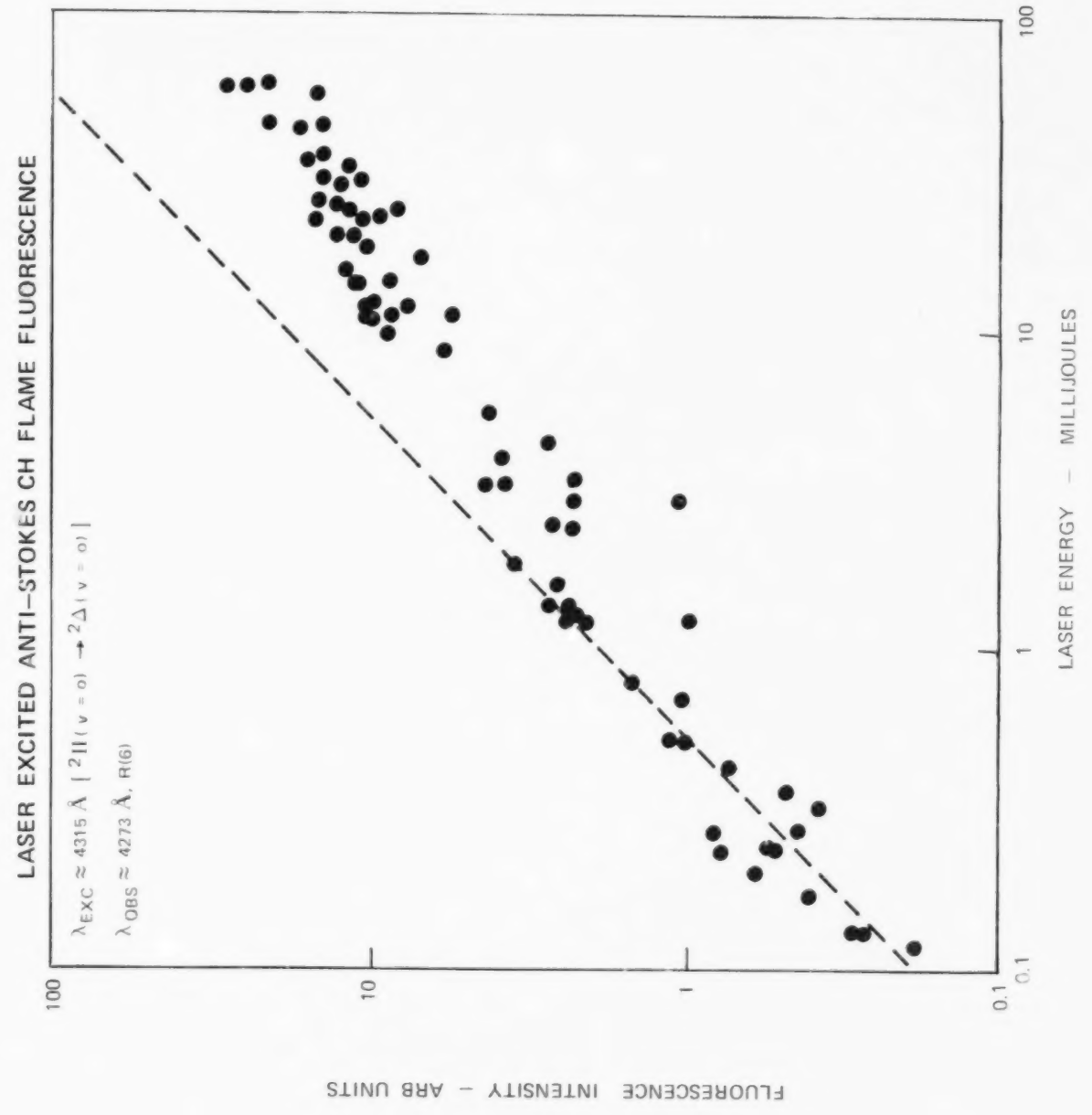

77-12-56-1

FIG. 16

LASER EXCITED CN FLAME FLUORESCENCE

$\lambda_{exc} \simeq 3842$ Å $[X^2\Sigma\ (v = 0) \rightarrow B^2\Sigma\ (v = 0)]$

$\lambda_{obs} \simeq 3880$ Å

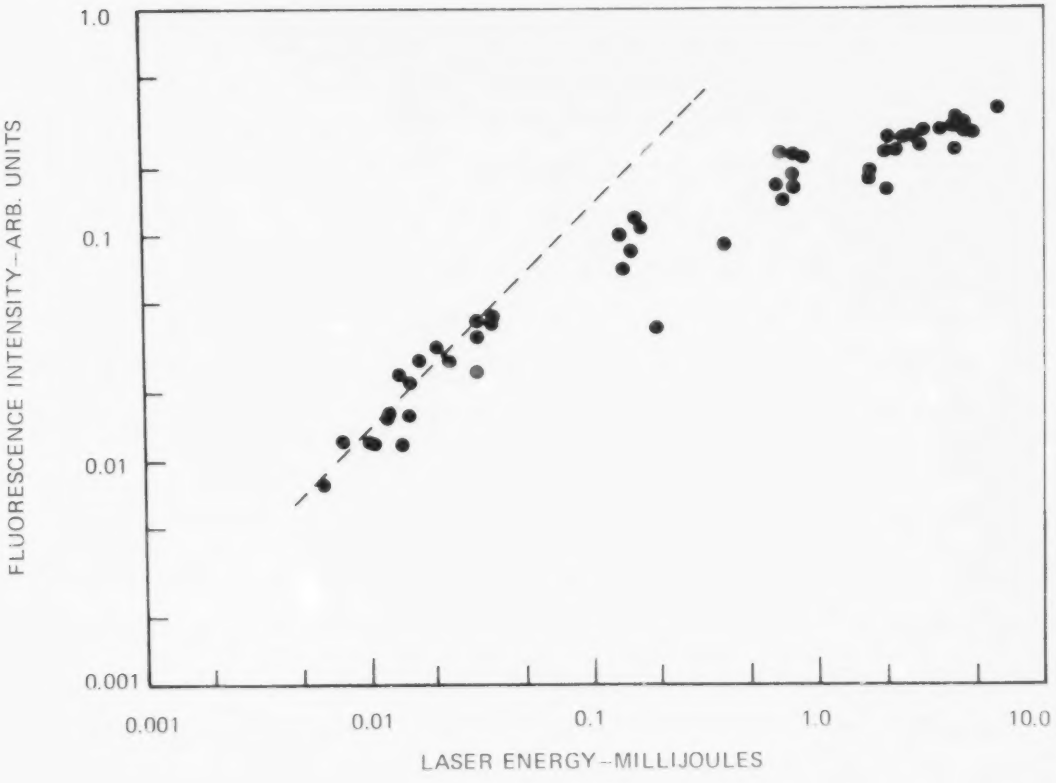

78-05-51-1

4335Å center wavelength and 100Å bandwidth positioned between the filament and photomultiplier, the calibration was made at the CH wavelength. In addition to the optical filter for center wavelength and bandwidth definition, two spatially separated pinholes were used in order to define the solid angle and filament area for which the radiated power was observed. From Planck's formula for blackbody radiation and accounting for the emissivity of the filament, the radiated power striking the photomultiplier was computed and compared with the photomultiplier output voltage. The tube calibration was performed only for the CH spectral region. A separate calibration was not performed for CN since there is only a slight difference in the sensitivity of the photomultiplier at the CH and CN wavelengths of 4315 and 3880Å, respectively.

The laser-induced fluorescence power is proportional to $\Omega V\epsilon$, where: Ω is the light collection solid angle; V is the sample volume size, and equal to the product of sample length, ℓ, and laser beam cross sectional area A; ϵ is the spectrometer efficiency. The product $\Omega_A \ell\epsilon$ is required in order to evaluate the concentration from fluorescence power. A useful means to this end involves observation of Rayleigh scattered light for the purpose of determining the product $\Omega\ell\epsilon$, and an independent measurement of laser beam area, A. The Rayleigh scattering is governed by

$$Q_r = Q_i \; n\left(\frac{\partial\sigma}{\partial\Omega}\right)(\Omega\ell\epsilon), \tag{18}$$

where Q_r is the scattered Rayleigh intensity; Q_i, the intensity of the incident laser pulse; n, the number density of Rayleigh scatters; and $\frac{\partial\sigma}{\partial\Omega}$, the Rayleigh differential scattering cross-section. The Rayleigh scattering is observed from room air. For this case, both n and $\frac{\partial\sigma}{\partial\Omega}$ are known. By measuring both Q_r and Q_i, where use is made of the results of the photomultiplier calibration in order to evaluate Q_r, it is possible to evaluate $(\Omega\ell\epsilon)$ from Eq. (18). Rayleigh data were taken at laser wavelengths corresponding to both CH and CN excitation. In the case of CH, the Rayleigh signal exceeded the maximum fluorescence signal by a factor of almost seven. On the other hand, for CN the Rayleigh signal was about half of the

fluorescence signal. A substantial part of this difference is due to the fact that fluorescence power is proportional to the Einstein coefficient, A_{21}, as in Eqs. (2, 3 and 4). A_{21} for CN exceeds that for CH by about a factor of ten, whereas the Rayleigh signal is about the same at the CH and CN wavelengths.

The area of the focused laser beam, A, which is required for the fluorescence measurements, was determined by measuring the laser energy through a series of apertures of well known size. The diameter of the beam was taken as equal to that particular aperture which passed 80 percent of the laser energy incident upon it. The minimum attainable laser spot size at the CH wavelength was about 1 mm diameter. The spot size actually used for the CH measurements was 2.5 mm diameter. For high laser spectral intensity and saturation, minimum spot size is desired. On the other hand, since fluorescence power is proportional to laser beam area, small spot size is not desirable from this point of view. The spot size chosen for the measurements represents a compromise between these two considerations.

As part of the required calibration measurements, it is necessary to determine what fraction of the emitted fluorescence is measured by the spectrometer. The spectrometer has a linear dispersion of 16Å/mm. Since the slitwidth for all fluorescence measurements was 0.4 mm, the spectrometer bandwidth was of order 6Å. On the other hand, the fluorescence is expected to be emitted over a much broader bandwidth since rapid rotational equilibration occurs in the excited state prior to fluorescence. In order to determine the fluorescence bandwidth for CH, the laser was set to operate at 4290Å and the fluorescence was measured as a function of wavelength by tuning the spectrometer. These results are given in Fig. 17. By comparison of Fig. 17 with Fig. 10, it is clear that the laser-induced fluorescence spectrum approximates the flame spectrum. The exception is, of course, the Rayleigh signal present in Fig. 10. Because of the foregoing similarity and the extreme difficulty of taking data pulse by pulse as in Fig. 17 with the Phase-R laser, the bandwidth factor or fraction of the total fluorescence actually observed, was determined in the case of both CH and CN by referring to flame spectra.

FIG. 17

LASER EXCITED CH FLUORESCENCE SPECTRUM

$\lambda_{EXC} \simeq 4290$ Å

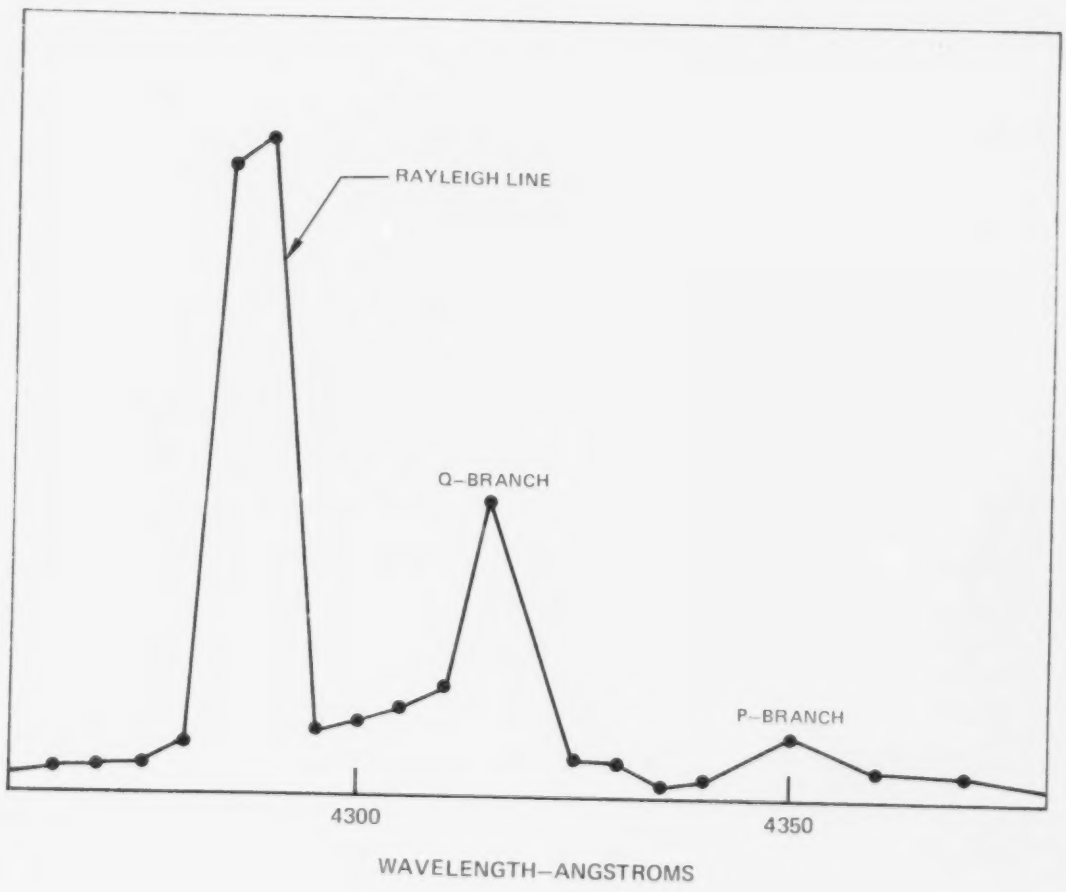

78-02-172-1

Experimental Results

Data Analysis Procedure

In order to evaluate species concentration from the measured fluorescence power, a procedure is used which was first described by Baronavski and McDonald (Ref. 5). This procedure is applicable in the important, practical situation where it is possible to saturate a transition only partially. For a two level system, the fluorescence power in exact form is given by

$$S_F = (hc/\lambda_F)(A_{21}/4\pi)\Omega_c V_c N_1 B_{12} \epsilon \nu \left[\frac{Q_{21} + A_{21}}{I_{L\nu}} + (B_{12} + B_{21}) \right]^{-1}, \qquad (19)$$

where the spectrometer efficiency and bandwidth factors ϵ and ν, respectively, have been included. Appropriate to conditions of near saturation where $(I_{L\nu})^{-1}$ is small, S_F is developed in a Taylor series expansion about $(I_{L\nu})^{-1}=0$. The two leading terms in this expansion are

$$S_F \approx (hc/\lambda_F)(A_{21}/4\pi)\Omega_c V_c \epsilon \nu \left[N_1 - \frac{N_1(Q_{21} + A_{21})}{(B_{21} + B_{12})I_{L\nu}} \right] \qquad (20)$$

In order that this approximate expression for S_F be valid, it is necessary that the coefficient of $(I_{L\nu})^{-1}$ be less than unity, i.e., $(Q_{21}+A_{21})/(B_{21}+B_{12}) < 1$. This means physically that the combined quenching and radiative decay rates may not exceed those associated with stimulated emission and absorption of radiation. It is evident from Eq. (20) that S_F has a linear dependence on $(I_{L\nu})^{-1}$. In a plot of S_F versus $(I_{L\nu})^{-1}$, the intercept on the S_F axis gives N_1, and the negative slope of this straight line is proportional to $(Q_{21}N_1)$ permitting separate determination of both N_1 and Q_{21}. Aside from the fundamental constants h and c and the fluorescence wavelength λ_F, it is necessary to know A_{21} and the product $(\Omega_c V_c)$ in order to evaluate N_1 by the intercept method. The value for A_{21} is taken from the literature values; it may not be determined by the techniques described in this work. The quantity $(\Omega_c V_c)$ follows from apparatus calibration via Rayleigh scattering of light and from laser beam cross-sectional area determination via insertion of calibrated

apertures. The presence of the term $(B_{21} + B_{12})$ in Eq. (20) causes no additional uncertainty. This term may be written in the form

$$(B_{21} + B_{12}) = B_{12}\left(1 + \frac{B_{21}}{B_{12}}\right) = \left(1 + \frac{g_1}{g_2}\right) \tag{21}$$

where g_1 and g_2 are the degeneracies of levels 1 and 2. Since $B_{12} = (\lambda^3/8\pi hc)A_{21}$, it follows that

$$(B_{21} + B_{12}) = (\lambda^3/8\pi hc)A_{21}\left(1 + \frac{g_1}{g_2}\right) \tag{22}$$

Accordingly, the term involving stimulated rates has been expressed in terms of a radiative rate and level degeneracies.

The concentration N_1 in Eq. (20) is the population of the particular rotational level excited by the laser and not the total species concentration. It is related to the total species concentration, N, by appropriate Boltzmann factors. Boltzmann factors applicable to CH and CN are those which account for both lambda and spin doubling in the case of CH and spin doubling alone for CN. Spin doubling occurs since the ground states of CH and CN, as given in Fig. 1, are $^2\Pi$ and $^2\Sigma$, respectively, where in both cases $2S' + 1 = 2$ or $S' = 1/2$. Lambda doubling is present for the CH Π-state but it does not occur for the CN Σ-state. The most general Boltzmann factor, applicable to a molecule with both lambda and spin doubling is given in Eq. (7). An approximate expression for the total partition function, Q, in Eq. (8) is given by

$$Q \approx (2-\delta_{0,\Lambda})(2S'+1)(kT/hcB_r)(1-e^{-hc\omega/kT}). \tag{23}$$

If Eq. (23) is substituted in Eq. (7), the fractional, Boltzmann population, with insertion of appropriate expressions for G_v and F_J, is given by

$$\frac{N_{v,J}}{N} = \frac{(hcB_r/kT)(2J+1)}{(2S'+1)}\,(1-e^{-hc\omega/kT})\,e^{-J(J+1)hcB_r/kT} \tag{24}$$

This is the fractional population in each of the two spin doublet states appropriate to a given state of rotation, J. Since the factor $(2-\delta_{0,\Lambda})$ factors out of the final expression, Eq. (24) is appropriate for the analysis of both CH and CN.

Calculation of Concentration and Quenching

In order to explain the procedure used to evaluate N_1 and Q, a representative example is treated in detail. The example chosen is appropriate to CH measurement with the oxy-acetylene welding torch for which saturated fluorescence data are given in Fig. 14. In order to apply the Baronavski-McDonald procedure (Ref. 5) it is necessary to plot the inverse of the laser energy versus the fluorescence intensity. This is done for only those laser energies which correspond to near saturation. Such a plot is given for CH in Fig. 18 and for CN in Fig. 19. The results in Fig. 19 were obtained from the data given in Fig. 16 for CN. In Fig. 18, the least mean squares fit to the data results in a straight line with a negative slope as would be expected from Eq. (20). The slope and intercept in Fig. 18 are required in order to compute N_1 and Q. In order to evaluate the species concentration, N, Eq. (24) is required. Table II lists the numerical values of the quantities required to calculate N_1, N and Q from Eqs. (20) and (24). The parameters $\Delta\nu$, τ and E_L are related to the laser spectral intensity by $I_{L\nu} = (E_L/\tau)/A\Delta\nu$. Results for N_1, N and Q for both types of burners and for both CH and CN are summarized in Table III. There are no essential differences between the calculational procedures for CH and CN.

Discussion

The fluorescence results given in Table III for species concentration from slot-burner measurements may be compared directly with the corresponding values determined from absorption. The concentrations measured by absorption exceed those from fluorescence by about a factor of two for CH and four for CN. Although the precision of the absorption results is quite good, it is not possible to assign similar, small uncertainties to the fluorescence results. The principal sources contributing to the uncertainty in concentration determined from fluorescence are as follows. The calibration factor (Ω/ε), is determined with an uncertainty of 25-50 percent. This is due to a lack of reproducibility in the Rayleigh scattering energy for a given laser pulse energy. The explanation for this lack of reproducibility may be related

CH CONCENTRATION DATA REDUCTION

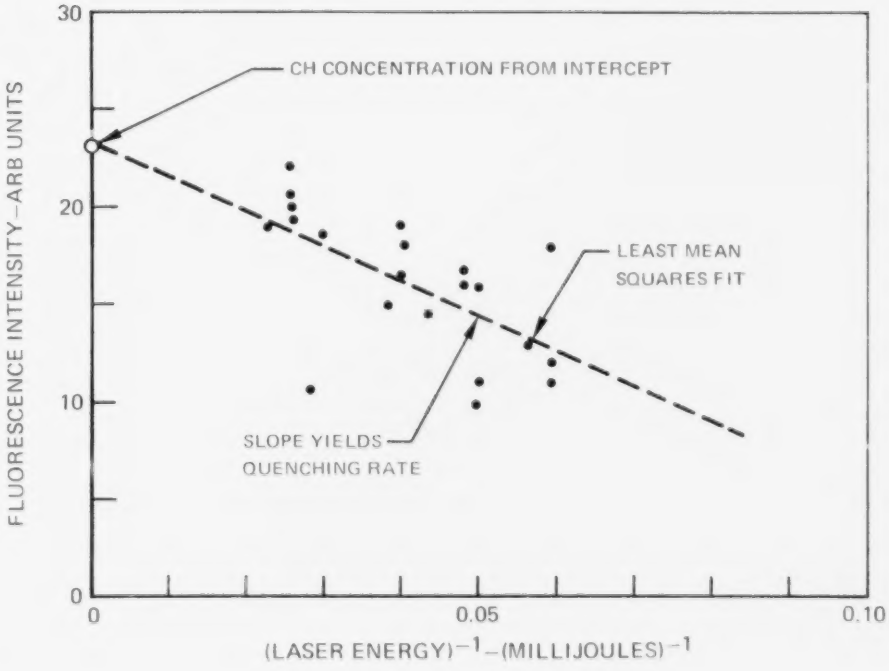

78-02-36-4

FIG. 19

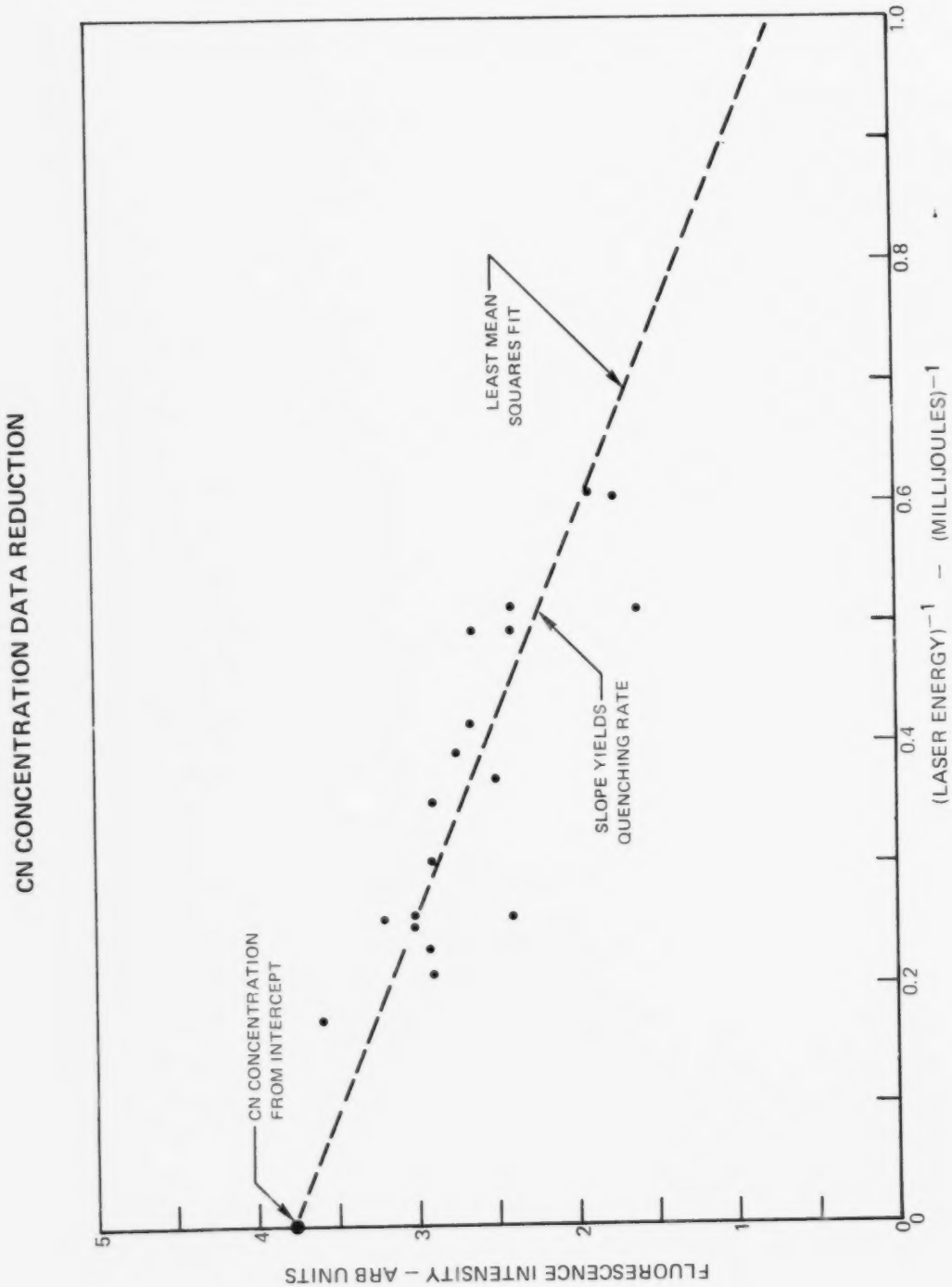

78-02-130-3

TABLE II

Numerical Values Used in Sample Calculation of N_1, N and Q for CH

S_F,	extrapolated fluorescence power (Fig. 18 intercept)	1.37×10^{-8} Watts
λ_F,	fluorescence wavelength	4315Å
A_{21},	spontaneous decay rate	1.97×10^{6} sec^{-1}
A,	laser beam area	4.9×10^{-2} cm^2
ν,	bandwidth factor	0.14
$(\Omega l \epsilon)$,	calibration factor (from Rayleigh data)	2.3×10^{-5}
g_1,	degeneracy of lower level	13
g_2,	degeneracy of upper level	15
$\Delta\nu$,	laser spectral width	10.74 cm^{-1}
τ,	laser pulse length	280×10^{-9} sec
E_L,	laser energy at saturation	50 mJ
T,	rotational temperature (from Table I)	2600°K
B_r,	rotational constant	14.457 cm^{-1}
ω,	vibrational constant	2862 cm^{-1}

TABLE III

Summary of Results of Fluorescence Measurements for CH and CN

	N_1 (cm^{-3})	N (cm^{-3})	Q (sec^{-1})
CH (welding torch)	2.4×10^{12}	4.0×10^{13}	1×10^{9}
CH (slot burner)	4.2×10^{12}	7.1×10^{13}	3×10^{9}
CN (slot burner)	1.2×10^{12}	8.1×10^{13}	2×10^{9}

to laser mode switching from pulse to pulse which results in a varying laser intensity at the Rayleigh focal volume. Since the calibrations were performed in room air, there may also be a varying Mie contribution from dust particles. With improved experimental procedures, this uncertainty can be substantially reduced. The beam quality of the flashlamp-pumped dye laser is relatively poor; it is undoubtedly not Gaussian and, indeed, its intensity distribution is unknown and, most likely, varies from pulse to pulse. This introduces an uncertainty in the measurement of the focused beam diameter. Indeed even in the case of a Gaussian beam, Daily (Ref. 26) has shown recently, for example, that the absence of a constant intensity distribution across the focal volume leads to anomalous apparent saturation intensities. It is estimated that the uncertainty in beam cross-sectional area could be as high as 50 percent, which implies a 25 percent uncertainty in beam diameter. As mentioned above, it was very difficult to determine the spectral distribution of laser excited fluorescence for both CH and CN since it was not possible in practice to repetitively pulse the dye laser for the dye/solvent combinations which were used. For CN, the bandwidth factor, v, was estimated from CN flame emission; however, because of the band overlaps in Fig. 11, this was an imprecise procedure. Accordingly, the uncertainty in v for CH is of order 25 percent and for CN of order 50 percent. If the above uncertainties are added to those associated with photomultiplier calibration, selection of an appropriate value of A_{21}, and determination of extrapolated fluorescence power from curves such as are given in Figs. 18 and 19, one concludes that there is a factor of 2 uncertainty in the fluorescence results for CH with the CN results being less certain by a factor of about 3. These uncertainties can go either way and in summary then, it appears that there is a definite discrepancy between the absorption and fluorescence results.

There is one very plausible explanation for the concentrations measured by fluorescence to be lower than those from absorption. The fluorescence power is proportional to sample volume size. In this work the sample volume is taken as the product of laser beam cross-sectional area and spectrometer slit width. The laser beam is focused to near its minimum spot size which is comparable to the radial

flame dimension. If there is a concentration gradient across this dimension, which is likely in these small, high pressure flames, the sample volume size is in effect overestimated which leads to an underestimate of the concentration. There is no information available regarding these gradients. However, CH flame emission data for the welding torch taken with a narrow 10-20 micron spectrometer slit width indicated a very pronounced dependence of the emission intensity with only slight horizontal displacements of the burner. This suggests that such concentration gradients are indeed present, and these may well be the root of the present discrepancy.

Clearly, for accurate saturated fluorescence measurements, the measurement focal volume should be considerably smaller than the characteristic spatial gradient scale. However, since the fluorescence signal level is proportional to the sample volume size, detection considerations may limit the gradient scale to which saturated laser fluorescence is applicable. In the experiments reported here, the laser focal diameter was limited by the poor beam quality of the flashlamp-pumped dye laser. With laser pumped dye lasers the quality is substantially better permitting finer scale probing. Within beam quality and signal detection limitations, an alternative for fundamental studies of fluorescence involves the use of burners with small gradients, e.g. a flat flame at reduced pressure.

In the fluorescence section of the Task I technical report (Ref. 1) estimates were made of the laser spectral intensities required for saturation of CH in Table XVII and the detection limits for species measurements were given in Table XX. It is of interest here to compare these latter estimates with results actually obtained in this work. For the CH welding torch measurements reported herein, the number of measured photons, based upon the photomultiplier tube calibrations, is calculated to be 8.3×10^3. When the number of photons calculated in Table XX is adjusted for the concentration and calibration factors, 4.5×10^3 photons are predicted. It is quite gratifying that this agrees with the above measured number within a factor of two. The laser spectral intensity required to saturate CH in this work was $I_{L\nu} = 3.4 \times 10^5$ Watts/cm^{2}cm^{-1}. This is about two orders-of-magnitude

smaller than the value 4×10^7 Watts/cm^2 cm^{-1} given in Table XVII of Ref. 1. This difference may be explained by the fact that the quenching rate of CH in Ref. 1 was taken as 1×10^{12} sec^{-1}, whereas the measured rate is 3×10^9 sec^{-1}. The smaller, actual quenching rate makes saturation correspondingly easier to achieve. The rate in Ref. 1 for CH was taken as identical with that for the quenching of excited NO γ-band emission by water vapor. This procedure was adopted since no data for CH were available at the time. In retrospect then, this procedure overestimated the laser spectral intensities required to achieve saturation. In the case of CN as well, the laser spectral intensity experimentally required to saturate was 1×10^5 Watts/cm^2 cm^{-1}, again two orders-of-magnitude smaller than that estimated in Table XVII of Ref. 1 due to the measured quenching rate being much smaller than the values assumed earlier.

In brief summary, the CH and CN investigations conducted during the Task II program yielded encouraging results in regard to the feasibility of saturated laser fluorescence for radical determinations in flames. It was found possible to saturate the fluorescence intensity of both CH and CN with readily achieved levels of laser spectral intensity, in the range of 10^5 to 10^6 Watts/cm^2 cm^{-1}. The achievement of partial saturation permitted the determination of the CH and CN concentrations in the flame as well as the excited state quenching rates via the procedure described first by Baronavski and McDonald (Ref. 5). As far as can be ascertained at this time, use of a simple two level model appears to be applicable as well to species measurements of multi-leveled systems, e.g. CN. This is consistent with the findings of Baronavski and McDonald in regard to C_2, which is not a simple two level system either. The fluorescence measurements of these radicals was probably low, based on the comparison with the absorption measurements, due most probably to sharp spatial gradients of the species in the small, high pressure flames examined here. In Section III, the conclusions of the saturated laser fluorescence investigations are discussed and recommendations for future research indicated.

SECTION II

CARS INVESTIGATIONS IN FLAMES

Introduction

Coherent anti-Stokes Raman spectroscopy (CARS) has recently come to prominence for combustion diagnostics based upon the pioneering investigations of Taran and his coworkers (Refs. 27, 28-31) at ONERA in France. The effect was originally discovered in the early sixties by Maker and Terhune (Ref. 32) and remained essentially in the province of nonlinear optics until Taran's application of it for gas phase diagnostics. In the United States, Harvey and his coworkers (Refs. 33-37) have conducted numerous investigations into the technique. Barrett has demonstrated both cw CARS generation (Ref. 38) and pure rotational CARS (Ref. 39). Broadband CARS generation in a single pulse has also been obtained (Ref. 40). All of the experimental work to be reported herein has been broadband or multiplex CARS for reasons to be elaborated upon later. Publications describing investigations into CARS are appearing at an ever increasing rate and the technique apparently will have a major impact in molecular structure and biological studies. Several very good reviews of CARS have appeared recently (Refs. 35, 37, 41).

CARS is probably best understood by reference to Fig. 20. Incident laser beams at frequencies ω_1 and ω_2 (often termed the pump and Stokes beams respectively) interact through the third order nonlinear susceptibility $\chi^{(3)}(-\omega_3, \omega_1, \omega_1, -\omega_2)$ to generate a polarization field which produces coherent radiation at frequency $\omega_3 = 2\omega_1 - \omega_2$. When the frequency difference $\omega_1 - \omega_2$ is close to the frequency of a Raman active resonance, the magnitude of the radiation at ω_3, then at the anti-Stokes frequency relative to ω_1, can become very large. Large enough, for example, that with the experimental arrangement described herein, the CARS signals from room air N_2 are readily visible. The incident beams, however, must be so aligned that the three wave mixing process is properly phased. For gases which are nearly dispersionless, phase-matching occurs when the beams are mixed collinearly, i.e., aligned.

CARS -- COHERENT ANTI–STOKES RAMAN SPECTROSCOPY

- APPROACH

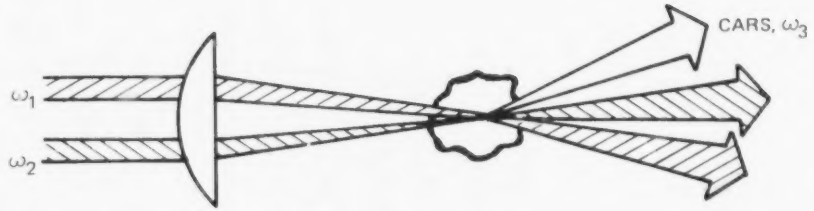

- ENERGY LEVEL DIAGRAM

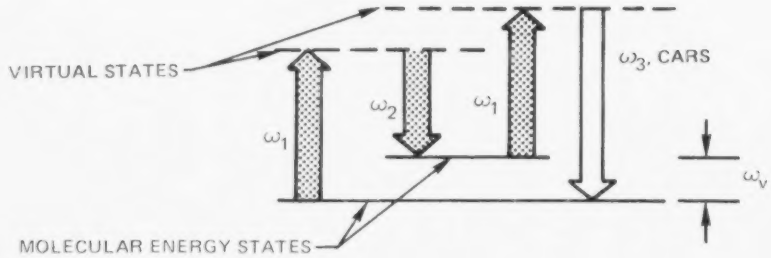

- SPECTRUM

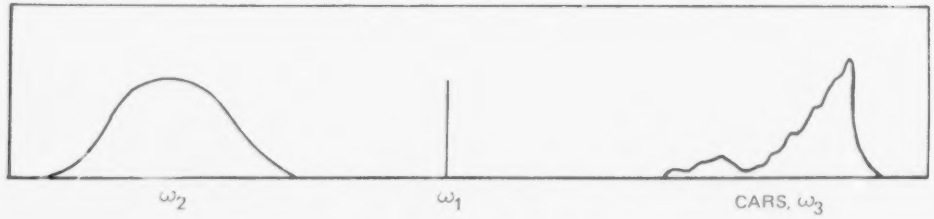

78-02-154-3

FIG. 20

Although easy to implement, collinear phase-matching possesses a drawback from a diagnostic standpoint, namely, potentially poor and ambiguous spatial resolution. A technique to circumvent this difficulty, which employs a crossed-triple-beam, phase-matching scheme, was developed during the course of the contract and will be described shortly. Assuming a fixed narrowband pump frequency, ω_1, the CARS spectrum at ω_3 can be mapped out piecewise by scanning a variable frequency, narrowband laser source at ω_2. Or, as depicted, if a broadband source at ω_2 is employed, the entire CARS spectrum can be generated simultaneously permitting fast, time-resolved measurements of flucutating phenomena.

CARS offers very promising potential for the diagnostic probing of high interference environments such as those typical of combustion processes for two reasons. First, in contrast to spontaneous Raman phenomena, CARS is a fairly strong process leading to signal levels typically many orders of magnitude larger than those from Raman scattering. Second, the CARS signals are coherent. Consequently, all of the CARS radiation can be collected. Contrast this with the situation pertaining in the normal Raman process where photons are scattered over 4π sr and are collected only over a limited solid angle, Ω. For f/3 optics, only 1 percent of the signal is collected in an isotropic, incoherent scattering process. Furthermore, since the CARS radiation can be collected in an extremely small solid angle, discrimination against background luminosity and laser induced particulate interferences, e.g. incandescences (Ref. 42), fluorescences, is greatly facilitated. Thus, CARS is expected to offer signal to interference ratio (S/I) improvements of many orders of magnitude over spontaneous Raman scattering. Based upon calculations presented in the Task I review report (Ref. 1) CARS appears capable of probing practical combustion environments successfully over a broad range of operating conditions.

Before CARS can be practically implemented, however, a number of questions needed to be addressed such as spatial resolution, computer synthesis of CARS flame spectra, feasibility and practicality of single pulse thermometry, the effects of soot particulates and species sensitivity limitations. The investigations conducted during the Task II experimental program and reported herein sought to answer these

questions and to provide an experimental foundation on which to base future avenues of relevant development. In the section which follows, the experimental apparatus employed in these investigations will be described. Then BOXCARS, a nomen for a crossed-beam, phase-matching technique will be described. BOXCARS provides fine and unambiguous spatial resolution for CARS diagnostics of spatially inhomogeneous media. Thermometry investigations, scanned and single pulse, in premixed flat flames are described. Then thermometry investigations in a highly sooting diffusion flame are described. The section concludes with an initial examination of CARS CO detection sensitivity in flames.

Experimental Approach

Although CARS has no threshold per se and can be generated with cw laser sources (Ref. 38), high intensity pulsed laser sources are required for the probing of high interference environments to generate CARS signals well in excess of the various sources of interference. Because CARS is highly nonlinear in its temperature and density dependences, signal averaging in temporally fluctuating media will obscure and distort the CARS spectrum rendering it of little utility or leading to measurement errors. Thus, measurements in fluctuating environments require the CARS spectrum to be generated and captured with each laser pulse. Hence, the individual laser pulses must be energetic enough to provide a statistically large number of CARS signal photons in each spectral detection interval. So restricted, laser selection narrows to a choice between ruby and frequency-doubled neodymium (2xNd) with the latter probably preferable.

2xNd lasers can be operated at a repetition rate generally an order of magnitude higher than ruby, at least 10 pps versus 1 pps. In an instrumental application, this obviously expedites data collection. In the laboratory, it permits the use of boxcar averagers and spectral scanning techniques (when applicable). At 10 pps or better, the experiment behaves much like a cw experiment permitting "tweaking" of adjustments, while the experiment is running, an important feature for the critical alignment requirements of CARS experiments. If a portion of the pump laser is split off to pump a Stokes beam dye laser, 2xNd lasers at 5320Å can pump very efficient

dyes in the 5500-6500Å region of the spectrum, while ruby lasers must pump lower efficiency near ir dyes. Furthermore, the CARS radiation from 2xNd resides in a region of higher photomultiplier tube quantum efficiency than does the CARS from 6943Å, a small advantage. The ruby laser wavelength disadvantages are mitigated by frequency doubling to 3471Å. Whether one would encounter desirable or undesirable (from background constituents) two-photon resonant-enhancement effects for combustion diagnosis is not known at this time. This is also true of using the third harmonic of neodymium at 3533Å. As an aside, one interesting feature of operating in this region is that the CARS signals would be about 144 times stronger from 2x ruby relative to ruby, and 19.5 times stronger for 3xNd than 2xNd on the basis of wavelength scaling alone. Considerations of harmonic generation efficiencies would diminish these gains however. For the investigations reported herein, a frequency-doubled neodymium laser was selected based on the foregoing rationale. In some early investigations of CARS (Ref. 27), the Stokes beam was generated via stimulated Raman scattering of the pump beam. Such an approach is limited to probing only stable species from which stimulated Raman is readily produced, is not suitable for broad-band CARS generation, and thus, is not very versatile. A more flexible scheme is to employ a tunable dye laser, generally pumped by splitting off a portion of the pump laser. CARS configurations employing 2xNd lasers and dye lasers pumped by a fraction of the 2xNd output are also being used at, among other places, the Naval Research Laboratory, Stanford University and Oregon State University.

In Fig. 21 is shown a schematic of the CARS setup used for the Task II experimental investigations. Various configurations were used during the course of the investigations as will be apparent but the major features remained the same. In Fig. 22, a photograph of the experimental set up is shown. Referring to Fig. 21, the output of a Quanta-Ray neodymium laser (Model DCR-1A) is frequency doubled to generate a horizontally polarized, "primary" green beam at 5320Å. The primary green and residual 1.06μ are separated in a splitter section and the residual 1.06μ doubled to generate a "secondary" green beam. Depending on the condition of the flashlamps in the laser and the frequency doublers, the primary green is typically between 1.5

FIG. 21

UTRC CARS EXPERIMENTAL ARRANGEMENT

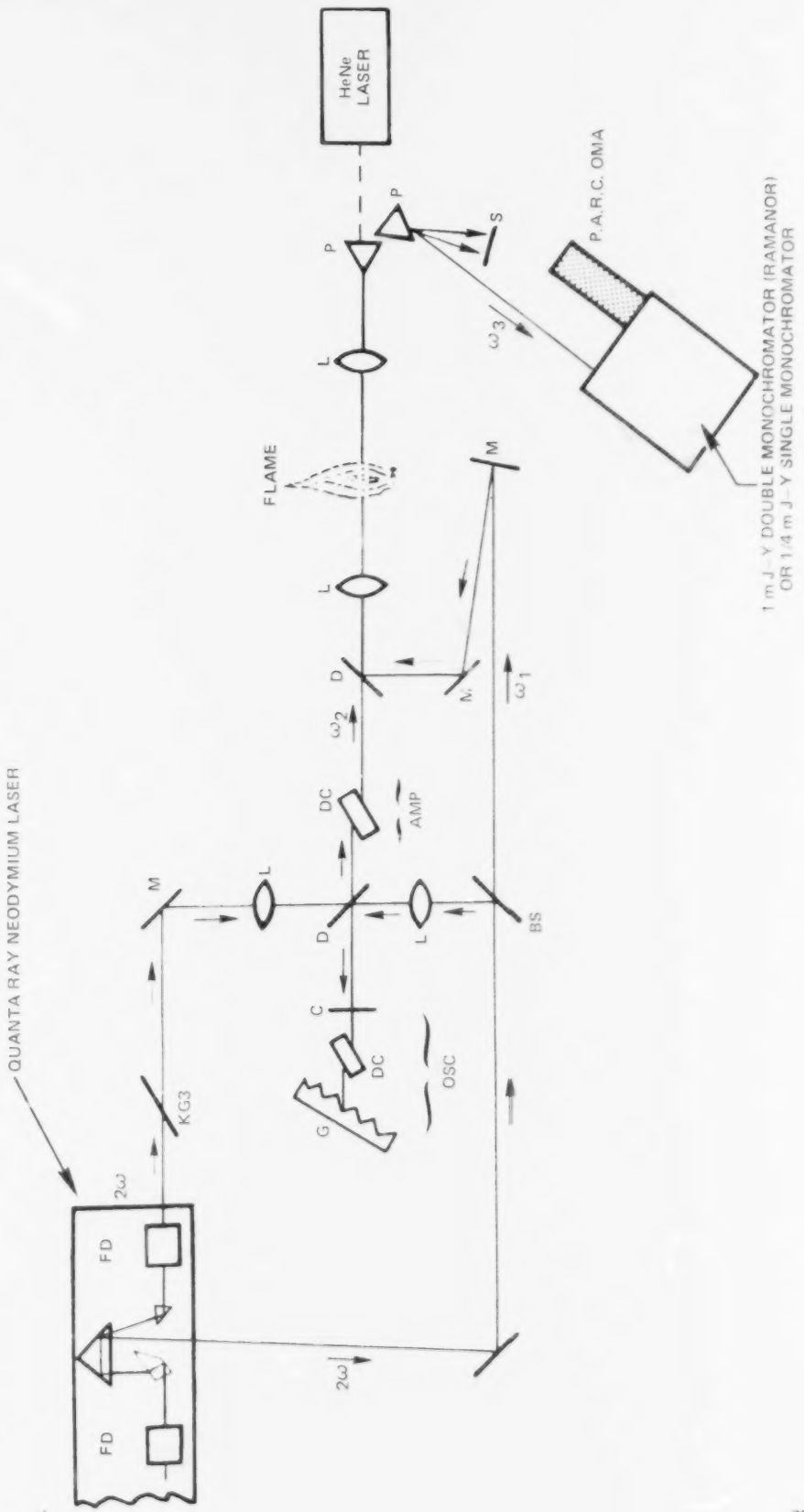

78-02-164-2

FIG. 22

CARS EXPERIMENTAL APPARATUS

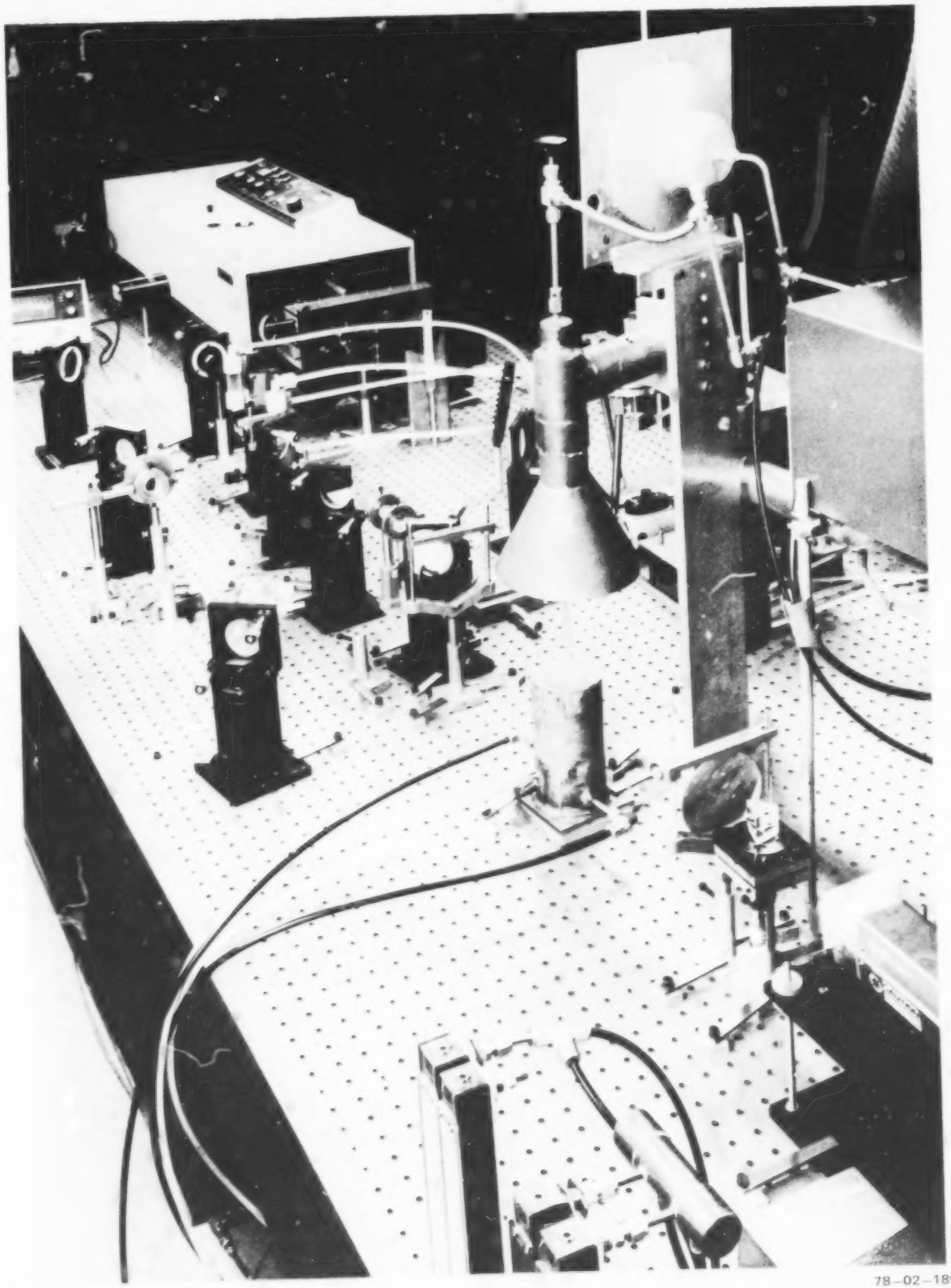

78-02-189-2

78-65-A

to 2.5 W (150 to 250 mJ pulses, 10 pps, 10^{-8} sec pulse duration). As seen in the figure, part of the primary is split off by the beamsplitter, BS, focussed, and reflected by the dichroic, D, to axially pump a flowing dye cell oscillator. The output from the dye laser is amplified in a flowing dye cell axially pumped by the secondary green. The secondary green passes through a piece of KG3 air-cooled, Schott glass placed at the Brewster angle to absorb any remaining 1.06μ. The secondary green is focussed off the same dichroic as the primary and pumps the dye in the amplifier cell. The oscillator and amplifier cells are in flow series. A small, magnetically coupled, stainless steel gear pump circulates the dye from a 1.5 liter reservoir through a 0.6μ filter to remove and prevent large air bubbles. The dye cells are oriented at Brewster's angle and produce a horizontally polarized output; actual oscillator efficiencies vary between 20-30 percent while the amplifier operates between 40 and 50 percent efficiency. One problem with coaxially pumped configurations is the existence of 5320$\mathring{A}$ focal points or high intensity regions on the various optical elements. Furthermore, many of the optical elements require dichroic coatings. Although much of the work to be reported herein employed coaxial pumping schemes, the system has recently been converted to off-axis, dye laser pumping, as seen in Fig. 22, with comparable or slightly improved efficiencies. The pump and Stokes beams are combined at a second dichroic and collinearly focussed into the region under study to generate the CARS radiation. Optical delay can be inserted into the primary pump leg to ensure that the pump and Stokes laser pulses are temporally overlapped. The Stokes, pump and CARS beams are recollimated and then dispersed with a double extra dense flint prism. The pump and Stokes beams are trapped, while the CARS passes through cutoff filters prior to analysis by a 1-m double monochromator (Ramanor, HG2S, Jobin Yvon) or to an optical multichannel analyzer, OMA (Princeton Applied Research) fitted to a 1/4 m spectrograph equipped with either a 1200 or 2400 gr/mm holographic grating. Recently the 1 m double monochromator has been modified to accept the OMA as well. The experimental configuration displayed is capable of very intense CARS generation. With collinear phase-matching, CARS generation from N_2 in room air is readily visible and easily phot-

graphed as shown in Fig. 23. The CARS beam is annular as shown and is an artifact of the unstable or diffraction-coupled resonator employed on the neodymium laser. The laser output is an annulus with outer to inner radius ratio (magnification) of about 3.2.

To produce the broadband Stokes laser output desired for single pulse CARS work, a variety of dye oscillator cavity configurations were tested. Bandwidths on the order of 100 cm^{-1} FWHH are desired since the vibrational band separation in N_2 is about 30 cm^{-1}. A 1200 gr/mm grating at low dye concentrations ($\sim 5 \times 10^{-5}$ M) resulted in a bandwidth of only $\sim$ 15 cm^{-1}. As the dispersion in the cavity was reduced by employing successively less dispersion, i.e., 600 gr/mm or 150 gr/mm gratings or various density prisms, the bandwidth increased. With the low dispersion required to obtain adequately large bandwidth, however, control of the laser center frequency was lost, i.e., the laser would oscillate off-axis at the wavelength corresponding to maximum gain. Consequently, no dispersion was employed at all. Rather, a flat-flat Fabry-Perot oscillator arrangement was adopted and the bandwidth appropriately centered by selection of appropriate dyes and dye concentration (Ref. 40). Small adjustments in the Stokes laser center frequency are also possible by varying the cavity mirror separation. Bandwidths vary from 100 cm^{-1} to 200 cm^{-1} depending on oscillator pump energy and whether the dye amplifier is used. By using mixtures of two different dyes, very broad bandwidths are possible, i.e., 250 to 300 cm^{-1}. For N_2 thermometry, which requires the Stokes laser to be centered at 6073$\mathring{A}$, Rhodamine 640 (Ref. 43) at a concentration of about $5(10^{-5})$M in ethanol is employed.

For single pulse CARS diagnostics or for spectral scanning of laminar (i.e. steady) situations it is important that the dye laser spectrum be smooth and reproducible from pulse to pulse. In Fig. 24 are shown five OMA traces of the broadband dye laser spectrum. Each spectrum corresponds to a single laser pulse and was obtained by gating the intensifier stage of the OMA with a $\sim$ 100nanosecond pulse. Each channel corresponds to 1.4$\mathring{A}$. As seen the spectra are fairly smooth and reproducible from pulse to pulse.

FIG. 23

CARS GENERATION FROM AIR AT 4733Å

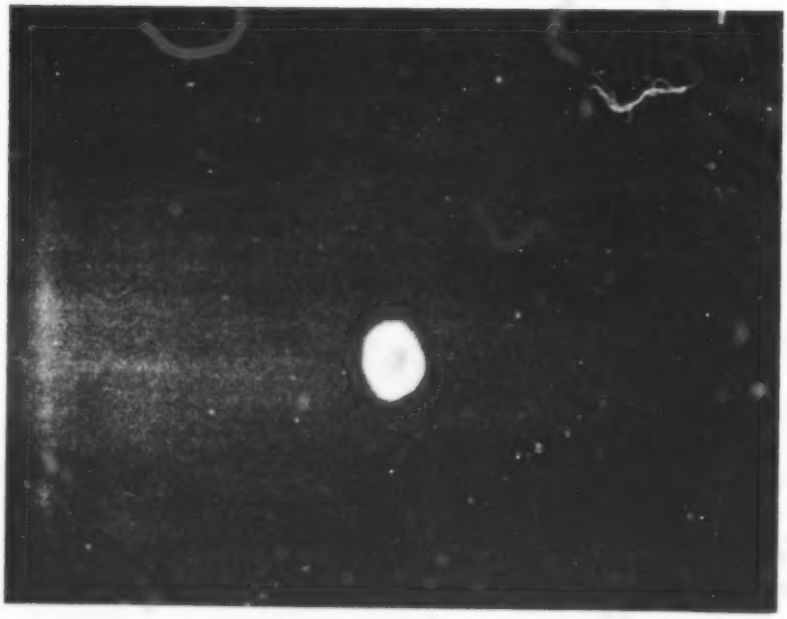

78-02-108-2

FIG. 24

BROAD BAND DYE LASER SPECTRAL STABILITY

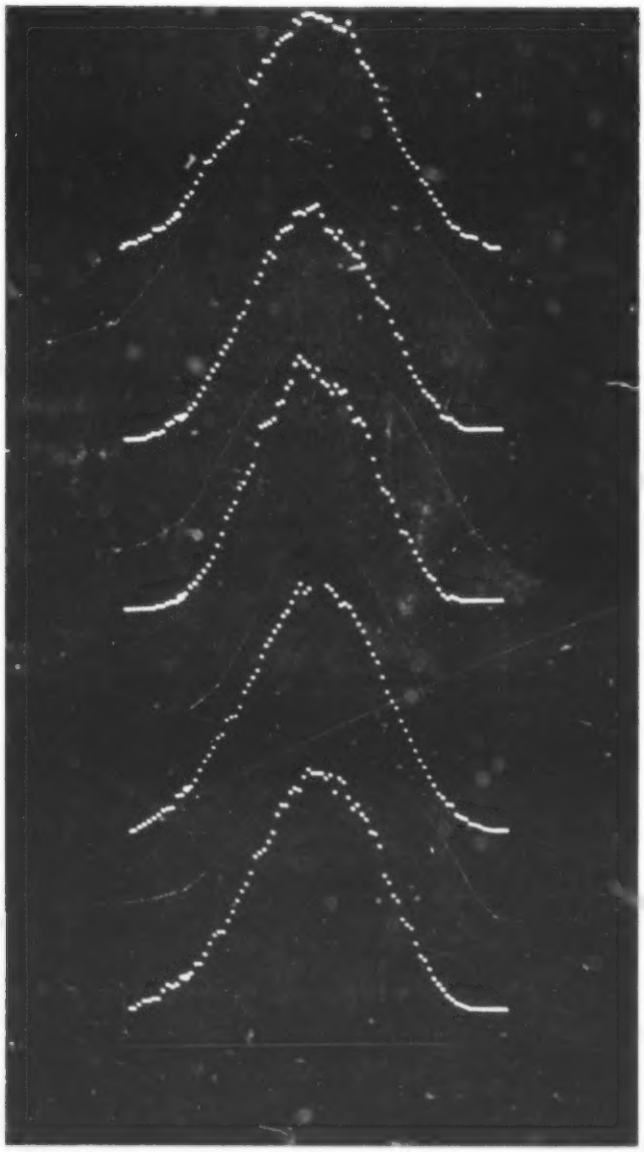

C17a-1

1.4 Å CHANNEL

78-02-108-1

In broadband CARS, either the linewidth of the pump laser or the resolution of the monochromator determine the ultimate resolution of the spectrum. The 1-m double monochromator has a limiting resolution of about 0.5 cm^{-1} in the visible. The 2xNd laser has a linewidth of about 1.2 cm^{-1} and thus limited the resolution of the CARS spectra to around this value. However, as will be seen, this moderate resolution is more than sufficient. The large pump laser linewidth is detrimental, however, in regard to the strength of the CARS radiation. In this regard it would be desirable to have the pump linewidth comparable to the Raman linewidths of the hot flame gases, ~ 0.1 cm^{-1}.

BOXCARS: Crossed-Beam Phase Matching

As mentioned previously, the incident pump and Stokes laser beams must be aligned in a precise manner so that the CARS generation process is properly phased. The general phase-matching diagram for three wave mixing is shown in Fig. 25a and requires that $2\vec{k}_1 = \vec{k}_2 + \vec{k}_3$. $\vec{k}_i$ is the wave vector at frequency ω_i with absolute magnitude equal to $\omega_i n_i/c$, where c is the speed of light and n_i, the refractive index at frequency ω_i. Since gases are virtually dispersionless, i.e., the refractive index is nearly invariant with frequency, the energy conservation condition $\omega_3 = 2\omega_1 - \omega_2$ indicates that phase-matching occurs when the input laser beams are aligned parallel to each other, Fig. 25b. Collinearity, however, possesses a problem in regard to spatial resolution. Since the CARS signal is coherent and undergoes an integrative growth process, the spatial resolution cannot be well defined by imaging techniques such as those successfully employed in spontaneous Raman approaches to yield fine resolution. Since the CARS signal generation scales as the intensity product $I_1^2 I_2$ the incident laser beams are generally tightly focussed for diagnostic purposes when collinear phase-matching is employed. For diffraction-limited beams, the interaction is assumed to occur primarily within a cylindrical volume of diameter φ and length ℓ given by (Ref. 30)

$$\varphi = \frac{4\lambda f}{\pi D} \qquad \ell = \frac{\pi \varphi^2}{2\lambda} \tag{25}$$

FIG. 2b

CARS PHASE MATCHING APPROACHES

a) GENERAL

b) COLLINEAR

c) BOXCARS

where f is the focussing lens focal length; D, the beam aperture incident on the lens; and λ, the wavelength, In Table IV, the probe volume focal diameter, cross-sectional area and length are tabulated for various focal length lenses for a 1 cm diameter beam at 5320Å.

TABLE IV

Collinear Phase-Matched CARS Probing Volume

Focal length (cm)	Diameter (cm)	Area (cm^2)	Length (cm)
10	6.11 (-4)	2.93 (-7)	1.22 (-2)
20	1.22 (-3)	1.17 (-6)	4.88 (-2)
50	3.06 (-3)	7.35 (-6)	3.05 (-1)
100	6.11 (-3)	2.93 (-5)	1.22

Depending on the specific diagnostic circumstance, i.e., the focussing lens to measurement point separation, the spatial resolution may be less than that which is desired. Although the resolution is very good for short focal length lenses, gas breakdown may limit the input beam intensities leading to diminished CARS signal levels. Many laser beams are not diffraction-limited resulting in much poorer spatial resolution than that tabulated here. For example, for a "three times diffraction limited" beam divergence angle, the linear resolution would be about an order of magnitude poorer. Specifically, in Fig. 26, CARS radiation curves of growth are displayed for beam divergence angles of 1 and 2 milliradians and various practical focal length lenses. The calculations were made using a plane wave analysis applicable to the parameter range selected (Ref. 44) corresponding to so-called "loose focussing." As is readily apparent in Fig. 26 significant CARS generation occurs well before the focal region in the prefocal regions. If the coherence length is sufficiently large, significant growth could occur beyond the focal region as well. To make the situation worse, in the presence of density gradients the resolution further degrades since CARS scales as the square of the

FIG. 26

COLLINEAR CARS CURVES OF GROWTH

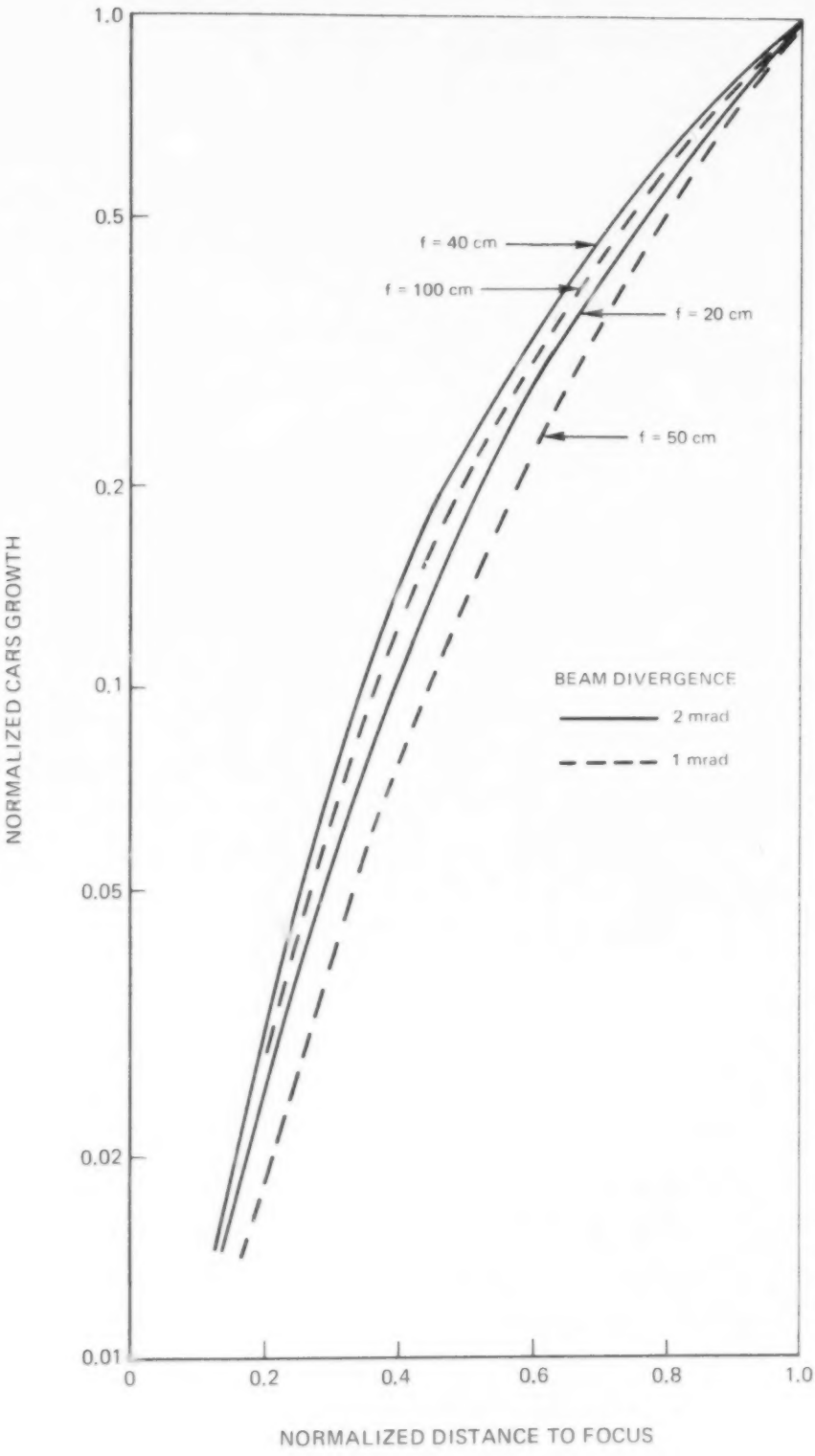

78-02-108-4

gas density. For probing of a hot flame operating at atmospheric pressure, significant contributions to the CARS signal may originate from the cool, high density regions adjacent to the flame. For example, in the experimental setup used here, initial attempts to record flame spectra with 40 cm focal length lenses on a 7.5 cm dia burner were unsuccessful due to a dominance of room air N_2 contributions. With a piece of Schott glass GG495, which transmits the laser and Stokes beams but absorbs the CARS beam, it was determined that about 10-15 percent of the total room air CARS signal was generated in the first 32 cm from the lens. With the flame ignited, the CARS signal from the hot, low density flame gases was substantially less than the cold, room air contribution.

CARS signal contributions may derive also from the various elements in the optical train, e.g., lenses, when collinear phase-matching is used. These could be significant when low gas densities or weak resonances are being probed. Clearly it would be desirable to avoid beam overlap and potential three wave mixing in all regions except the desired measurement location. In an effort to avoid collinearity, one could attempt to introduce the pump and Stokes beams at a slight angle to one another. As phase mismatch is deliberately introduced in this manner, the CARS signal generating efficiency will diminish. At $\Delta k\ell \approx 3$, where Δk is the magnitude of the phase mismatch, i.e., $|2\vec{k}_1 - \vec{k}_2 - \vec{k}_3|$, the CARS efficiency will have decreased by an order of magnitude (Ref. 35). Accepting this loss of power for the moment and if a 0.1 cm spatial resolution is desired, then a Δk of 30 cm^{-1} would be tolerable. At wavelengths of 5320Å (ω_1) and 6073Å (the N_2 ground vibrational state Stokes wavelength), a 30 cm^{-1} phase mismatch would be produced at an angular separation of only 1^o assuming no dispersion. Although one could operate in this manner, it is clearly inefficient and the actual spatial resolution will depend very critically on the precise angular separation. During the course of the Task II experimental investigations, CARS has been generated using crossed ω_1 and ω_2 beams as will be described in the CO studies, but no systematic study of the scaling of the signal generation efficiency or spatial resolution was attempted.

A method which permits large angular separation of the input frequencies, while still satisfying the phase matching requirement is depicted in Fig. 25c (Ref. 45). In this approach the ω_1 pump beam is split into two components which are crossed at a half angle of α. The ω_2 Stokes beam is introduced at angle θ producing phase-matched CARS at angle φ. Based upon the shape of the phase-matching diagram, Fig. 25c, this technique has been termed BOXCARS. The appropriate phase-matching angles are readily related from simple geometric considerations as follows:

$$n_2\omega_2 \sin\theta = n_3\omega_3 \sin\varphi \tag{26}$$

$$n_2\omega_2 \cos\theta + n_3\omega_3 \cos\varphi = 2n_1\omega_1 \cos\alpha \tag{27}$$

Neglecting dispersion, Table V lists several examples of phase-matching angles for BOXCARS generation from N_2 assuming a pump wavelength of 5320Å

TABLE V

BOXCARS Phase-Matching Angles

θ	α	φ	θ	α	φ
5	4.38	3.89	60	50.7	42.5
10	8.81	7.78	70	57.8	47.1
15	13.2	11.6	80	64.1	50.1
20	17.6	15.5	90	69.4	51.2
25	21.9	19.2	120	78.7	42.5
30	26.2	22.9	150	82.1	22.9
40	34.7	30.1	180	82.9	0
50	42.9	36.7			

The very large angles shown lead to interesting phase-matching configurations which may be of utility in certain laboratory studies. In general, the smaller angles are of most interest for diagnostic applications where input and output optical apertures are limited.

It is also interesting to note that the angular separation $\theta-\alpha$ between ω_2 and the adjacent ω_1 component is generally large enough to preclude significant CARS generation between these individual components. However, it was in conjunction with small angle BOXCARS experiments that phase mismatched CARS generation between these adjacent components was first observed. Although the interaction zone has not been analyzed in detail, BOXCARS generation can clearly occur only where all three beams overlap leading to unambiguous spatial resolution. By proper design this interaction zone can be made acceptably small for most diagnostic applications, e.g., less than 1 mm.

Experimentally, BOXCARS was demonstrated using the front end optical arrangement shown in Fig. 27. The primary pump beam after passing through the first beamsplitter is split at a second beamsplitter and sent to an additional mirror. The remaining ω_1 beam reflects from the original beam combining dichroic but appropriately displaced from ω_2. All three beams, ω_1, ω_1 and ω_2 are aligned parallel to each other in a single plane and sent to the focussing lens. If the beams are aligned properly, they will cross at the focal point of the lens, by definition. However, due to wavefront sphericity they may not necessary waist at the crossing point. To ensure that the minimum beam waist occurs at the crossing point, adjustable telescopes are added in each leg. At high laser intensities, the beams are readily visualized near the focal region via the room air Rayleigh scattering. The telescopes are then adjusted to visually produce minimum waisting at the crossing point. Also inserted in the ω_2 leg is a rotatable optical flat. Rotation of the flat permits displacement of the ω_2 beam on the focussing/crossing lens permitting the phase-matching angle θ to be varied. After passing through the crossing point, the four beams, i.e., CARS @ ω_3, ω_1, ω_1, ω_2 are recollimated by a second lens, generally the same focal length as the focussing lens. Two of the components, ω_1 and ω_2, are trapped although they could be sent to a reference leg if desired to generate a normalizing signal. The CARS radiation and the remaining ω_1 are dispersed with a prism and the CARS sent to appropriate instrumentation. It should be noted that generally at small angles ($\alpha < 10^{\circ}$), the ω_1 and ω_3 CARS radiation, although angularly

FIG. 27

BOXCARS EXPERIMENTAL ARRANGEMENT

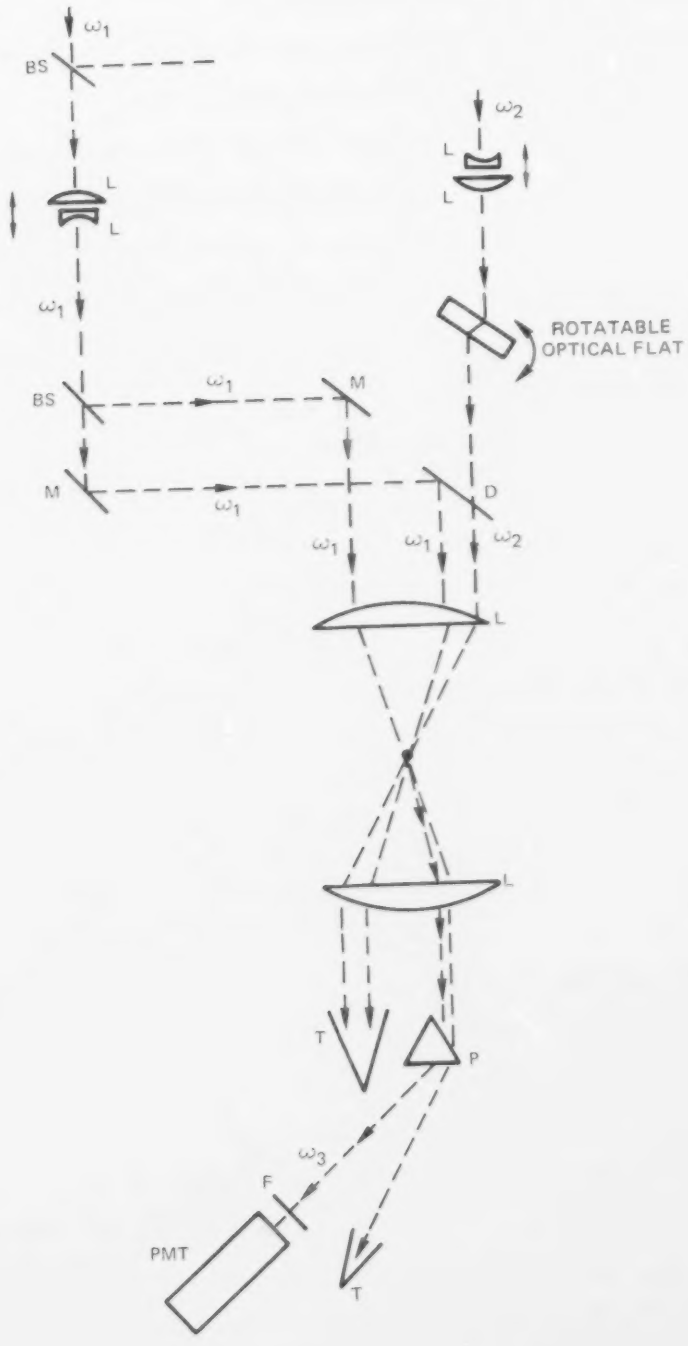

78-02-153-1

separated, are not necessarily spatially separated which depends on the beam diameters used. In all of the work reported here, this was always the case and a prism was used to separate the ω_1 and ω_3 radiations.

In the initial demonstrations of BOXCARS, an 89 mm diameter, 483 mm focal length lens was employed and CARS was generated from room air N_2. α was selected to be 3.1°; θ and φ were 3.6° and 2.8° respectively. That the detected signal was indeed CARS was verified by separately blocking either of the two ω_1 or ω_2 components which led to the expected disappearance of the signal. Most convincing was the effect on the signal of rotating the optical flat through which ω_2 was transmitted, which as previously mentioned varies the phase-matching angle θ. In Fig. 28, the variation of the CARS signal with deviation in θ from the optimum phase-matching angle is shown. The angular mismatch was calculated based upon the measured angle of the optical flat, its thickness and assuming its refractive index to be 1.5. Roughly, each 0.1 degree of angular deviation corresponds to a calculated phase mismatch $|\Delta k|$ of about 20 cm^{-1}. The CARS signal displays little variation in magnitude for misalignments up to 0.1°. Beyond that the signal declines fairly slowly with increasing phase mismatch. The variation in signal is not symmetric about the optimum angle. The slower decrease in signal with increasing negative angular misalignment is probably due to a larger interaction length as ω_2 draws closer to ω_1 than when its separation from ω_1 increases.

In the initial experiments just reported, the spatial resolution was not very good. The resolution was measured by examining the CARS signal generated from a translatable 1 mm thick microscope slide. All of the signal generation occurred within a 1.3 cm extent. Integrating the respective piecewise contributions revealed that the total signal grew from 10 to 90 percent over a distance of about 4 mm. For the sooting flame studies to be reported later, slightly larger angles were employed and the resolution improved. In these studies a 305 mm focal length lens was used and the angles were $\alpha = 5.0$, $\theta = 5.7^\circ$ and $\varphi = 4.4^\circ$. The resolution measured with a 0.15 mm slide cover is shown in Fig. 29. Signal generation occurred within a 2.5 mm extent and the 10 to 90 percent growth in the integral occurred over an

FIG. 28

BOXCARS INTENSITY VARIATION WITH ANGULAR DETUNING

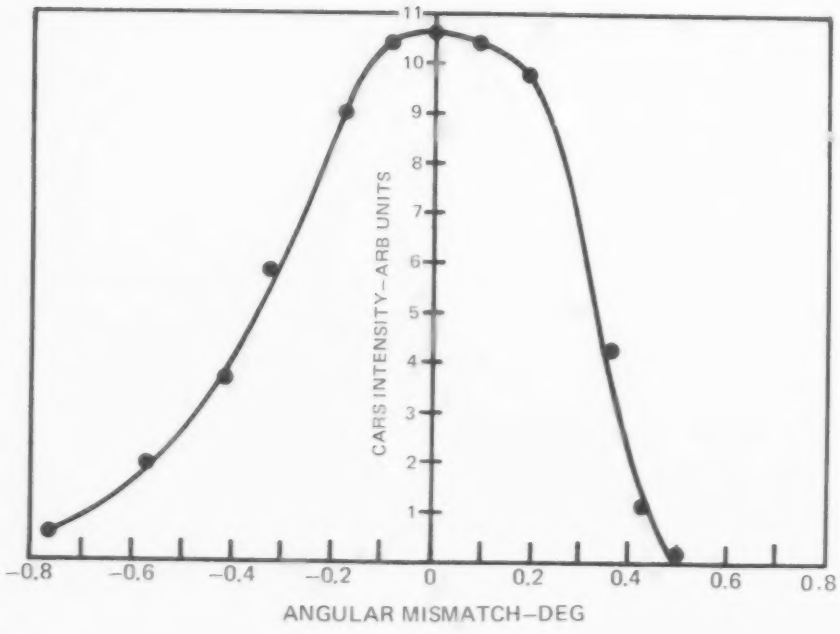

78-02-108-7

FIG. 29

BOXCARS SPATIAL RESOLUTION

f = 305 mm

$\theta = 5.7^{o}$ $\alpha = 5.0^{o}$ $\phi = 4.4^{o}$

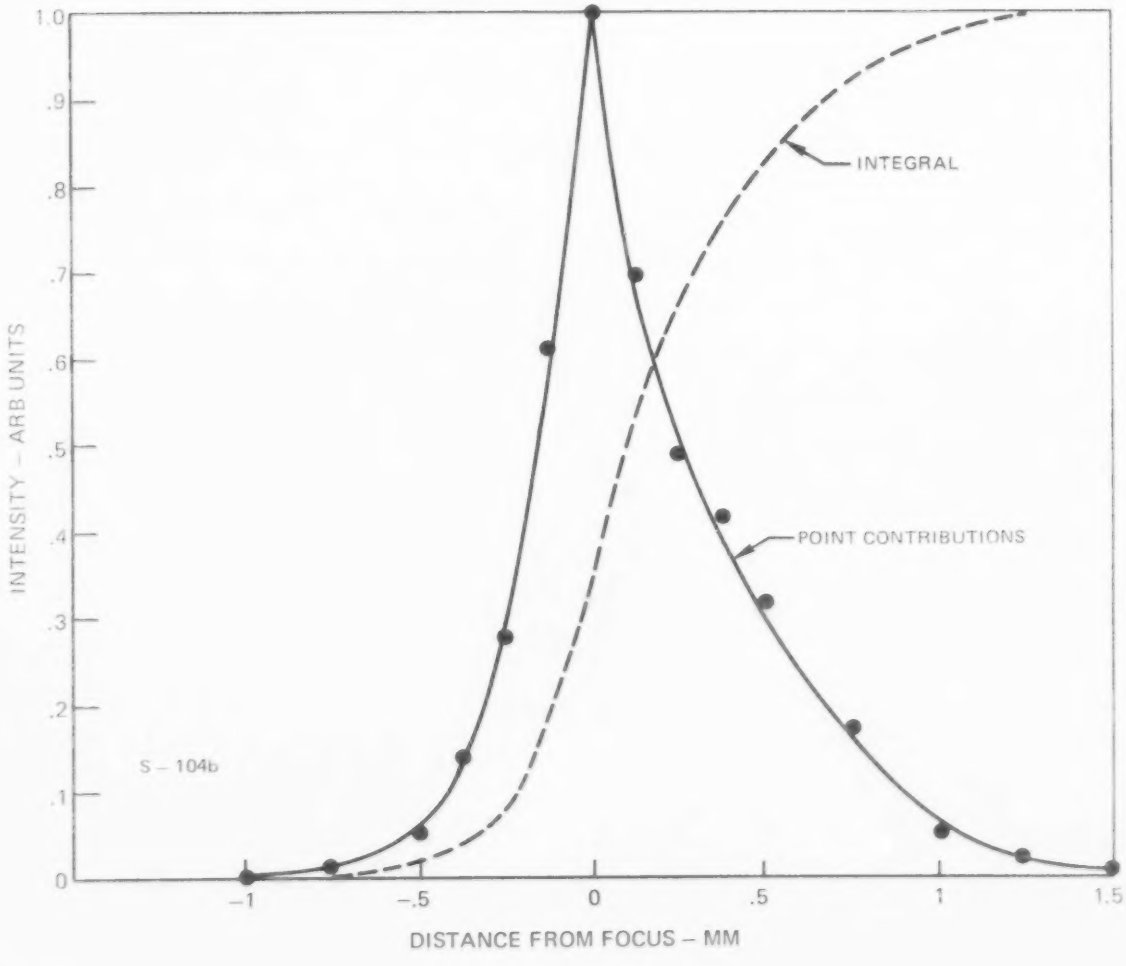

78-02-111-1

extent of 0.9 mm. The focal beam diameters were measured by translating a 25μ pinhole across the attenuated focal spots. The diameters at the $1/e^2$ points were found to be 380μ for the ω_1 and 480μ for the ω_2 beams. These measurements imply beam divergences of 1.6 milliradians for the dye laser (after expansion in the 2x telescope) and 0.9 milliradians for the primary ω_1 component (before contraction at the 0.7x telescope). The spatial resolution although certainly not poor could be improved by using larger intersection angles and smaller focal waists. The latter can be achieved by either beam expansion prior to focussing, use of a smaller f number crossing lens or both.

At larger angles and for the longer focal lengths required in practical applications, a single conventional focussing lens generally would be quite heavy and expensive. One can then first cross the beams and use individal lenses on each leg. An alternative would be to investigate the use of large, corrected, acrylic Fresnel lenses.

An interesting aspect of BOXCARS that has not yet been explored concerns the employment of crossed polarizations (Ref. 46). In isotropic media such as gases, the third order nonlinear resonant susceptibility can be expressed as (Ref. 47)

$$\chi_{ijkl}(-\omega_3, \omega_1, \omega_1, -\omega_2) = \chi_{xxxx}[(1-2\rho)\delta_{ij}\delta_{kl} + \rho(\delta_{ik}\delta_{jl} + \delta_{il}\delta_{jk})] \qquad (28)$$

where the indices i, j, k, l refer to the polarization orientation of the frequencies ω_3, ω_1, ω_1 and ω_2. ρ is the depolarization of the Raman mode and δ_{ij}, the Kroneker delta (=1, i=j; =0, i≠j). In N_2, ρ is extremely small and equal to 0.022 (Ref. 48). Hence

$$\chi_{ijkl} \approx \chi_{xxxx}\,\delta_{ij}\delta_{kl} \qquad (29)$$

With conventional CARS, where only one ω_1 input pump beam is employed, j ≡ k, and hence, for CARS to be observed, the Stokes polarization must be parallel to the pump polarization, k = l. The CARS radiation will then exhibit the same polarization, i = j, as the pump and Stokes beams and is generated via χ_{llll}. With BOXCARS, however, one has independent control of the j and k polarizations. If j and k are

parallel, then the Stokes beam must have the same polarization for CARS to be generated, as in conventional CARS. However if j and k are orthogonally polarized, and the Stokes beam is aligned along one of the pump components, then the CARS radiation will emerge orthogonally polarized to the Stokes beam.

This gives rise to an interesting instrumental approach to thermometry. One way to measure temperature (Appendix I) is to ratio the CARS from a hot band, e.g., v = 1, to CARS from the ground state band, v = 0. If the Stokes beam contains two orthogonally polarized components corresponding respectively to wavelengths necessary to generate CARS from the hot and ground state band, then the CARS so generated from each band would be orthogonally polarized. The two CARS components could be separated with a polarization splitter and temperature ascertained from the ratio of the two. In contrast to the broadband techniques to be subsequently described, such an approach offers backend (detection) simplicity. It obviously would be more complicated on the front end (laser) side than broadband CARS approach. Hence, in addition to obvious spatial resolution advantages, BOXCARS may offer other instrumental benefits as well.

Flat Flame Thermometry

Unlike spontaneous Raman spectra which depend linearly on and, hence, mirror quantum state population distributions, CARS spectra are much more complex representative of the nonlinear nature of the three wave mixing process. Although some simple schemes were first proposed to derive temperature information from CARS spectra, there seems to be widespread consensus that computer modelling will be required for accurate temperature measurements. In fact as confidence develops in the analytical modelling procedures, simplified data reduction schemes will most likely emerge. A computer model is an important adjunct to experimental studies of CARS spectra. Initially, the model predictions guide the experimenter in judging the validity of the experimental approach. This is particularly true of CARS research in flames where signal contributions may emanate from other than the desired region under study. As confidence grows in the experimental technique and the results

therefore, the model can be revised and updated. Ultimately, if necessary, the model will provide a data reduction capability, preferably in real time. During the Task II experimental program, the close interaction between the experimental results and the model predictions was quite evident.

Computer Modelling of CARS Spectra

Under Corporate funding, a computer model to synthesize CARS spectra as a function of density, temperature and background was formulated by R. J. Hall of UTRC. The model is currently capable of generating N_2 and CO spectra and is described in detail in Appendix I. A block diagram of the model is shown in Fig. 30. Briefly, upon inputting selection of the molecular species of interest together with density and temperature, the model calculates the state populations $n_{v,J}$ and energies, $h\omega_{v,J}$, where h is Planck's constant and v, J the vibrational and rotational quantum numbers for the state of interest. Next the program computes the complex third order nonlinear susceptibility. Recall that the CARS radiation is proportional to the square of the absolute value of the susceptibility. The third order nonlinear susceptibility may be written as

$$\chi^{(3)} = \sum_j (\chi' + i\chi'')_j + \chi^{nr} \qquad (30)$$

where $(\chi' + i\chi'')_j$ is the resonant susceptibility associated with transition j and χ^{nr} is the nonresonant susceptibility contribution of the electrons and remote resonances. The resonant contribution may be expressed as

$$(\chi' + i\chi'')_j = K_j \frac{\Gamma_j}{2\Delta\omega_j - i\Gamma_j} \qquad (31)$$

where the detuning frequency $\Delta\omega_j = \omega_j - (\omega_1 - \omega_2)$ has been introduced. ω_j is the frequency of a particular possible transition from $v,J \rightarrow v',J'$ and equal to $|\omega_{v,J} - \omega_{v',J'}|$. Selection rules govern which transitions are allowed. Γ_j is the Raman linewidth for the transition denoted by j. K_j is the modulus of the susceptibility and equal to

FIG. 30

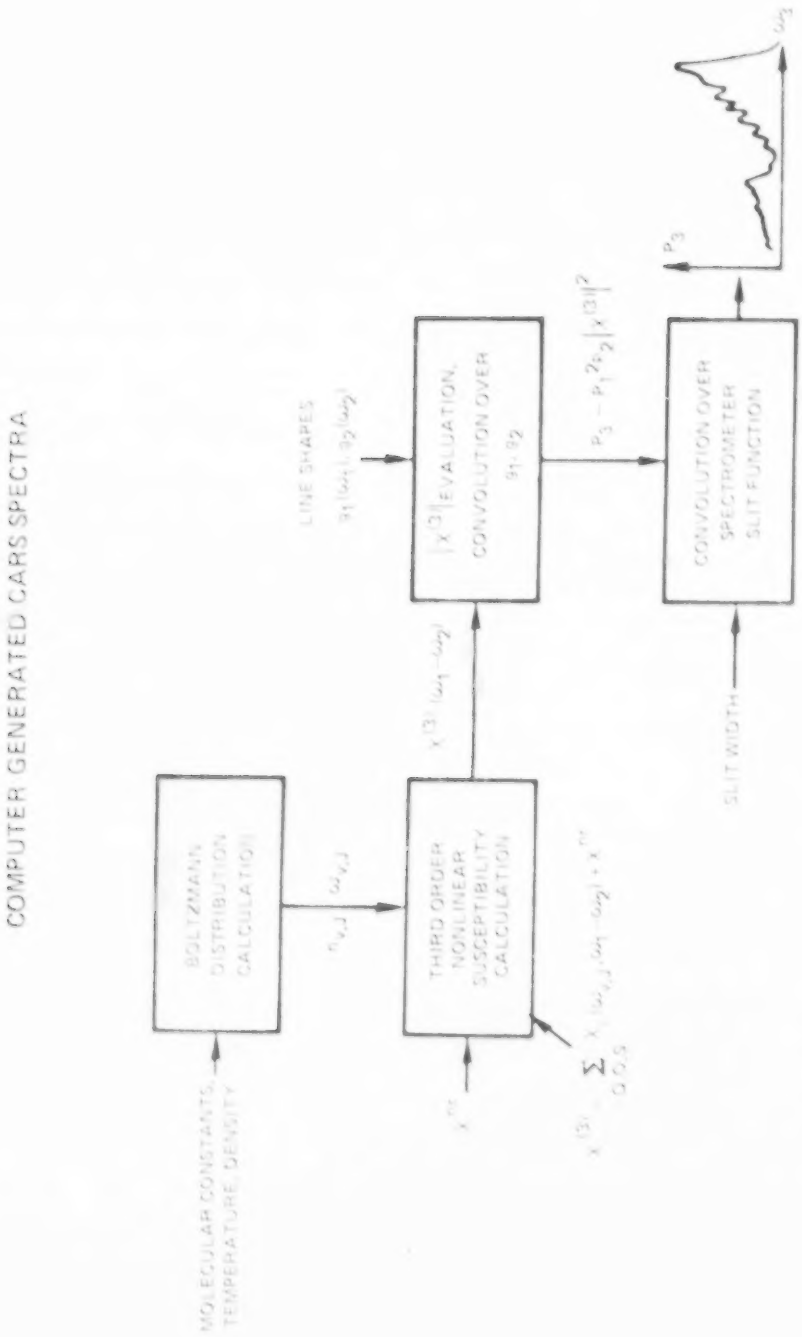
COMPUTER GENERATED CARS SPECTRA
MOLECULAR CONSTANTS, TEMPERATURE, DENSITY
BOLTZMANN DISTRIBUTION CALCULATION
THIRD ORDER NONLINEAR SUSCEPTIBILITY CALCULATION
LINE SHAPES
$|\chi^{(3)}|$ EVALUATION, CONVOLUTION OVER Γ_1, Γ_2
$P_3 \sim P_1^2 P_2 |\chi^{(3)}|^2$
CONVOLUTION OVER SPECTROMETER SLIT FUNCTION
SLIT WIDTH
P_3
ω_3

$$\chi_j = \frac{\pi c^4}{\hbar \omega_j^4} n \Delta_j \varepsilon_j \left(\frac{\partial \sigma}{\partial \Omega}\right)_j \frac{1}{\Gamma_j} \qquad (4)$$

where $\hbar$ is Planck's constant divided by 2π; n, the total species number density; Δ_j, the normalized population difference between the levels involved in the transition; ε_j, linestrength factor equal to (v_j+1); and $(\partial\sigma/\partial\Omega)_j$, the Raman cross section for the transition. The susceptibility is calculated by summing over all appropriately allowed transitions and selecting a value for the nonresonant susceptibility. The susceptibility emerges from this subroutine as a function of $\omega_1-\omega_2$. Next the square of the absolute value of the susceptibility is calculated together with a convolution over the function $g(\omega_1)^2 g(\omega_2)$, where $g(\omega_i)$ is the laser lineshape at frequency ω_i. This accounts for the scaling of the CARS radiation as $I_1^2 I_2$ where I_i is the laser intensity at frequency ω_i. In the program, Gaussian fits to the laser lineshapes are used. The ω_1 halfwidth is 1.2 cm^{-1} and ω_2 linewidth appropriate to the experimental value, typically 150 to 300 cm^{-1}. Finally the CARS spectra is convoluted over a monochromator slit function, generally taken to be triangular. At the display terminal, plots are available of the susceptibility, and the CARS spectrum before and after the monochromator slit convolution.

Scanned Flame Spectra

CARS spectra from flame N_2 have been studied on premixed flat flames sustained on a 7.5 cm dia burner consisting of either a water cooled bundle of hypotubes or a sintered porous plug. Early spectra (Ref. 49) were obtained using collinear phase matching and Ar shield gas between the focussing lens and the burner, and between the burner and the recollimating lens. In this manner, room air N_2 contributions were suppressed. Improved quality spectra were subsequently obtained using BOXCARS at small crossing angles. Such a spectrum is displayed in Fig. 11. The experimental spectrum was obtained using 100μ entrance and exit slits on the monochromator, corresponding to a monochromator resolution of about 1 cm^{-1}. The output of the monochromator photomultiplier is fed to a two channel boxcar averager (PAR Model 162) fitted with gated integrators (PAR Model 164). For broadband CARS spectra

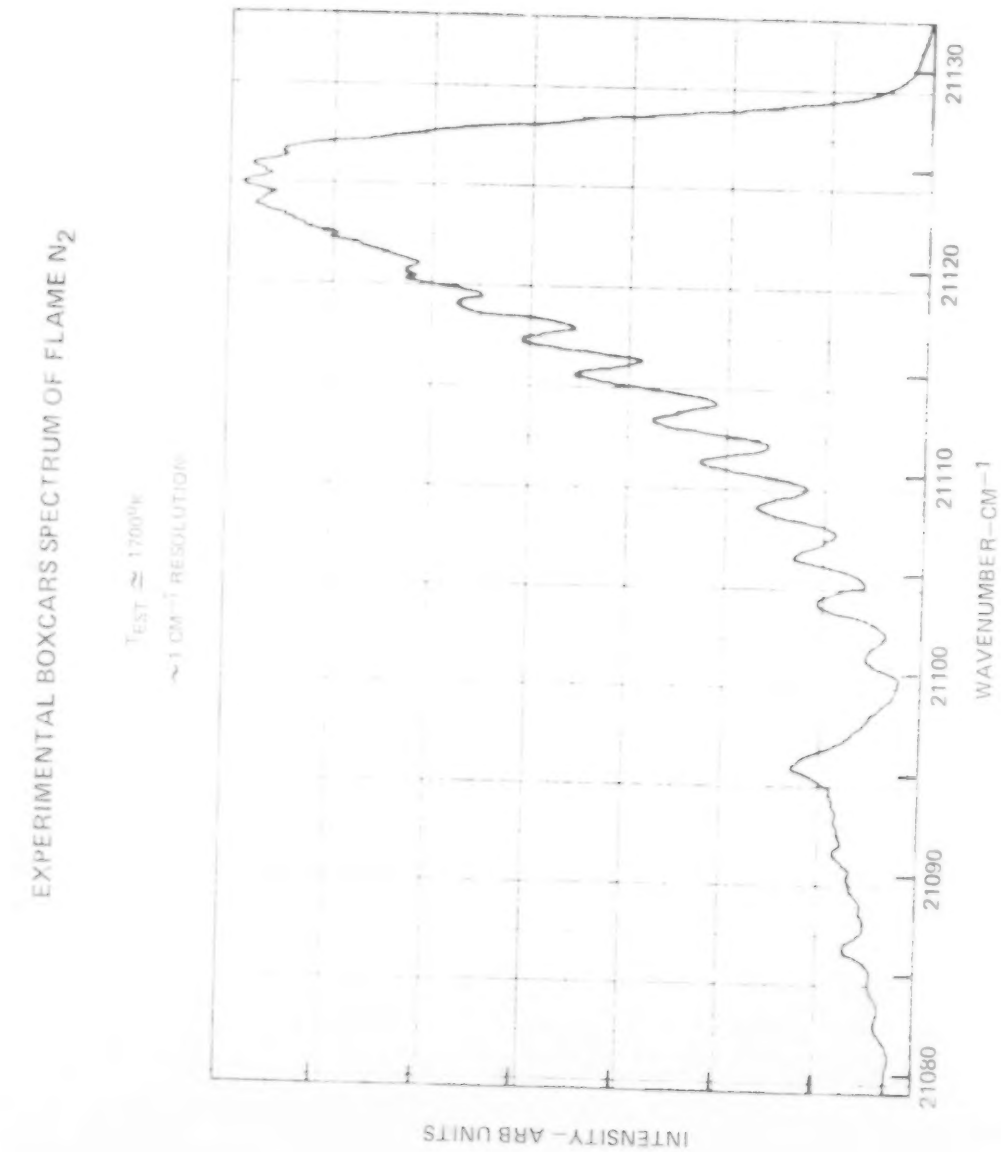
EXPERIMENTAL BOXCARS SPECTRUM OF FLAME N_2
$T_{EST} \simeq 1700^{\circ}K$
$\sim 1\ CM^{-1}$ RESOLUTION
INTENSITY – ARB UNITS
21080
21090
21100
21110
21120
21130
WAVENUMBER–CM^{-1}

from laminar flames, the monochromator signal can be normalized to the total integrated CARS signal. The latter is obtained by splitting off a small fraction of the CARS signal which is monitored by a second photomultiplier fitted with a narrow-band interference filter to ensure that only CARS is collected. For these flames at low air and CH_4 flowrates, radiation corrected thermocouple measurements (Ref. 50) indicated a temperature just below 1700°K. Earlier, spontaneous Raman measurements (Ref. 50) gave temperatures between 1625 and 1675°K.

In Fig. 32 is the computed CARS spectrum which produced the best fit to the experimental spectrum. The computation was performed at 1650°K and 1.25 cm^{-1} slit width. As seen, excellent agreement is obtained except for some features in the hot band. In the ground state vibrational band (v=0) the low lying Q branch transitions are unresolved and pile up to form a broadened band. At higher rotational quantum numbers, due to the rotational-vibrational interaction, the even Q branch peaks are clearly seen. The odd rotational quantum number transitions, which have a nuclear spin weighting equal to half of the even numbered Q branch transitions, do not stand out. The first hot band is also clearly visible. Initially in comparing the experimental and analytical spectra it was noticed that the various even Q branch peaks did not coincide. However, when the rotational constant was updated from the value in Herzberg's treatise, coincidence was obtained. The experimental peaks in the hot band are reproducible and are believed to be valid. Depending on the exact value of the vibrational frequency selected, these peaks can be duplicated in the model predictions. The analytical curve shown corresponds to the set of molecular constants given in Ref. 51. As more refined values of the molecular constants become available, agreement of the analytical and experimental spectra can be anticipated to improve. In the meantime, empirical procedures can be adopted if desired. Also uncertain in the model are the Raman linewidths. As discussed in Appendix I, linewidth variations have been studied. Good agreement is obtained assuming constant values for the linewidths throughout and the model sensitivity is not very acute to the selection. Better fine structure agreement may also require more accurate knowledge of the Raman linewidths and their scaling behavior. For

FIG. 32

COMPUTED CARS SPECTRUM FOR FLAME N_2

T = 1650°K 1.25 CM^{-1} RESOLUTION

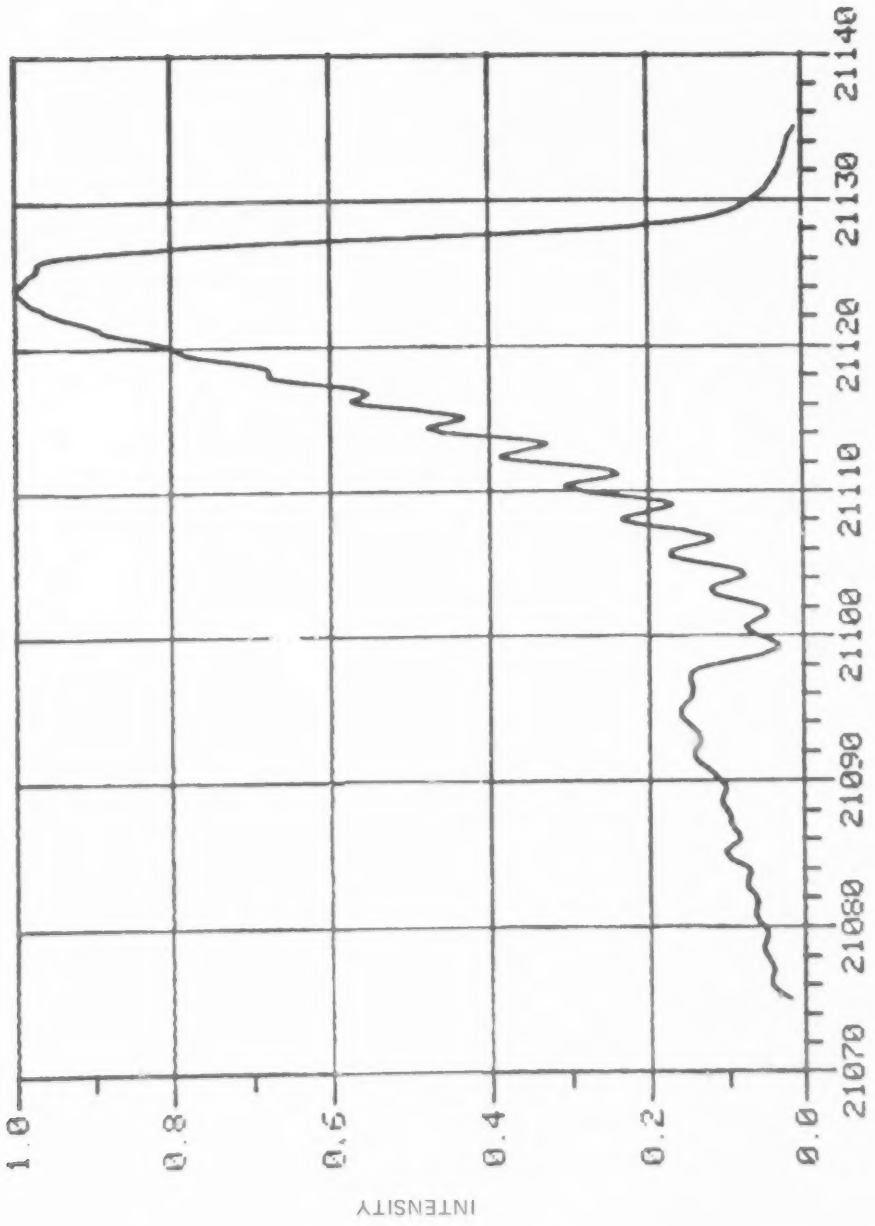

78-02-36-1

the most part, modelling is fairly well in hand and the use of CARS for flame thermometry should pose no unusual problems.

Single Pulse Thermometry

As mentioned earlier, for turbulent flame work, the CARS spectrum must be captured in a single pulse due to the highly nonlinear dependence of CARS on temperature and density. Scanning the spectrum over a period of time would result in an accumulation of terms involving self- and cross-correlations between the density and temperature fluctuations. This obviously would render the spectrum ambiguous from a data reduction standpoint. Furthermore, single shot thermometry leads to a determination of the temperature probability distribution function from which the magnitude of turbulent temperature fluctuations can be obtained.

Single pulse, CARS spectra of flame N_2 were obtained using an optical multichannel analyzer (OMA, PARC) fitted to a 1/4 m monochromator containing a 2400 gr/mm holographic grating. A single CARS pulse was captured using a photographic shutter. Since the laser operated at 10 pps, setting the shutter at a 90 millisecond duration guarantees capturing only one pulse and with high probability. In Fig. 33 is shown the single pulse CARS spectrum of flame N_2 from the previously described flat flame. Collinear phase-matching was employed since these particular tests preceded the demonstration of crossed-beam phase-matching. Each point on the spectrum corresponds to 0.39Å (1.74 cm^{-1}). Also shown as the thin solid line is the computed CARS spectrum at 1700°K but now convolved over a 2.7 cm^{-1} slit function corresponding to the combined monochromator-OMA resolution. This was determined by examining the spectrum of a thin atomic line. As seen the agreement between the OMA trace and the model prediction is quite good. The data presented in Fig. 33 thus demonstrate the feasibility of single pulse CARS thermometry.

In subsequent experiments with the OMA it was found that the OMA vidicon tube was extremely vibration sensitive. In the single pulse thermometry experiments, the mechanical optical shutter was mounted directly in front of the entrance slit, and attached to the monochromator. The slight undulation on the OMA trace apparent in

SINGLE PULSE CARS SPECTRUM OF FLAME N_2

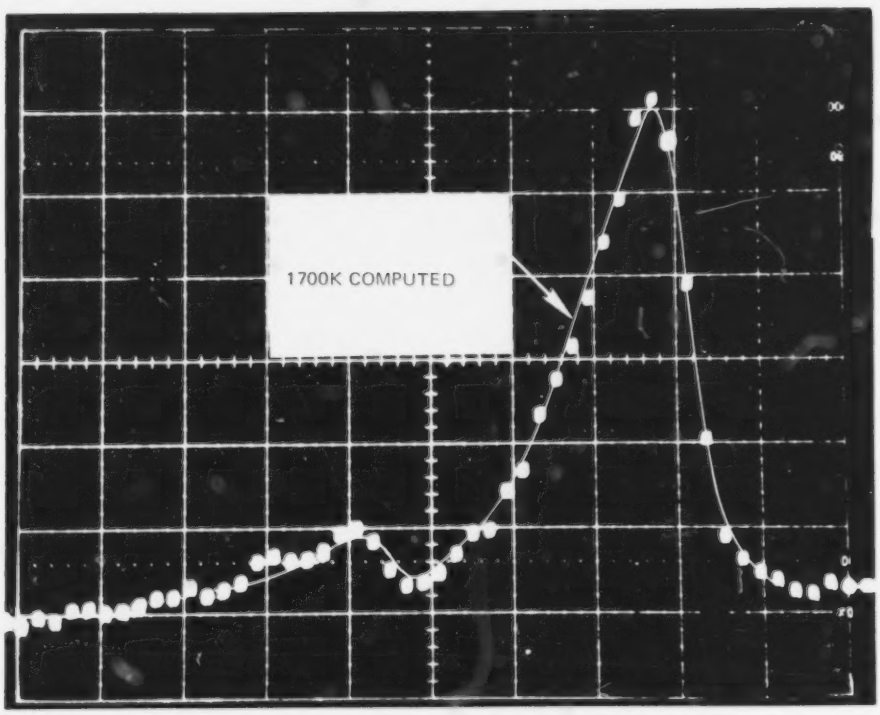

0.4Å PER CHANNEL

the hot band and baseline is probably due to shutter induced vibrations. Vidicon tubes, due to this vibration sensitivity, are probably unsuited for operation in high vibration environments such as combustor test cells. One possible solution which exploits the coherence of the CARS signal is to locate the OMA remotely from the test cell itself, possibly in the control room and transmit the CARS signal to the detector. For thermometry only the relative shape of the spectrum is important and small misalignment jitter may be tolerable. An alternate course is to choose a solid state diode array (e.g. reticon) for multichannel detection.

At the lower spectral resolution currently encountered with state-of-the-art multichannel detectors, the CARS spectra still exhibit fine temperature sensitivity as shown in the model calculations presented in Fig. 34. As temperature increases, the ground state band broadens substantially and the hot band increases as shown. Temperature may be obtained by detailed curve fitting, by the breadth and slope of the ground state band possibly, or by the ratio of the hot to ground state peaks. In fact, qualitatively, low resolution CARS spectra resemble spontaneous Raman spectra and, hence, should be amenable to the same mechanics used to reduce spontaneous Raman data. The low resolution spectra are believed to display enough temperature sensitivity to perform temperature measurements with a resolution of at least 50°K.

Sooting Flame Temperature Measurements

Based upon the Task I review (Ref. 1) together with experience gathered while attempting spontaneous Raman measurements in simulated combustors (Ref. 52), CARS is of great interest because of its potential for operation in the highly particle laden environments typical of practical devices. To investigate this potential CARS generation was studied in a laminar, sooting, propane diffusion flame. Such a flame was studied extensively earlier in conjunction with studies of laser modulated particulate incandescence interferences in Raman scattering diagnostics (Ref. 42). The flame is generally sustained on a stainless steel tube, 0.6 cm i.d., and established by merely flowing propane through the tube. The flame resembles that from

LOW RESOLUTION CARS SPECTRA

SLIT WIDTH 2.7 CM^{-1}

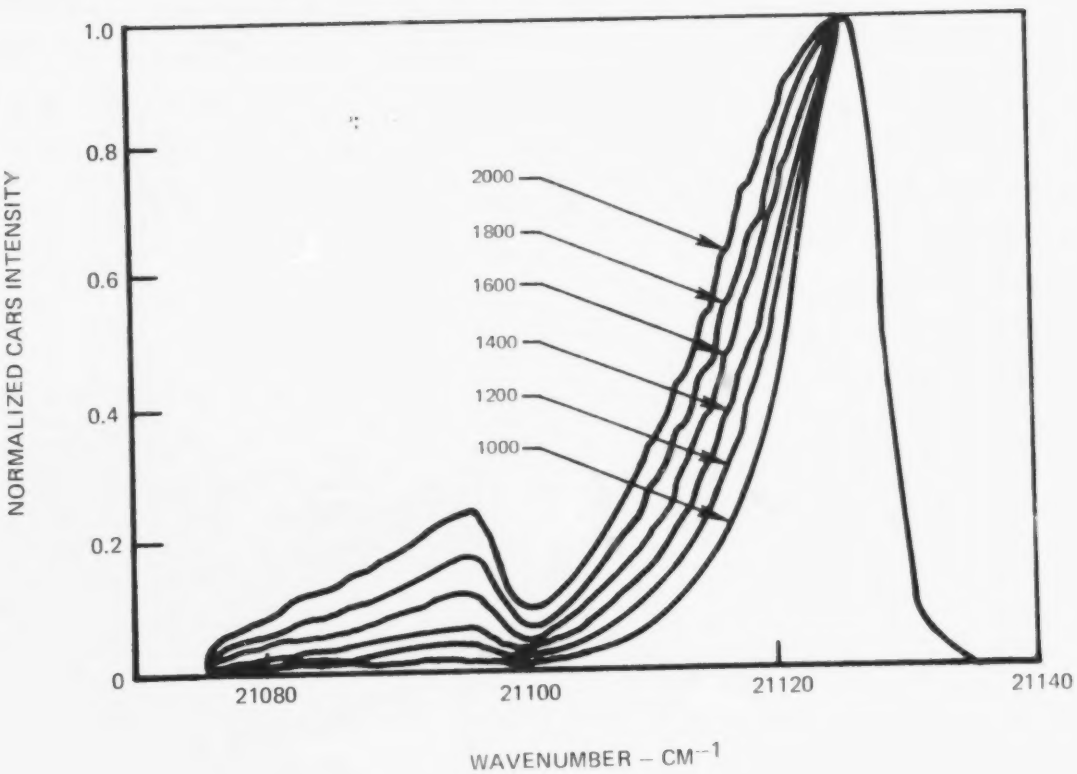

77-11-92-1

a candle and is highly sooting. Previous Mie scattering measurements (Ref. 50) indicated a soot number density on the order of 10^{10} cm^{-3} with an average particle diameter of 400Å. This is a very high soot level producing an attenuation in transmitted light of tenths of percent per mm pathlength. The requisite spatial resolution was achieved via the previously described BOXCARS approach using an 89 mm dia, 305 mm focal length lens. The phase-matching angles of $\alpha = 5.7^{\circ}$ and $\theta = 6.5^{\circ}$ gave the resolution shown in Fig. 29, approximately 0.4 mm in diameter by 1 mm long.

With a two dye component mixture in the dye laser, which produces very broad bandwidths (~ 270 cm^{-1}), the BOXCARS signals were weak necessitating an increase in the monochromator slit width to 400μ, or a resolution of 4 cm^{-1}.* With 4 cm^{-1} resolution, the calculated CARS spectra are not too dissimilar qualitatively from the 2.7 cm^{-1} resolution curves shown in Fig. 34. The broadened ground vibrational state and first hot band are readily apparent and the resolution is sufficient for temperature determinations.

In Fig. 35 is shown one of the first BOXCARS spectra from the highly sooting, laminar propane diffusion flame. As is apparent this spectrum bears no resemblance to the hot N_2 spectra calculated in Fig. 34. The strong spectral feature seen arises from C_2 which has a major Swan band transition at 4737Å midway between the N_2 bands at 4733Å (v=0) and 4740Å (v=1). Swan bands are known to be degraded to the violet (higher wavenumbers) in contrast to the N_2 CARS spectrum. The signal in Fig. 35 consists of both incoherent and, unfortunately, coherent features. The incoherent contribution is ascertained by blocking one of the ω_1 or ω_2 beams, or rotating the optical flat in the ω_2 Stokes beam to phase mismatch the three wave mixing process. Incoherent interferences are generally suppressible in coherent spectroscopy. Coherent features are obviously more problematical. Here the

*It was subsequently discovered that the photomultiplier tube used for the sooting flame measurements was fairly noisy which restricted the tube voltage and, hence, the tube gain, at which good results could be obtained. With the better tube now in use, smaller slit widths probably could have been used.

BOXCARS SPECTRUM FROM LAMINAR, C_3H_8, DIFFUSION FLAME

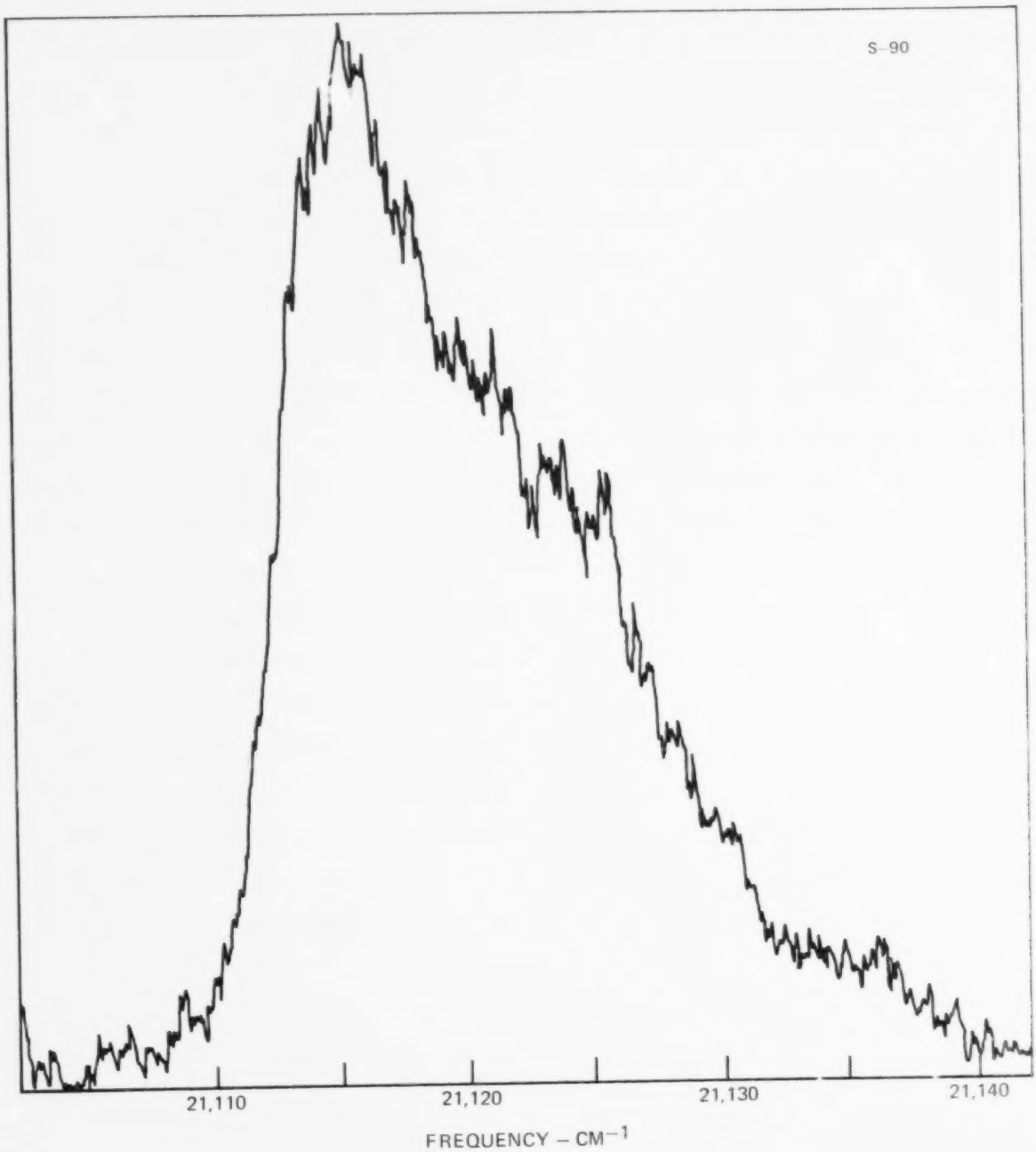

77-12-64-1

coherent feature arises from three wave mixing in laser produced C_2. At the high laser intensities used to produce CARS, significant soot vaporization will occur (Ref. 42), even on a nanosecond time scale. A major product of vaporizing soot is C_2. CARS can be electronically resonantly enhanced when either the CARS radiation itself or the pump component resides near an electronic transition (Ref. 53). The CARS generation in the laser produced C_2 vapor is resonantly enhanced due to the coincidence of the CARS and C_2 electronic transition frequencies. In Fig. 35, the coherent contribution was approximately 25 percent of the total interference and roughly comparable to the CARS N_2 ground state peak. The shoulder in the slope of the Swan spectrum arises from the CARS from the N_2 ground state. Although this result may at first seem discouraging, it is important to bear in mind that the flame was highly sooting and the signal/coherent interference is of order unity. In fact this situation was readily improved. How the improvement came about will be more understandable if reference is made to studies performed in regard to the scaling of the incoherent interferences.

An optical collection system was set up at right angles to the central BOXCARS axis and laser induced emissions examined through blocking and narrowband interference filters. In Fig. 36, the temporal variation of the emissions is shown together with the laser pulse signature for reference. The laser pulse is approximately 10 nsec FWHH in reality, but stretched somewhat in the 31000A photomultiplier (RCA) used here due to its 3 nsec rise and fall time. As seen the emissions at 4733, 5050, and 6864Å exhibit risetimes comparable to the laser pulse. This is due to the fact that there are no effective soot heat transfer processes other than vaporization (Ref. 42) resulting in flashed vaporization of the soot surface. The emissions at 5050 and 6864Å are laser modulated soot incandescences while that at 4733Å is incandescence and primarily, Swan emission at 4737Å within the filter bandpass. The 6864Å trace displays a long tail probably due to the shifting graybody radiation distribution as the particles cool, or possibly, but less likely, some fluorescence contribution.

LASER INDUCED SOOT EMISSIONS

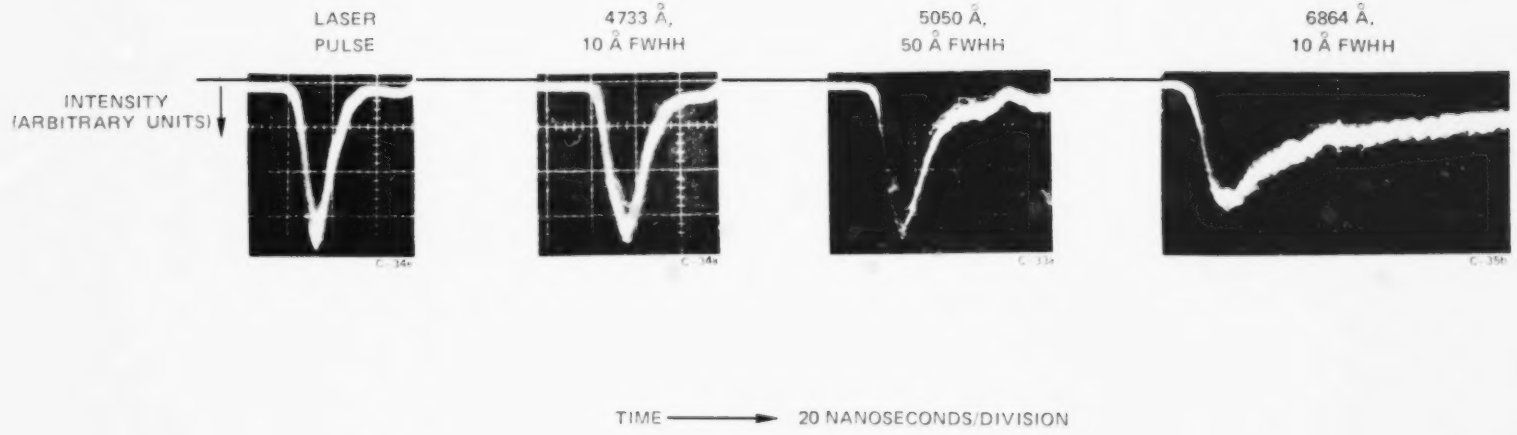

FIG. 36

77-12-64-3

Quantitatively the emissions are quite interesting. By comparing those at 4733Å and 5050Å, the Swan emissions are found to be about an order of magnitude larger than the incandescence contribution. Furthermore, the two emissions display substantially different response to the exciting laser wavelength. For example, the two high intensity ω_1 (5320Å) beams produce slightly more incandescence than does the lower intensity ω_2 beam (6073Å). This is expected due to the saturation behavior of the incandescence described in Ref. 42. The Swan emissions at 4737Å are much more pronounced with the 6073Å excitation, however, than with the 5320Å, probably due to absorption of the broadband 6073Å by three Swan bands residing within the dye laser profile. The Stokes dye laser width of 270 cm^{-1} centered at 16466 cm^{-1} encompassed three strong Swan transitions at 16,333, 16,502, and 16,653 cm^{-1}. Similar results were found for the incoherent interference component when recording the BOXCARS spectrum. Whether the enhanced Swan emission at 4733Å by the Stokes beam (6073Å) is via a direct vapor excitation process or vapor phase absorption leading to increased heating of the laser irradiated soot particle has not been determined.

The result did suggest decreasing the dye laser spectral bandwidth to decrease the C_2 Swan absorptions and to increase the CARS signal strength. Returning to single dye component mixtures decreased the Stokes laser bandwidth by about two to 150 cm^{-1} (still quite sufficient for single pulse multiplex CARS) and quite significantly resulted in about a factor of two increase in dye laser energy as well. Furthermore, since the CARS signal from N_2 using horizontally polarized laser sources is horizontally polarized, Eq. (29), an additional factor of two discrimination against incoherent interferences is obtained by insertion of a polarization filter in the CARS detection system. In so doing, the spectrum shown in Fig. 37 was obtained. Also shown for comparison is the computed CARS spectrum at 2300°K for a 4 cm^{-1} slit width resolution and 0.1 cm^{-1} assumed Raman linewidths. As seen the computer model prediction fits the experimental spectrum fairly well. The adiabatic flame temperature for propane-air is 2250°K (Ref. 54). The rough character of the

FIG. 37

BOXCARS SPECTRUM OF N_2 IN A HIGHLY SOOTING LAMINAR PROPANE DIFFUSION FLAME

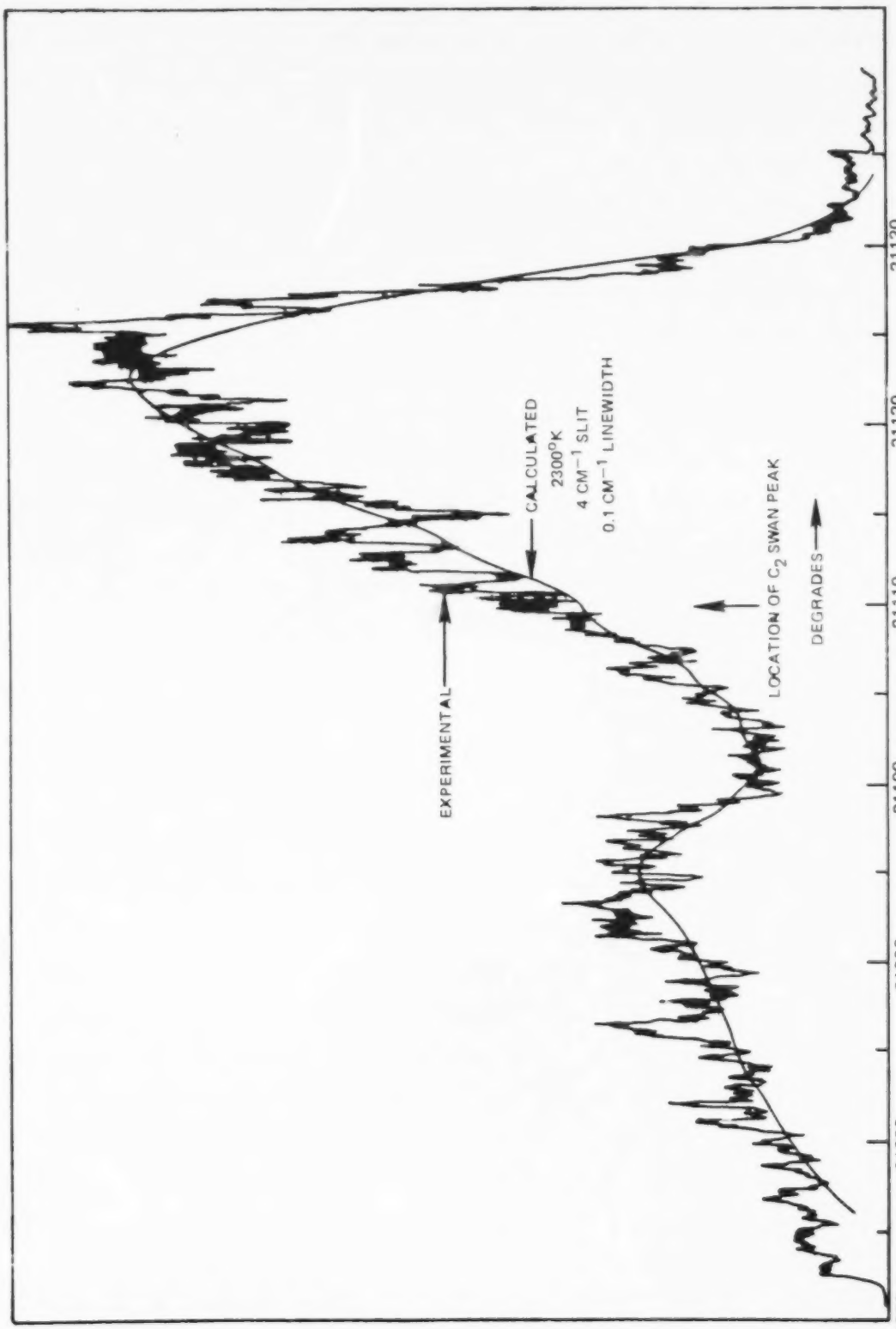

78-1-25-2

experimental spectral trace reflects the compromise made in the number of pulses averaged over, the desire to record the spectrum in a reasonable period of time (10 cm^{-1}/min) and use of a very short output time constant on the averager. Also shown is the location of the beginning of the Swan band head at 21,110 cm^{-1} which peaks at 21,115 (Fig. 35) and degrades to higher wavenumbers. A small amount of electronically resonantly-enhanced CARS from laser produced C_2 is probably present but its contribution is quite small. This result is very encouraging since the soot densities in the laminar propane flame are very high which bodes well for the practical utility of CARS diagnostics.

CO Species Concentration Measurements

Species detection sensitivity is limited for the conventional CARS approach, not due to an inadequacy of signal as is often the case in spontaneous Raman scattering, but due to the presence of the background nonresonant susceptibility. The nonresonant susceptibility is essentially an electronic contribution from all of the molecules present. Species sensitivity limitation is best illustrated by considering the case of a single resonance in the presence of background. The susceptibility may be expressed as before

$$\chi = \chi' + i\chi'' + \chi^{nr} \tag{33}$$

where χ', χ'' and χ^{nr} are respectively the resonant and nonresonant components of the susceptibility. The square of the absolute value of the susceptibility is

$$|\chi|^2 = \chi'^2 + 2\chi'\chi^{nr} + \chi^{nr^2} + \chi''^2 \tag{34}$$

or in the case of a very weak resonance

$$|\chi|^2 \approx \chi^{nr^2} + 2\chi'\chi^{nr} \tag{35}$$

Since χ' varies from negative to positive about line center, the presence of a species in low concentrations is apparent by a similar modulation in the CARS background susceptibility profile. In broadband CARS, the background nonresonant

susceptibility profile merely mirrors the Stokes laser profile. In narrowband, scanned CARS, it reflects the tuning power variation of the Stokes laser. When the species concentration becomes very low, i.e., $\chi' \ll \chi^{nr}$, the "signal" is lost in the background susceptibility profile.

Model Calculations

The foregoing situation is quite evident in the detailed computer calculations of flame CO, some of which are summarized in Fig. 38. There, computer calculations are displayed as a function of CO concentration in the post flame region of an atmospheric pressure CH_4-air flame at 1700°K. The background susceptibility was calculated from the values at 6943Å in Ref. 55 assuming a postflame composition of 70% N_2, 20% H_2O and 10% CO_2. Any variation in the nonresonant susceptibility with wavelength was not accounted for. In the absence of data on the nonresonant susceptibility of H_2O vapor it was assumed to be that of methane. Since H_2O is a major constituent resulting from hydrocarbon combustion, knowledge of its nonresonant susceptibility would be quite valuable. Changes in the composition of flame products which result when varying amounts of CO are produced are not accounted for in the model. The spectra in Fig. 38 have not been convoluted with a spectrometer slit function, but do reflect the limited resolution attainable with a 1.2 cm^{-1} pump laser line. Also note that the ordinate scale is not the same from plot to plot. In all cases shown, the destructive interference dip caused by the resonant portion of the susceptibility going negative is apparent, but clearly less so as the concentration decreases. At the larger concentrations shown, the CO spectrum clearly rises out of the nonresonant background and displays a pronounced hot band. The computer calculations display vividly the species sensitivity limitations of CARS. At the 0.5 percent CO level, the destructive interference causes the spectrum to dip by only about 12 percent and at 0.1 percent CO only by 2 percent. For scanned, laminar flame studies this places very stringent requirements on the pulse-to-pulse stability of the CARS signal. For single pulse work, it places high resolution requirements on the detection system. For the nonresonant susceptibility

COMPUTED FLAME CO SPECTRA

$T = 1700^{O}K$

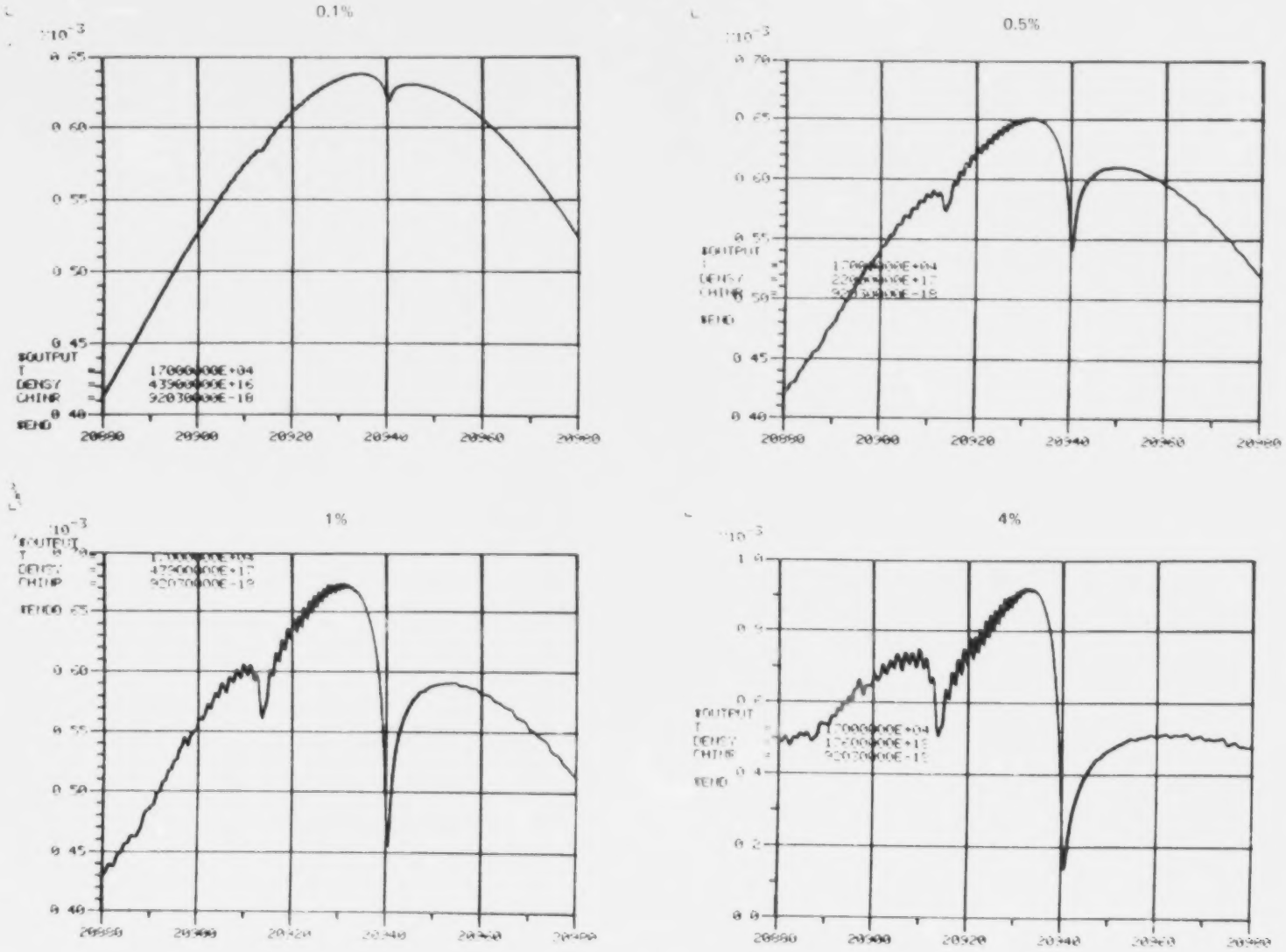

FIG. 38

78-02-153-2

69

selected for these calculations, it would be difficult to measure CO levels below a few tenths of a percent. If the nonresonant susceptibility were larger, the detection sensitivity would be even less. The calculated spectra are quite sensitive to the nonresonant susceptibility value selected. As an example, the 4 percent CO spectrum shown in Fig. 38 but convolved over a 2 cm^{-1} slit function was compared with a similar 4 percent CO spectrum but with double the nonresonant susceptibility used for the Fig. 38 calculations. For double the nonresonant susceptibility, the destructive interference dip from the nonresonant profile decreased to a 33 percent drop compared with 55 percent previously, the ground state band peak to destructive dip ratio decreased from 4 to 2, and the hot band peak to ground state peak height ratio increased to 0.86 from 0.79.

Experimental Approach

Unlike the thermometry studies of flame N_2, one must be quite careful experimentally with species concentration measurements when using collinear phase-matching. For thermometry, one need only eliminate the potential resonant contributions from cool N_2 adjacent to the flame zone. Argon can be conveniently used as a purge gas. In attempting CO measurements, wherein the CO is modulating a non-resonant background, purge gas selection is quite important. Argon, for example, has a slightly larger nonresonant susceptibility than N_2 (Ref. 55), while Helium with a susceptibility more than an order of magnitude lower appears to be the best choice.

With a short focal length lens, f = 20 cm, the cool regions adjacent to the 7.5 cm dia burner apparently did not pose a problem. For example, spectra showed virtually no variation between the situation when room air was adjacent to the burner regions through which ω_1 and ω_2 passed, and when Helium shields were used. The problem encountered with collinear phase-matching, however, was apparently a lack of CO concentration profile uniformity across the "flat" flame. To produce large levels of CO, the flat flame porous plug burner was operated fuel rich, either with excess CH_4 or CO. At these high equivalence ratios, the flat flame exhibited some diffusion flame behavior, i.e., a blue conical outer secondary flame zone was clearly evident. Based on subsequent experience with improved spatial resolution

approaches, it appears that the collinear phase-matched CO spectra were spatially averaged. This appears to be the case even when measurements are made 7 mm above the burner surface. Initial dissatisfaction with collinear phase-matching arose due to lack of agreement between the experimental and computed spectra which led to a suspicion that the results were spatially averaged. Subsequent experience indicates that: (1) the nonresonant susceptibility appears to be quite sensitive to flame conditions and is probably difficult to calculate a priori and (2) the model calculations are fairly sensitive to the magnitude of the nonresonant susceptibility.

BOXCARS was attempted in an effort to improve the spatial resolution. Even at small crossing angles, however, the resolution was apparently too fine and the CARS signals from the flame were very weak. Recall that the CARS radiation strength scales as the square of the interaction length. It should be pointed out the weak CARS signals encountered at high resolution are due in part to the large pump laser bandwidth, 1.2 cm^{-1}, currently existing in the experimental setup. If the laser could be spectrally condensed with no loss of energy to 0.4 cm^{-1} or 0.1 cm^{-1}, the CARS signal would increase by one and two orders of magnitude respectively. The signals would also increase inversely with reductions in the Stokes laser bandwidth. For broadband CARS, it is desirable to keep the Stokes laser bandwidth as small as possible, but yet broad enough to avoid severe distortion of the CARS spectrum.

Based upon experimentation with low angle BOXCARS, it was discovered that CARS generation between the adjacent ω_1 and ω_2 components (Fig. 27), although not perfectly phase matched, could be substantial. Upon attempting crossed-beam, phase-mismatched CARS, the nonresonant CARS signal from the flame was found to be within the detection sensitivity of the apparatus. Consequently, the CO studies reported here employed this crossed-beam, phase-mismatched approach. A 305 mm focal length lens was used and the pump and Stokes lasers were crossed at an angle of 1.8°. At this angular separation, the beams intersected only over the burner and near its centerline. Hence no contributions from cool regions outside the burner were possible. The spatial resolution was checked in the usual way by monitoring the CARS signal generated from a translatable microscope slide and is shown in

Fig. 39. As seen, all of the signal is generated within a 2.5 cm extent but the CARS originates predominantly within ± 0.5 cm of the crossing point.

An interesting aspect of crossed-beam, phase-mismatched CARS is the direction of the emergent CARS signal radiation. One possibility is for the CARS beam to emanate in the direction suggested by Fig. 25a. This was found not to be the case. Rather the CARS emerged between the crossed Stokes and pump beams indicating that the CARS generation occurs along the nominal phase-matching direction in the medium, despite the fact that ω_1 and ω_2 are angled.

To measure the amount of CO produced in the flame, an uncooled quartz microprobe was used to sample the centerline CO concentration the level of which was indicated by a Beckman Model 864 ndir analyzer. Sampling with uncooled probes in high pressure flames is subject to some uncertainty, and the microprobe results may only be roughly indicative of the actual CO levels (Ref. 56).

Measurements

In Fig. 40 is shown the CARS spectrum recorded for an ndir reading of 3.9 percent CO in a CO-CH_4-air "flat" flame. The spectrum was obtained 7 mm above the burner surface . Due to various fluctuations in the laser, flame, etc., even the averaged CARS signal is subject to fluctuations on the order of about ± 10 percent. In the spectrum shown, 100μ slits corresponding to a nominal 1 cm^{-1} resolution were employed. Also shown as the series of points is the 4 percent CO model calculation in Fig. 38 convolved over a 1 cm^{-1} slit function. As seen the agreement between the experimental spectrum and the model calculation is quite good.

The quality of the spectra degraded rapidly, however, at lower CO concentrations indicated by the quartz microprobe sampling system. For given CH_4-air settings, the CO spectra obtained at lower CO flame levels as the CO doping level was reduced did not behave as those shown in Fig. 38. Modulation of the CARS spectrum was apparent at the 2 percent level and to the trained eye at 1 percent in the presence of the random spectral fuctuations. The spectra had the qualitative appearance of CO levels within a higher nonresonant susceptibility. It is not

CROSSED-BEAM, PHASE MISMATCHED CARS SPATIAL RESOLUTION

1.8° CROSSING ANGLE, 305MM FOCAL LENGTH LENS

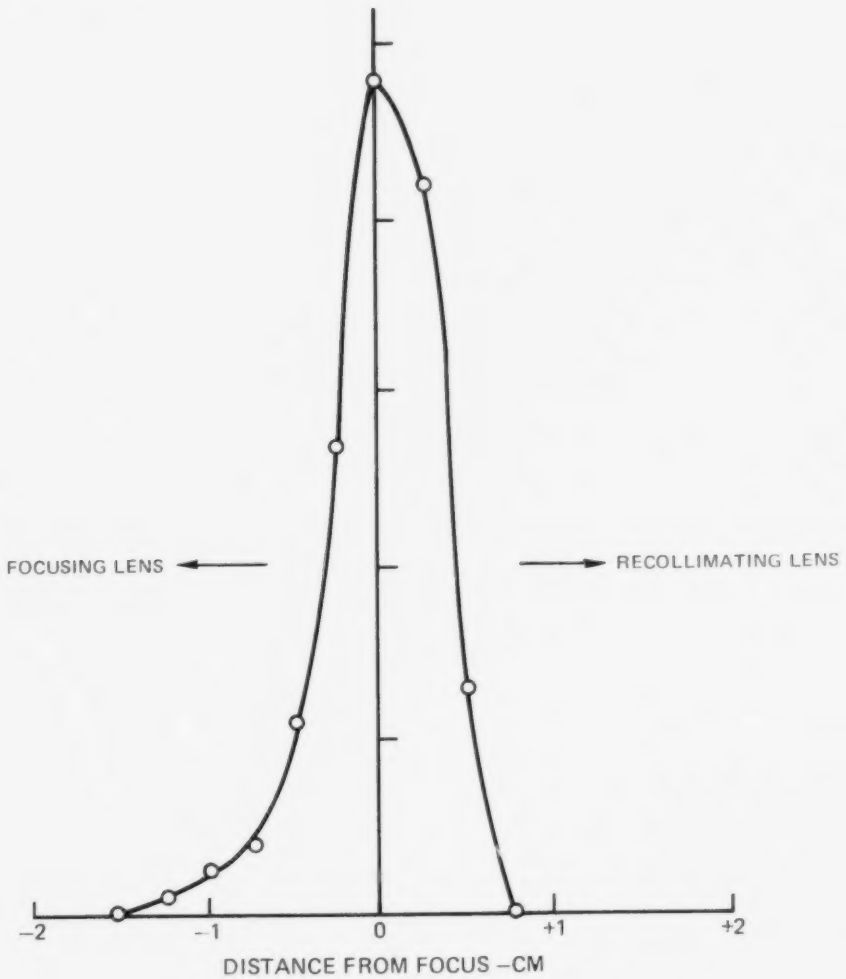

78-02-195-3

FIG. 40

CROSSED-BEAM, PHASE MISMATCHED, CARS SPECTRUM OF FLAME CO

- COMPUTER MODEL
  - $T = 1700^0K$
  - $\chi^{nr} = 9.2\,(10^{-19})\,CM^3/ERG$
  - $CO = 4\%$
  - MEASURED CO (+4DIR) 3.9%

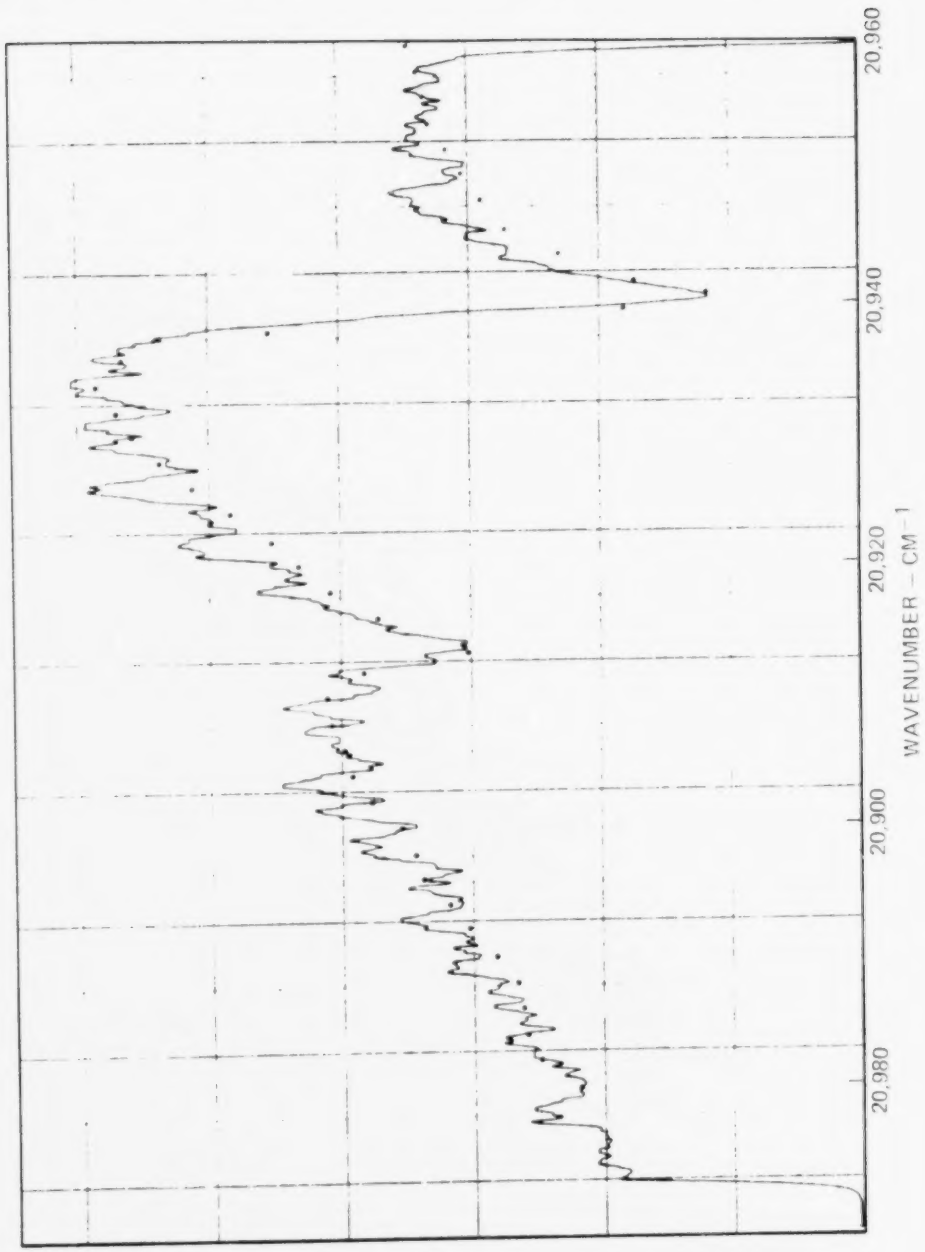

78-02-195-2

beyond the realm of possibility, however (Ref. 56), that the CO in the flame is actually lower than that indicated by the sampling system due to CO_2 reduction in the high pressure ($\sim$ 680 torr), hot quartz microprobe and sampling lines. CO measurements with a water-cooled quartz microprobe indicated a CO level comparable to the uncooled probe in CH_4-air mixtures, however.

CARS spectral differences were noted at the nominal 4 percent level depending upon how the CO was produced. In Fig. 41 is shown the CARS CO spectrum obtained in a rich CH_4-air flame with no added CO. Assuming for the moment that the microprobe sample was correct, this spectrum differs markedly from that shown in Fig. 40 in which large amounts of CO were added to the flame. One explanation for the Fig. 41 spectrum is that the nonresonant susceptibility is larger than before. CH_4 has a nonresonant susceptibility over twice that of N_2 and to produce the 4 percent CO level, over twice the CH_4 flow relative to that required to sustain the flame was employed. It is also possible, however, that under these conditions the CO level in the flame was lower than that indicated by the ndir analyzer as previously mentioned. Incidentally, the large peak in the center of the ground vibrational state band is real and reproducible and does not result from CO. Its assignment is unknown, perhaps originating from a hydrocarbon fragment.

CARS measurements of CO species concentration in the presence of an uncertain nonresonant susceptibility requires a three parameter model fit involving the concentration, temperature and nonresonant susceptibility. An important question yet to be thoroughly studied concerns the uniqueness of a three parameter fit to species concentration data. Clearly species concentration measurements would not be possible in an unknown, nonresonant background if uniqueness does not exist. Experimentally, measurements were possible only to the 1-2 percent level at best. Analytically species concentration measurements would be practically possible to the 0.5 percent level or so (Fig. 38) for the nonresonant susceptibility assumed. Clearly CARS approaches which lead to a cancellation of the background nonresonant susceptibility, some of which are reviewed in Ref. 1, would seem desirable for species concentration measurements.

Conclusions based upon all of the foregoing CARS investigations are summarized in Section III which follows, together with recommendations for future developmental efforts.

FIG. 41

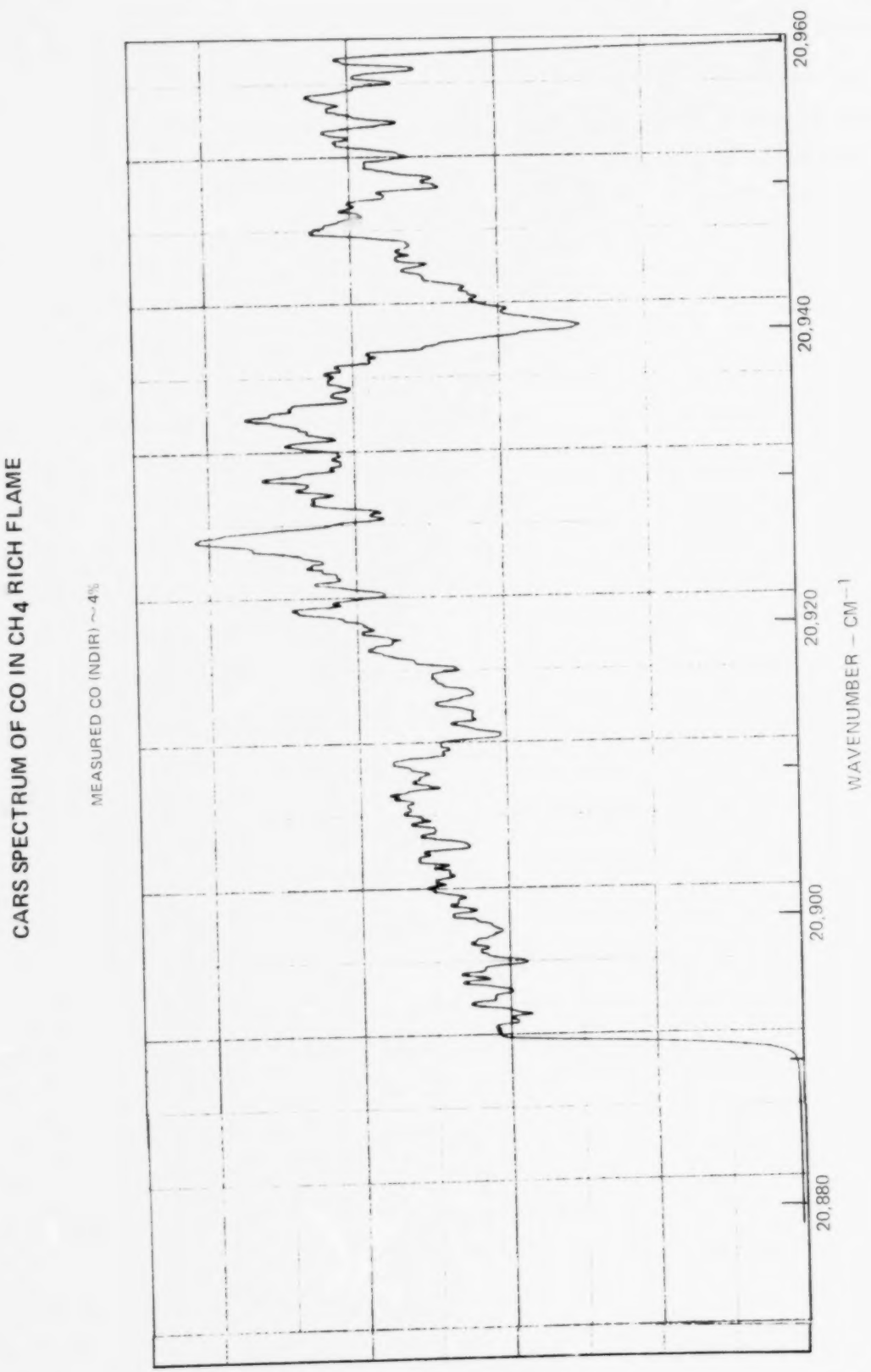
CARS SPECTRUM OF CO IN CH_4 RICH FLAME
MEASURED CO (NDIR) ~4%
20,960
20,940
20,920
20,900
20,880
WAVENUMBER – CM^{-1}
78-02-195-1

SECTION III

CONCLUSIONS AND RECOMMENDATIONS

Saturated Laser Fluorescence Investigations

The Task II experimental investigations of laser fluorescence have shown that it is possible to saturate laser excited molecular fluorescence from the flame radicals CH and CN. Accordingly, this permits determination of these radicals without the inherent imprecision arising from uncertain analytical quenching corrections in unsaturated fluorescence. The laser spectral intensities required to achieve saturation are readily attainable and in the 10^5 to 10^6 Watts/cm^2 cm^{-1} range for CH and CN. Fluorescence signals were obtained in very hot flames from concentrations, as determined by absorption, of ~ 60 ppm for CH and 150 ppm for CN, thus confirming the sensitivity of the saturated fluorescence technique. Based upon the signal levels experienced, saturated fluorescence should be capable of detecting minority flame species at the ppm concentration level. Combining the saturated fluorescence investigations with absorption serves to assess rigorously the validity of the saturated fluorescence approach. The saturated fluorescence results were lower by a factor of two for CH and four for CN than the species concentrations determined by absorption. This discrepancy is believed due to the possibility that the region of CH and CN production was smaller than the fluorescence sample volume. In effect the sample volume is overestimated, leading to an underestimate of the species concentration required to produce a certain fluorescence intensity level. Furthermore, the results of this work indicate that the two-level saturated fluorescence theory appears to be applicable to molecules, such as CN, which, in reality, are considerably more complex. CN, for example, approximates a three level system from an electronic energy level viewpoint and is even more complex when the various vibrational and rotational level are accounted for. This is consistent with findings of Baronavski and McDonald who successfully applied the two level model to C_2 which is also considerably more complex than a two-level system.

It would be desirable to repeat the CH and CN experiments reported here with an improved experimental approach. In this way, the optimistic conclusions reached in these first experiments concerning the viability of saturated laser fluorescence detection could be more definitively checked. Key to an improved experiment is an improved beam quality, narrower linewidth, repetitively pulsed dye laser. Improved beam quality would permit greater experimental versatility and permit much smaller focal diameters to be achieved. This would eliminate the previously supposed problem of a measurement volume larger than the radical production region. Narrower linewidth than that employed here would permit higher spectral intensities to be attained and allow more selective excitation of the fluorescence spectrum. Repetitive pulsing at 10 to 20 pps would permit the employment of boxcar averaging techniques for greatly improved signal to noise ratio and permit the fluorescence spectrum to be continuously scanned. Laser pumped dye lasers could provide the improved beam quality, narrower linewidth, and repetition rate required to upgrade the fluorescence experiments. A suitable drive laser would be a pulsed neodymium laser system similar to the CARS driver operating at either the second or third harmonic. For CH and CN the third harmonic at 3533Å would be used to pump suitable dyes directly to probe these radicals at 4315 and 3883Å, respectively. For NO, the third harmonic would pump a tunable dye laser which in turn would be frequency-doubled to probe the NO γ bands at 2265Å. For OH at 3064Å and NH at 3350Å, the second harmonic at 5320Å would pump a tunable dye laser which would be frequency doubled to the appropriate absorptions. For C_2 no frequency doubling of the second harmonic pumped dye laser is necessary. The 10 nanosecond pulse length of the Q-switched neodymium laser ensures high intensities which result in efficient dye laser and various harmonic generation efficiencies. The 10-20 pps repetition rate of such a laser permits the use of commercially available boxcar averagers. Laser pumped dye lasers can also be spectrally condensed much more efficiently and to fairly narrow linewidths, ~ 0.1Å. Quite interesting, with such a system, it would be possible to perform both the absorption and the fluorescence measurements simul-

taneously using the spectrally narrow dye laser. By using the same laser source for absorption and fluorescence, one is assured that the interaction region is the same for both measurements. To reduce the concentration gradients in the flame, it would be desirable to perform the initial experiments on a low pressure flat flame, multipass if necessary.

Subsequent to the investigations of CH and CN, it is recommended that the applicability of saturated fluorescence to other molecules be explored. Due to its extreme importance, NO would be the most logical candidate molecule to investigate. This is quite convenient experimentally, in that the neodymium third harmonic pumped dye laser used for the CH work would be tuned to a slightly higher wavelength and then frequency doubled. The high sensitivity, in-situ, spatially precise detection of NO via saturated laser fluorescence is a very exciting possibility and should be explored in the near future. Due to its importance in combustion, investigations of OH hydroxyl radical detection would also be desirable.

CARS Investigations in Flames

Coherent anti-Stokes Raman spectroscopy is capable of providing both temperature and species concentration measurements in flames and the Task II experimental program in this area mirrored this duality. Although thermometry was accorded the major emphasis, much of the experience gained during the CARS investigations of flame N_2 is applicable to species detection applications, e.g. spatial resolution enhancement. During the Task II investigations, a crossed-beam phase-matching technique, termed BOXCARS, was devised which greatly improves upon and eliminates any ambiguity in regard to the spatial resolution of CARS. Conventional, collinear phase-matching can possess poor and ambiguous resolution particularly in the presence of density gradients. This was a major problem area for the diagnostic application of CARS which has now been overcome. The moderate (~ 1 cm^{-1}) resolution spectral scans of CARS from flame N_2 show excellent agreement with the predictions of the CARS computer code and demonstrate the suitability of CARS for thermometry. Single shot, lower resolution CARS spectra from flame N_2 obtained with an optical multi-

channel analyzer (OMA) also show good agreement with the code predictions and demonstrate the feasibility of single pulse thermometry. Such a capability will permit temperature probability distribution functions to be measured in turbulent combustion processes from which the magnitude of turbulent temperature fluctuations can be ascertained. Although coherent spectral interferences have been encountered in thermometry investigations in highly sooting flames, these seem to be well understood, not too serious and suppressible. With appropriate Stokes laser bandwidth selection and detection technique, CARS spectra of N_2 in highly sooting propane diffusion flames have been obtained permitting temperature determinations in such flames. This is believed to be the first temperature measurement in such flames with a remote, spatially precise technique. CARS is of intense interest because of its very promising potential for probing practical combustion environments. Based upon the Task II experimental investigations, which have certainly demonstrated this potential in laboratory studies, it is recommended that CARS thermometry now be attempted in a practical combustion facility, e.g., research scale furnace. Such attempts would serve to uncover new and unanticipated difficulties, if any, and provide the opportunity to explore the operational limits for CARS diagnostics in practical environments.

CARS CO spectra have been obtained at the 4 percent level which show quite good agreement with the model code predictions. The spectra are quite interesting, particularly with respect to the appearance of destructive interference effects. These occur because of the modulation of the nonresonant susceptibility profile by the real part of the resonant susceptibility. As the CO concentration level is reduced, this modulation of the nonresonant susceptibility background is reduced, and the "signal" disappears into the background profile. The CO detectability studies have demonstrated both experimentally and analytically that for typical combustion molecules such as CO, conventional CARS approaches are limited in species sensitivity to about the 0.5 percent level. Detectivity is quite sensitive to flame conditions. Conventional CARS measurements will require a three parameter fit to the spectrum to ascertain the concentration and further study is required to

demonstrate the uniqueness of such fitting procedures. If indeed the spectra are unique, then species concentrations measurements can be made based upon the shape of the spectrum and not necessarily from the magnitude of the signal which would be quite advantageous. Unfortunately, conventional CARS permits measurements generally only to the several tenths of a percent level. To increase the concentration sensitivity of CARS, the relative contribution to the CARS signal from the nonresonant susceptibility must be reduced. There are several approaches to accomplish this end as reviewed in Ref. 1 such as resonance enhancement, double resonance exploitation, and polarization orientation approaches. The latter two have only been demonstrated in liquids. Resonance enhancement has been demonstrated in I_2, but is not widely applicable since many molecules of combustion interest have resonances too far into the ultraviolet to be easily accessible. The most promising near term approach involves polarization orientation. With conventional phase-matching this involves the use of "three colors." Three beams at frequencies ω_o, ω_1 and ω_2 are used and by proper arrangement of the polarization directions, it is possible to greatly reduce or eliminate the nonresonant susceptibility contribution. With crossed-beam phase-matching (BOXCARS) it is not necessary to employ a third frequency since the pump beam is already split into two components and angled. It is recommended that polarization orientation BOXCARS investigations be pursued as an avenue toward enhancing the species sensitivity capabilities of CARS.

SECTION IV

REFERENCES

1. Eckbreth, A. C., P. A. Bonczyk and J. F. Verdieck: Review of Laser Raman and Fluorescence Techniques for Practical Combustion Diagnostics. EPA Report R77-952665-6, February 1977.

2. Eckbreth, A. C., P. A. Bonczyk and J. F. Verdieck: Laser Raman and Fluorescence Techniques for Practical Combustion Diagnostics. Appl. Spect. Rev., Vol. 13, pp. 15-164, January 1978.

3. Piepmeier, E. H.: Theory of Laser Saturated Atomic Resonance Fluorescence. Spectrochimica Acta, Vol. 27B, pp. 431-443 (1972).

4. Daily, J. W.: Saturation Effects in Laser Induced Fluorescence Spectroscopy. Appl. Opt., Vol. 16, pp. 568-571, March 1977.

5. Baronavski, A. P. and J. R. McDonald: Measurement of C_2 Concentrations in an Oxygen-Acetylene Flame: An Application of Saturation Spectroscopy. J. Chem. Phys., Vol. 66, pp. 3300-3301, April 1, 1977.

6. Mitchell, A. C. G. and M. W. Zemansky: Resonance Radiation and Excited Atoms Cambridge University Press (1971).

7. Pearse, R. W. B. and A. G. Gaydon: The Identification of Molecular Spectra Fourth Ed., Chapman and Hall, London (1976).

8. Eckbreth, A. C. and J. W. Davis: Spatial Resolution Enhancement in Coaxial Light Scattering Geometries. Appl. Opt., Vol. 16, pp. 804-806, April 1977.

9. Bleekrode, R. and W. C. Nieuwpoort: Absorption and Emission Measurements of C_2 and CH Electronic Bands in Low-Pressure Oxyacetylene Flames. J. Chem. Phys., Vol. 43, pp. 3680-3687, November 15, 1965.

10. Jessen, P. F. and A. G. Gaydon: Study of the Absorption Spectra of Free Radicals in Flames. Comb. and Flame, Vol. 11, pp. 11-16, February 1967.

11. Bleekrode, R.: Absorption and Emission Spectroscopy of C_2, CH and OH in Low-Pressure Oxyacetylene Flames. Philips Res. Repts. Suppl. No. 7, pp. 1-64 (1967).

12. Jessen, P. F. and A. G. Gaydon: Estimation of Carbon Radical Concentration in Fuel-Rich Acetylene-Oxygen Flames by Absorption Spectroscopy. Twelfth Symposium (International) on Combustion, pp. 481-489, The Combustion Institute (1969).

REFERENCES (Cont'd)

13. Bulewicz, E. M., P. J. Padley and R. E. Smith: Spectroscopic Studies of C_2, CH and OH Radicals in Low Pressure Acetylene and Oxygen Flames. Proc. Roy. Soc., Vol. A315, pp. 129-148 (1970).

14. Bulewicz, E. M., P. J. Padley and R. E. Smith: Elementary Combustion Processes in Cyanogen and Oxygen and Hydrogen Flames: Spectroscopic Studies. Fourteenth Symposium (International) on Combustion, pp. 329-341, The Combustion Institute (1973).

15. Beenakker, C. I. M., P. J. F. Verbeck, G. R. Mohlmann and F. J. de Heer: The Intensity Distribution in the CH ($A^2\Delta$ - $X^2\Pi$) Spectrum Produced by Electron Impact on Acetylene. J. Quant. Spectros. Radiat. Transfer, Vol. 15, pp. 333-340 (1975).

16. Hesser, J. E. and B. L. Lutz: Probabilities for Radiation and Predissociation II. The Excited States of CH, CD and CH^+ and Some Astrophysical Implications. Astrophys. J., Vol. 159, pp. 703-718, February 1970.

17. Liszt, H. S. and W. H. Smith: RKR Franck-Condon Factors for Blue and Ultraviolet Transitions of Some Molecules of Astrophysical Interest and Some Comments on the Interstellar Abundance of CH, CH^+ and SiH. J. Quant. Spectros. Radiat. Transfer, Vol. 12, pp. 947-958 (1972).

18. Moore, C. E. and H. P. Broida: CH in the Solar Spectrum. J. Res. Natl. Bur. Std., Vol. 63A, pp. 19-53, August 1959.

19. Luk, C. K. and R. Bersohn: Time Dependence of the Fluorescence of the B State of CN. J. Chem. Phys., Vol. 58, pp. 2153-2163, March 1973.

20. Nicholls, R. W.: Franck-Condon Factors to High Vibrational Quantum Numbers III. CN. J. Res. Natl. Bur. Std., Vol. 68A, pp. 75-78, Jan.-Feb., 1964.

21. Jevons, W.: The More Refrangible Band System of Cyanogen as Developed in Active Nitrogen. Proc. Roy. Soc. (London), Vol. 112A, pp. 407-441 (1926).

22. Suchard, S. N.: Spectroscopic Data, Vol. I. Plenum Press (New York) (1974).

23. Jevons, W.: Report on Band-Spectra of Diatomic Molecules. The Physical Society (London) (1932).

24. Bennett, R. G. and F. W. Dalby: Experimental Oscillator Strengths of CN and NH. J. Chem. Phys., Vol. 32, pp. 1716-1719, June 1960.

REFERENCES (Cont'd)

25. Gaydon, A. G.: The Spectroscopy of Flames, 2nd Edition, J. Wiley and Sons (New York) (1974).

26. Daily, J. W.: Saturation of Fluorescence in Flames with a Gaussian Laser Beam. Appl. Opt., Vol. 17, pp. 225-229, January 15, 1978.

27. Regnier, P. R. and J. P. E. Taran: On the Possibility of Measuring Gas Concentrations by Stimulated Anti-Stokes Scattering. Appl. Phys. Lett., Vol. 23, pp. 240-242, September 1973.

28. Regnier, P. R., F. Moya and J. P. E. Taran: Gas Concentration Measurement by Coherent Raman Anti-Stokes Scattering. AIAA Paper 73-702, AIAA 6th Fluid and Plasma Dynamics Conference, Palm Springs, CA, July 1973.

29. Moya, F. S., S. A. J. Druet and J. P. E. Taran: Gas Spectroscopy and Temperature Measurement by Coherent Raman Anti-Stokes Scattering. Opt. Comm., Vol. 13, pp. 169-174, February 1975.

30. Regnier, P. R., F. Moya and J. P. E. Taran: Gas Concentration Measurement by Coherent Raman Anti-Stokes Scattering. AIAA J., Vol. 12, pp. 826-831, June 1974.

31. Moya, F., S. Druet, M. Pealat and J. P. Taran: Flame Investigation by Coherent Anti-Stokes Raman Scattering. pp. 549-575 in B. T. Zinn, Ed., Experimental Diagnostics in Gas Phase Combustion Systems, AIAA, New York, NY, 1977.

32. Maker, P. D. and R. W. Terhune: Study of Optical Effects Due to an Induced Polarization Third Order in Electric Field Strength. Phys. Rev., Vol. 137, pp. A801-A818, February 1965.

33. Begley, R. F., A. B. Harvey and R. L. Byer: Coherent Anti-Stokes Raman Spectroscopy. Appl. Phys. Letts., Vol. 25, pp. 387-390, October 1974.

34. Harvey, A. B., J. R. McDonald and W. M. Tolles: Analytical Applications of a New Spectroscopic Tool: Coherent Anti-Stokes Raman Spectroscopy (CARS) in Progress in Analytical Chemistry, Plenum Press.

35. Tolles, W. M., J. W. Nibler, J. R. McDonald and A. B. Harvey: A Review of the Theory and Application of Coherent Anti-Stokes Raman Spectroscopy (CARS). Appl. Spect., Vol. 31, pp. 253-272 (1977).

36. Nibler, J. W., J. R. McDonald and A. B. Harvey: CARS Measurement of Vibrational Temperature in Electric Discharges. Opt. Comm., Vol. 18, pp. 371-373, August 1976.

37. Nibler, J. W., W. M. Shaub, J. R. McDonald and A. B. Harvey: Coherent Anti-Stokes Raman Spectroscopy. pp. 173-225 in J. R. Durig, Ed., Vibrational Spectra and Structure, Vol. 6, Elsevier, Amsterdam (1977).

38. Barrett, J. J. and R. F. Begley: Low-Power CW Generation of Coherent Anti-Stokes Raman Radiation in CH_4 Gas. Appl. Phys. Letts., Vol. 27, pp. 129-131, (1975).

39. Barrett, J. J.: Generation of Coherent Anti-Stokes Rotational Raman Radiation in Hydrogen Gas. Appl. Phys. Letts., Vol. 29, pp. 722-724, December 1976.

40. Roh, W. B., P. W. Schreiber and J. P. E. Taran: Single-Pulse Coherent Anti-Stokes Raman Scattering. Appl. Phys. Letts., Vol. 29, pp. 174-176, August 1976.

41. Nibler, J. W. and G. V. Knighten: Coherent Anti-Stokes Raman Spectroscopy in A. Weber, Ed., Topics in Current Physics, Chapter 7, Springer Verlag, Stuttgart (1977).

42. Eckbreth, A. C.: Effect of Laser-Modulated Particulate Incandescence on Raman Scattering Diagnostics. J. Appl. Phys., Vol. 48, pp. 4473-4479, November 1977.

43. Exciton Chemical Company, Dayton, OH.

44. Shaub, W. M., A. B. Harvey and G. C. Bjorklund: Power Generation in Coherent Anti-Stokes Raman Spectroscopy with Focused Laser Beams. J. Chem. Phys., to be published.

45. Eckbreth, A. C.: BOXCARS: Crossed-Beam Phase-Matched CARS Generation in Gases. Appl. Phys. Lett., March 1978.

46. Rahn, L., Sandia Laboratories, Livermore, CA: private communication.

47. Hellwarth, R. W.: Third-Order Optical Susceptibilities of Liquids and Solids, Pergamon Press, Oxford (1977).

48. Penney, C. M., L. M. Goldman and M. Lapp: Raman Scattering Cross Sections. Nat. Phys. Sci., Vol. 235, pp. 110-112, February 1972.

49. Bonczyk, P. A., A. C. Eckbreth and J. A. Shirley: Species Composition and Temperature Measurements in Flames. Monthly Progress Report for the Period September 27, 1977 to October 26, 1977 for EPA Contract 68-02-2176, UTRC Report R77-952665-14, November 1977.

50. Eckbreth, A. C.: Applicability of Laser Raman Scattering Diagnostic Techniques to Practical Combustion Systems. Project SQUID Technical Report UTRC-4-PU, October 1976.

51. Suchard, S. N.: Spectroscopic Constants for Selected Diatomic Molecules. Air Force Report No. SAMSO-TR-74-82, Aerospace Corp., Los Angeles, CA (1974).

52. Eckbreth, A. C.: Laser Raman Thermometry Experiments in Simulated Combustor Environments. pp. 517-547 in B. T. Zinn, Ed., Experimental Diagnostics in Gas Phase Combustion Systems, AIAA New York, NY (1977).

53. Hudson, B., W. Hetherington III, S. Cramer, I. Chabay and G. K. Klauminzer: Resonance Enhanced Coherent Anti-Stokes Raman Scattering. Proc. Natl. Acad. Sci. U.S.A., Vol. 73, pp. 3798-3802, November 1976.

54. Kanury, A. M.: Introduction to Combustion Phenomena, Gordon and Breach, New York, p. 131 (1975).

55. Rado, W. G.: The Nonlinear Third Order Dielectric Susceptibility Coefficients of Gases and Optical Third Harmonic Generation. Appl. Phys. Letts., Vol. 11, pp. 123-125, August 1967.

56. Samuelson, G. S. and J. N. Harman, III: Chemical Transformations of Nitrogen Oxides While Sampling Combustion Products. J. Air. Poll. Cont. Asst., Vol. 27, pp. 648-655, July 1977.

APPENDIX I

CARS Spectra of Combustion Gases

by

R. J. Hall
United Technologies Research Center
East Hartford, Connecticut 06108

ABSTRACT

Computer-generated CARS spectra, necessary for temperature and species concentration measurements in combustion environments, are presented. The third-order, nonlinear electric susceptibility governing CARS generation from N_2 and CO has been programmed in terms of a Boltzmann distribution of vibration-rotation states and the normal Raman cross-sections. Finite pump laser widths and instrumental effects are accounted for by appropriate convolutions. Examples of flame temperature (N_2) and minority species concentration (CO) measurements using these theoretical spectra are presented.

Introduction

Coherent Anti-Stokes Raman Spectroscopy (CARS) is a nonlinear, three-wave optical mixing technique with considerable promise for combustion diagnostics (Refs. 1-7). Its high potential conversion efficiency and coherence make it well suited for thermometry and species concentration measurements in combustion environments; relative to normal Raman spectroscopy, CARS offers superior discrimination against incoherent fluorescence, background luminosity and particulate incandescence. The advantages and disadvantages of CARS for combustion diagnostics are discussed in Ref. (7).

Data reduction in CARS is less straightforward than in conventional Raman spectroscopy, however, a complication arising from spectral interference effects in CARS. Signal strength in normal vibrational Raman spectroscopy is a simple sum of contributions from neighboring transitions, resulting in a signal directly proportional to vibrational state population. A CARS signal, however, is affected by interferences between neighboring transitions and between resonant and nonresonant contributions to the electric susceptibility. These interference effects complicate CARS data reduction, and generally require that temperature or concentration measurements be made by fitting computer-generated theoretical spectra to experiment. This paper describes a model which generates synthetic CARS spectra, and gives examples of thermometry and minority species concentration measurement in an air-methane, atmospheric flame.

Theory

The basic theory of the CARS effect has been presented extensively elsewhere (Refs. 1-6). Thus, only the important results needed for calculations are summarized herein. For monochromatic, phase-matched pump lasers (powers P_1 and P_2) the CARS generated power at $\omega_3 = 2\omega_1 - \omega_2$ is proportional to:

$$P_1^2 P_2 |\chi|^2 \tag{1}$$

where χ is the complex, third order electric susceptibility. When the frequency difference $\omega_1 - \omega_2$ is tuned to a Raman-active molecular transition, resonance contributions to χ become important and we may write

$$\chi = \chi_R' + i\chi_R'' + \chi_{NR} \tag{2}$$

If homogeneously broadened transitions are assumed the resonant contributions to χ can be expressed as a sum over neighboring transitions:

$$\chi_R = \chi_R' + i\chi_R'' = \sum_j K_j \frac{\gamma_j}{2\Delta\omega_j - i\gamma_j} \tag{3}$$

where the j summation is over all Q, O, and S ($\Delta J = 0, \pm 2$) vibration-rotation transitions in the vicinity of $\omega_1 - \omega_2$, γ_j is the homogeneous linewidth (FWHM), and $\Delta\omega_j$ is the detuning $\omega_j - (\omega_1 - \omega_2)$. The modulus K_j can be shown to be related to the normal Raman scattering cross-section by the relationship

$$K_j = \frac{2c^4}{\hbar\omega_2^4} N\Delta_j \left.\frac{d\sigma}{d\Omega}\right|_j \gamma_j^{-1} \tag{4}$$

where N is the number density of the Raman-active molecule; Δ_j is the population difference between the upper and lower vibration/rotation states, and $\left.\frac{d\sigma}{d\Omega}\right|_j$ is the cross-section for spontaneous Raman scattering. In computing the Boltzmann factors

Δ_J, nuclear spin statistics are accounted for, and a Dunham expansion has been employed in the calculation of vibration/rotation energy levels. Mutual equilibrium between vibrational and rotational modes has been assumed at temperature T. For forward scattering, the spontaneous Raman cross-section can be expressed in terms of the components of the derived polarizability tensor:

$$\left.\frac{d\sigma}{d\Omega}\right|_Q = \left(\frac{\omega_2}{c}\right)^4 \frac{\hbar}{2M\omega_o} \left[\alpha'^2 + \frac{7}{45} b^J_{J,\nu} \gamma'^2\right] (v+1)$$

$$\left.\frac{d\sigma}{d\Omega}\right|_{O,S} = \left(\frac{\omega_2}{c}\right)^4 \frac{\hbar}{2M\omega_o} \left(\frac{7}{45} b^J_{J\pm 2} \gamma'^2\right) (v-1) \qquad (5)$$

where M and ω_o are the reduced mass and angular frequency of the molecular oscillator, the $b^J_{J'}$ are the Placzek-Teller coefficients (Ref. [illegible]) and α' and γ' are the derivatives (with respect to internuclear coordinate) of the mean molecular polarizability and anisotropy. v is the vibrational quantum number of the initial level, and the factor (v-1) is contributed by the vibrational matrix element.

The foregoing development is applicable to narrow band pump lasers. In practice, a broadband P_2 can be employed to generate a complete spectrum in a single shot, and P_1 may have an appreciable width. The frequency distribution of the scattered power for finite laser line widths can be derived from the macroscopic, third order polarization, whose frequency components are given by

$$P_3(\omega) = \int_{-\infty}^{\infty} d\omega' \, E_1(\omega') \int_{-\infty}^{\infty} d\omega'' \, \chi(\omega'-\omega'') \, E_1(\omega-\omega'+\omega'') \, E_2(-\omega'') \qquad (6)$$

where E_1 and E_2 are the Fourier components of the pump fields. The solution of Maxwell's Equations with (6) as source term gives a CARS intensity proportional to

$$\omega^2 \left|P_3(\omega)\right|^2 \qquad (7)$$

For a monochromatic P_1, use of a broadband P_2 generates the same spectrum as that obtained by tuning a monochromatic P_2. Because the CARS signal is linear in P_2, the signal can be represented as a superposition of the individual spectral elements of P_2. The achievable resolution is, therefore, dependent on the width of P_1.

There are consequently three medium parameters (N, T, χ_{NR}) which go into the calculation of a CARS spectrum, so that in principle a temperature or concentration measurement entails a three-parameter fit. In addition, the homogeneous linewidths γ_j are not well known, requiring an examination of the sensitivity of CARS spectra to reasonable variations in these widths.

A computer program based on Equations (2-6) has been written to generate CARS spectra numerically. The numerical scheme selects an appropriate spectral range $\omega_1-\omega_2$ and divides it into a number of discrete intervals. Based on the Boltzmann populations for the assumed T and N, the program calculates a value $\chi(\omega_1-\omega_2)$ from Equations (2-5) and performs the convolution integral (6) numerically.

In this analysis we have ignored population perturbations due to the pump lasers, as well as stimulated Raman effects. It has also been assumed that the fields $E(\omega_1)$ and $E(\omega_2)$ have the same polarization directions (Polarization Condition (1) of Ref . (9)).

Flame Thermometry and Concentration Measurement

We now consider the application of the foregoing theory to the problems of N_2 thermometry and CO concentration measurement in an air-methane, atmospheric flame. These calculations were performed in conjunction with the experiments of Ref. (10), in which vibration-rotation transitions were probed with a broad-band P_2. In these

experiments, a pulsed, frequency-doubled Nd:YAG laser and a dye oscillator pumped by a portion of the Nd laser output provided the two excitation beams. Details of the optical apparatus and flat flame burner are given in Ref. (10); pump laser parameters characteristic of the experiments are given in Table 1. Because the flame was probed in the postflame region, a nominal gas concentration of 70% N_2, 20% H_2O and 10% CO_2 has been assumed in these calculations. The calculations are applicable to both scanned and single pulse experiments.

Temperature measurement is best performed using a dominant molecular species such as N_2. In an atmospheric flame, the resonant CARS contribution from N_2 will be so much stronger than the nonresonant contribution ($|\chi_R| >> \chi_{NR}$) that χ_{NR} and N become relatively insignificant parameters. In the absence of significant interference with the nonresonant background, the temperature can be deduced from the qualitative shape of the CARS spectrum.

With T thus established, the interference between the CARS signal for a minority species such as CO and the background offers the promise of concentration measurements without having to make an absolute intensity measurement. This possibility arises because the CO resonant susceptibility modulates an approximately known background susceptibility. In the limit of dominant χ_{NR}, the susceptibility takes on the dispersive profile of χ_R'.

For the two molecules of interest in this study, N_2 and CO, the molecular polarizability parameters were calculated from the spontaneous cross-section and depolarization data of Ref. (11). For the homogeneous linewidths there is pure rotational data (Ref. 12) for both molecules, and some data for the $0 \rightarrow 1$ band Q-branches of N_2 (Ref. 13). However, it is fair to state that the magnitudes, J-dependence, and

temperature dependence of the widths are uncertain; consequently, we have assumed a constant nominal value of .1 cm^{-1} for both molecules. Nonresonant background susceptibilities have been taken from Ref. (14). Lacking an experimental value for the H_2O susceptibility, a value equal to that for CH_4 has been assumed. For the assumed postflame composition, χ_{NR} is calculated to have an STP value of 5.25×10^{-18} cm^3/erg, a value about 30 percent larger than that for pure N_2 (Ref. 14). Because the gas composition is not precisely known, and the H_2O nonresonant susceptibility is uncertain, the sensitivity of the predicted spectra to variations in the background susceptibility is examined.

N_2 Thermometry

Rotational temperatures can be most accurately inferred by probing the $0 \rightarrow 1$ Q branches with nearly monochromatic P_1 and P_2, making it possible to dispense with a monochromator. For a broadband P_2, high resolution can still be achieved if P_1 is not too broad. These calculations are concerned with experiments in which a broadband P_2 and narrowband P_1 are employed, but in which the monochromator resolution may not be sufficient to resolve individual Q-branches. In the low resolution case, inference of a vibrational-rotational temperature can utilize the relative strengths of the 0-1 and 1-2 band envelopes.

Figure 1 shows how the calculated N_2 spectrum at $T = 1700^{\circ}K$ evolves from the monochromatic spectrum, through the correction for finite pump laser widths, and through a final convolution with a triangular instrumental slit function. In the 0-1 band of the monochromatic spectrum, two distinct envelopes corresponding to the even and odd numbered Q branches are evident. The even rotational quantum number transitions are stronger because of a higher nuclear spin statistical weighting.

In the convolved spectrum, the low-lying Q-branches are unresolved, but at the higher quantum numbers the spacing between transitions due to vibration-rotation interaction (α_e) becomes sufficient to permit the resolution of even numbered Q branches. Also of interest is the disturbance of the 1-2 band by the 0-1 band that is evident in the spectra.

In Figure 2, the N_2 profile is compared for T = 1200°K and 2000°K. Of note here are the rapidly increasing modulation depth and 1-2 band strength for increasing temperature. The shift of the spectrum maximum evident in Figure 2 is due to the changes in the rotational Boltzmann distribution. These moderate resolution N_2 CARS spectra contain prominent spectral features which vary strongly with temperature, offering the potential for sensitive temperature determinations.

For low monochromator resolution, many of the spectral features cannot be resolved, and the "hot band" can be used for temperature determination. Figure 3 displays the calculated low-resolution spectra for a range of temperatures. For display purposes, the maxima of the different curves have been brought into coincidence. While the width of the 0-1 band broadens substantially with increasing temperature, the hot band intensity ratio is a much more sensitive function of temperature. This peak height ratio is shown as a function of T in Figure 4.

With regard to simplified data reduction, the expression $4 \exp(-2^{*}\omega_v/kT)$ does not provide a useful relationship between temperature and peak height ratio, and it appears that interference effects limit the utility of measuring the slope of the 0-1 band on its hot side (Ref. (3)). The best results will be obtained by analyzing experimental data with the aid of a computer model.

Because of the uncertainty in the Q-branch linewidth data, the sensitivity of the predicted N_2 CARS spectra to reasonable variations in these widths has been examined. Figure 5 displays the variation of peak height with γ for T = 1300°K, 1700°K, 2000°K. As seen, for linewidths greater than .1 cm^{-1}, the sensitivity is not great. For values less than .1 cm^{-1}, the sensitivity is somewhat greater. These results suggest that knowledge of the homogeneous linewidths is not critical for CARS thermometry.

Uncertainties in the value of χ_{NR} do not appear to have much impact on the predicted N_2 CARS spectra; varying χ_{NR} by $\pm$ 33 percent at T = 1700°K changes the predicted peak height by less than 10 percent.

A comparison of the theory and experimental data is shown in Figure 6. Radiation-corrected thermocouple and spontaneous Raman measurements had previously established a temperature in the range 1625-1700°K (Ref. 15). The CARS prediction for T = 1650°K is seen to be in quite good agreement with the corresponding experimental trace; a particularly good fit is obtained for the 0-1 band, where the moderate monochromator resolution permits the observation of individual Q-branches (Q(28)-Q(40)). This fit was obtained using a value of .0177 cm^{-1} for the rotational constant α_e (Ref. 16); use of the Ref. (17) value (.0187 cm^{-1}) in the theoretical program resulted in predicted wavelength assignments for the large J Q-branches that were incorrect by about 1 cm^{-1}. While the fit to the 0-1 band is excellent, and the overall height and width of the 1-2 band are well accounted for, the theory does not reproduce the finer features of the 1-2 hot band as well. In particular, there is a discrepancy concerning the prominent peak on the hot band. The predicted 1-2 features prove to be quite sensitive to the choice of vibrational anharmonic

constants; thus, more exact spectroscopic constants or linewidths may be needed for the theory to reproduce hot band fine structure accurately. If individual Q-branches can be resolved, however, it should suffice to fit the theory to the 0-1 band.

CO Concentration Measurement

It has been shown that N_2 thermometry essentially requires a one-parameter fitting of theoretical and experimental spectra. Measuring small CO concentrations O (1%) is more complicated, because the background susceptibility sets a lower limit on detectivity, and because the fitting may involve more than one parameter.

A sample calculated CARS spectrum is shown in Figure 7 for an assumed flame temperature of 1700°K and CO mole fraction of .04. The "theoretical" and convolved spectra display the expected destructive interference dip and a pronounced contribution from the $v = 1 \rightarrow 2$ hot band. This hot band contribution suggests that the CO CARS spectra may contain useful information about temperature as well as concentration; temperature variations show that the $0 \rightarrow 1$ and $1 \rightarrow 2$ bands in the CO spectra undergo changes similar to those in N_2 (Figure 3). The asymptotic limits of the convolved spectra follow the profile of P_2.

Figure 8 displays the effect of CO concentration variation at fixed T and χ_{NR}. As the CO concentration increases, its spectrum emerges from the nonresonant background, with the interference minimum and hot band features becoming more pronounced. For the assumed χ_{NR}, which is about 25 percent larger than the pure N_2 value (Ref. 14), a lower limit on CO detectivity of slightly less than 5×10^{-3} is implied. In reality, lower CO mole fractions could be accompanied by changed concentrations of gases like CH_4 which possess relatively high background susceptibility (Ref.), thus changing detectivity. The achievable detectivity in any particular experiment will depend strongly on the background gas concentration through χ_{NR}.

Because the moduli K_j are inversely proportional to the homogeneous linewidths, γ_j (Equation 4) it might be expected that the latter would be important

parameters in minority species CARS spectra. The variation of the predicted CO spectrum with γ_j exhibited in Figure 9 shows that knowledge of the homogeneous linewidths is not critical for minority species concentration measurements. The predicted sensitivity is, however, large enough to suggest a need for measurements of these linewidths for very accurate work. As the γ_j increase, the contribution of the resonant susceptibility, and thus the detectivity, are slightly reduced.

The agreement of these calculations with the experimental spectra of Refs. (10) is good, as shown in Figure 10, which compares a calculated spectrum for a CO mole fraction of .04 to an experimental trace. Simultaneous quartz microprobe/ndir analyzer measurements had established a CO mole fraction of about .04. The temperature of 1700°K employed in the calculations is consistent with the N_2 thermometry performed in the same experiment, and the fact that the ratio of spectrum extrema is well reproduced indicates that the background susceptibility is nearly correct. While the calculated spectra are sensitive to the value assumed for χ_{NR}, it was not found necessary to change this parameter from the nominal value assumed throughout these calculations. Reproduction of the slight asymmetry in the experimental spectrum did require an adjustment in the center frequency of P_2.

Parametric variations with N and χ_{NR} show, however, that these solutions are not unique, and that the inferred CO mole fraction is subject to an uncertainty determined by the uncertainty in χ_{NR}. In the limit of small N, Equation (2) gives

$$|\chi|^2 \sim \chi_{NR}\,(\chi_{NR} + 2\chi_R')$$

$$= \chi_{NR}^2\,(1 + \frac{2N}{\chi_{NR}}\,\chi_R'\,(\omega))$$

Thus, there will be a family of solutions determined by N/χ_{NR} = const. that have the same dispersive profile. A calculation with the computer model confirms that the experimental spectrum of Figure 10 can be fit with a CO mole fraction of .03 if χ_{NR} is taken to be .75 times its nominal value. This result demonstrates the need for a measurement of the H_2O nonresonant susceptibility, and suggests that CARS minority species measurements would be most accurately performed in conjunction with computer modelling of the majority species concentration profiles.

Conclusions

A computer model for CARS generation from N_2 and CO has been described. The model has been applied to the practical problems of N_2 thermometry and CO concentration measurement in an air-fed methane flame. In both cases, the CARS measurements obtained by fitting theoretical and experimental spectra are consistent with measurements obtained by other techniques. For experimental conditions in which individual Q-branches of the v = 0-1 band of N_2 could be resolved, a very precise fit of theory to experiment has been achieved. Under low resolution conditions, the N_2 hot band spectrum can be employed for temperature determination. An examination of the factors influencing predicted CARS spectra indicates that neither type of measurement is critically dependent on the values assumed for the homogeneous linewidths, with CO concentration measurement somewhat more sensitive than N_2 thermometry. The accuracy of CO mole fraction measurement is shown to be subject to an uncertainty determined by knowledge of the nonresonant susceptibility.

Acknowledgement

The author is greatly indebted to Dr. Alan Eckbreth for supplying the experimental spectra used in this paper and for many informative discussions of this subject.

References

1. N. Bloembergen, Nonlinear Optics, Benjamin, New York (1965).

2. P. D. Maker and R. W. Terhune, Phys. Rev. 137, A801 (1965).

3. F. Moya, et. al., "Flame Investigation by Coherent Anti-Stokes Raman Scattering," in Experimental Diagnostics in Gas Phase Combustion Systems, B. T. Zinn, Editor, AIAA, New York (1977).

4. W. M. Tolles, et. al., Applied Spectroscopy 31, 253 (1977).

5. J. W. Nibler and G. V. Knighten, "Coherent Anti-Stokes Raman Spectroscopy," in Topics in Current Physics, A. Weber, Editor, Springer Verlag, Freiburg (1977).

6. R. N. DeWitt, A. B. Harvey and W. M. Tolles, Theoretical Development of Third-Order Susceptibility as Related to Coherent Anti-Stokes Raman Spectroscopy (CARS), Naval Research Laboratory Memorandum Report 3260 (1976).

7. A. C. Eckbreth, P. A. Bonczyk, and J. F. Verdieck, "Review of Laser Raman and Fluorescence Techniques for Practical Combustion Diagnostics," Applied Spectroscopy Reviews 13, 15 (1978).

8. G. Placzek and E. Teller, Z. Physik 81, 209 (1933).

9. M. D. Levenson and N. Bloembergen, Physical Review B 10, 4447 (1974).

10. A. C. Eckbreth, Appl. Phys. Lett. 32, April 1, 1978.

11. C. M. Penney. L. M. Goldman and M. Lapp. Nature Phys. Sci. 235, 110 (1972).

12. K. S. Jammu, G. E. St. John and H. L. Welsh, Can. J. Phys. 44, 797 (1966).

13. W. H. Fletcher, private communication, October 1977.

14. W. G. Rado, Appl. Phys. Lett. 11, 123 (1967).

15. A. C. Eckbreth, Applicability of Laser Raman Scattering Diagnostic Techniques to Practical Combustion Systems, Project SQUID Technical Report UTRC-4-PU October 1976.

16. W. Benesch, et. al., Astrophysical Journal 142, 1227 (1965).

17. G. Herzberg, Molecular Spectra and Molecular Structure. I. Spectra of Diatomic Molecules, D. Van Nostrand Co., Inc., Princeton, NJ (1950).

Figure Captions

Fig. 1 Calculated CARS spectrum for flame N_2, T = 1700°K.
(a) CARS signal for monochromatic P_1, P_2.
(b) Signal for finite width, P_1, P_2 (Table 1).
(c) Convolution of (b) with triangular slit function, resolution 1 cm^{-1}.

Fig. 2 Computed N_2 CARS spectra for T = 1200, 2000°K. Slit width 1 cm^{-1}.

Fig. 3 Low resolution N_2 CARS spectra for temperature range 1000-2000°K. Slit width 2.7 cm^{-1}.

Fig. 4 Variation of hot band intensity ratio with temperature for flame N_2. Slit width 2.7 cm^{-1}.

Fig. 5 Sensitivity of predicted hot band intensity to assumed homogeneous linewidth. Flame N_2, slit width 2.7 cm^{-1}.

Fig. 6 Comparison of theoretical and experimental N_2 CARS signal for T = 1650°K. ——— experimental, ····· theoretical. Slit width 1.25 cm^{-1}, $\omega_2^{(0)}$ = 16540 cm^{-1}, $\Delta\omega_2$ = 200 cm^{-1}.

Fig. 7 Calculated CARS spectrum for 4% CO, T = 1700°K, χ_{NR} = 9.2 x 10^{-19} cm^3/erg
(a) CARS signal for monochromatic P_1, P_2.
(b) Signal for finite width P_1, P_2 (Table 1).
(c) Convolution of (b) with triangular slit function, slit width 2 cm^{-1}.

Fig. 8 Variation of predicted CARS spectra with CO mole fraction. All other parameters as in Fig. 7. Instrumental convolution has not been performed.

Fig. 9 Variation of predicted CO CARS spectra with homogeneous linewidth. All other parameters as in Fig. 7.

Fig. 10 Comparison of theoretical and experimental CO CARS spectra. ——— experimental, ····· theoretical. Slit width 1 cm^{-1}, $\omega_2^{(0)}$ = 16640 cm^{-1}. All other parameters as in Fig. 7.

Table 1

Nominal Pump Laser Parameters

$\omega_1^{(0)} = 18797\ cm^{-1}$ $\qquad$ $\omega_2^{(0)} = 16481\ cm^{-1}\ (N_2)$
$= 16654\ cm^{-1}\ (CO)$

Gaussian Widths (FWHM)

$\Delta\omega_1 = 1.2\ cm^{-1}$ $\qquad$ $\Delta\omega_2 = 150\ cm^{-1}$

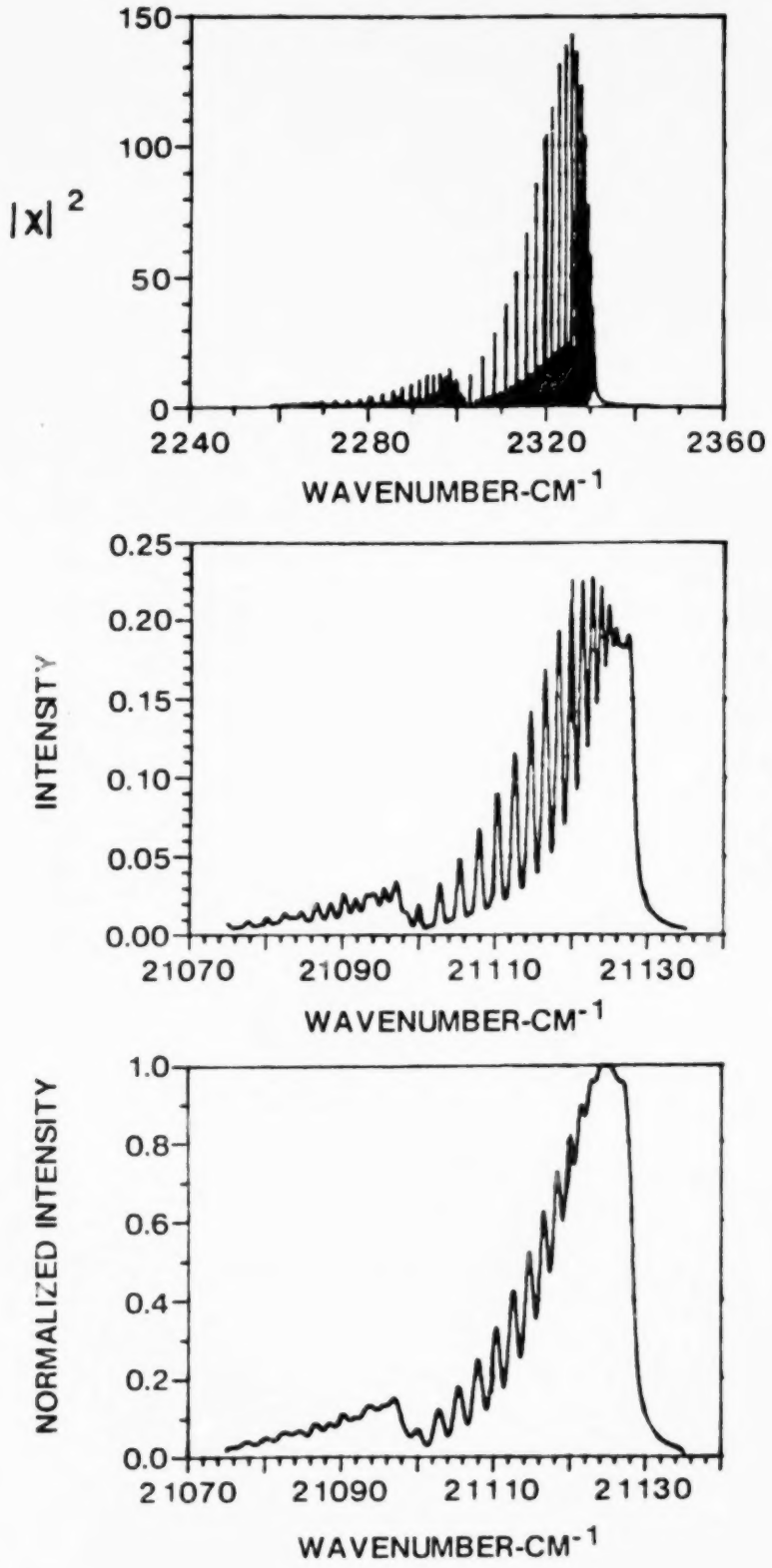
150
100
50
0
$|X|^2$
2240
2280
2320
2360
WAVENUMBER-CM^{-1}
0.25
0.20
0.15
0.10
0.05
0.00
INTENSITY
21070
21090
21110
21130
WAVENUMBER-CM^{-1}
1.0
0.8
0.6
0.4
0.2
0.0
NORMALIZED INTENSITY
21070
21090
21110
21130
WAVENUMBER-CM^{-1}

78-01-176-1

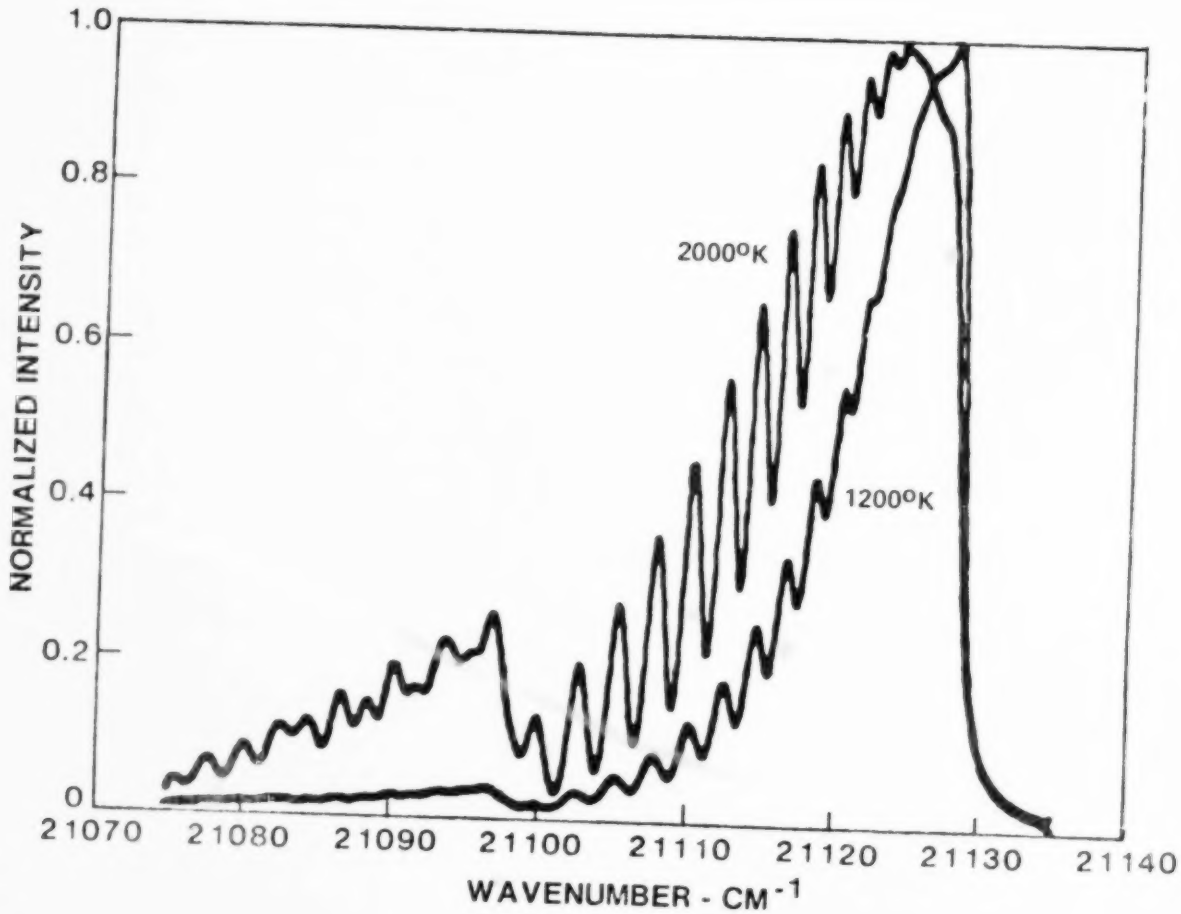
1.0
0.8
0.6
0.4
0.2
0
NORMALIZED INTENSITY
2000°K
1200°K
21070
21080
21090
21100
21110
21120
21130
21140
WAVENUMBER - CM-1

78-02-133-1

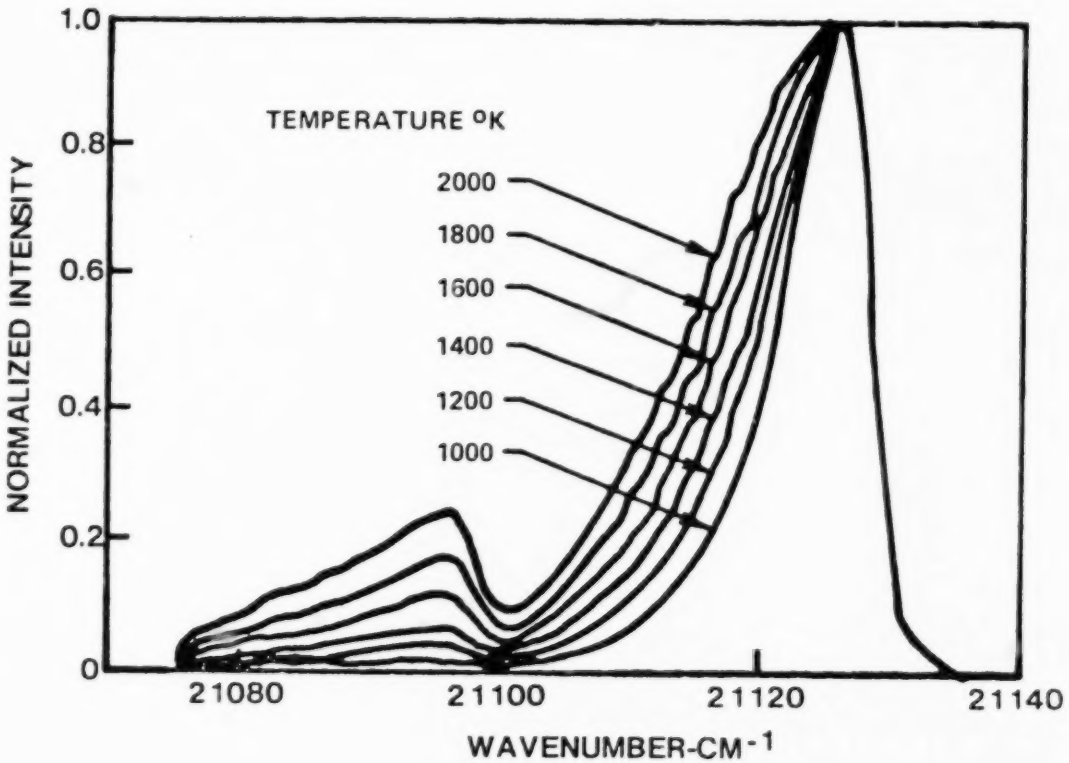
1.0
0.8
0.6
0.4
0.2
0
NORMALIZED INTENSITY
TEMPERATURE °K
2000
1800
1600
1400
1200
1000
21080
21100
21120
21140
WAVENUMBER-CM-1

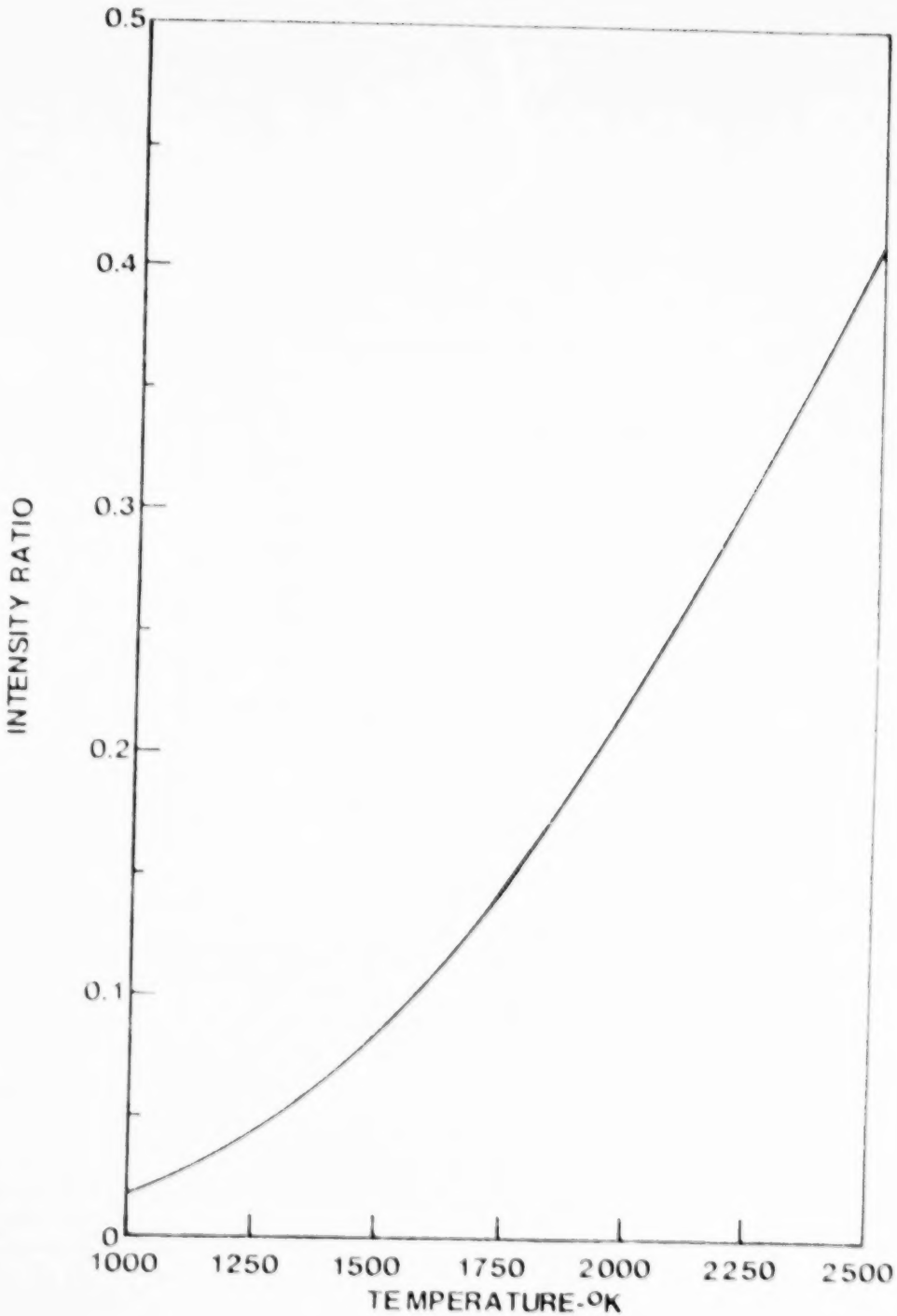
0.5
0.4
0.3
0.2
0.1
0
INTENSITY RATIO
1000
1250
1500
1750
2000
2250
2500
TEMPERATURE-°K

78-03-176-3

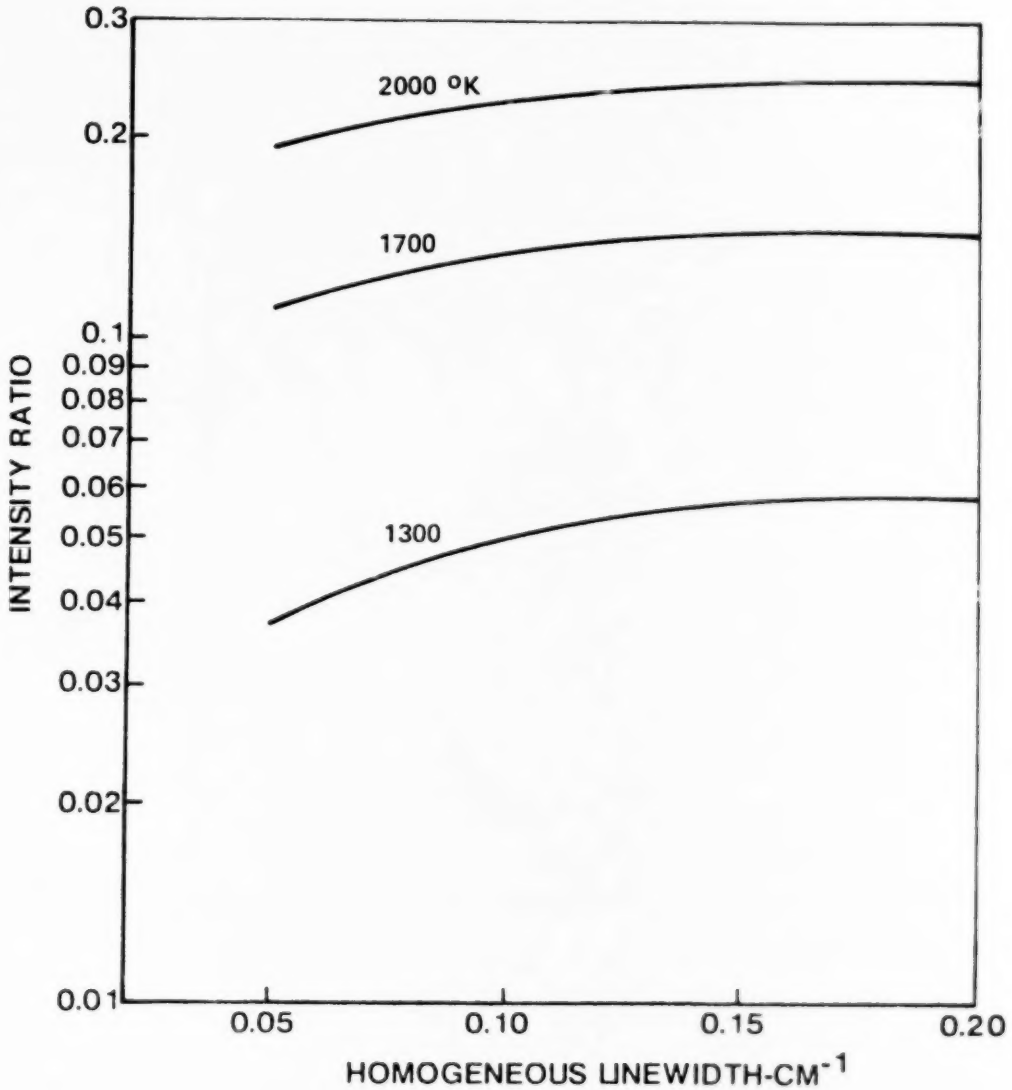
0.3
0.2
0.1
0.09
0.08
0.07
0.06
0.05
0.04
0.03
0.02
0.01
INTENSITY RATIO
2000 °K
1700
1300
0.05
0.10
0.15
0.20
HOMOGENEOUS LINEWIDTH-CM^{-1}

78-01-176-4

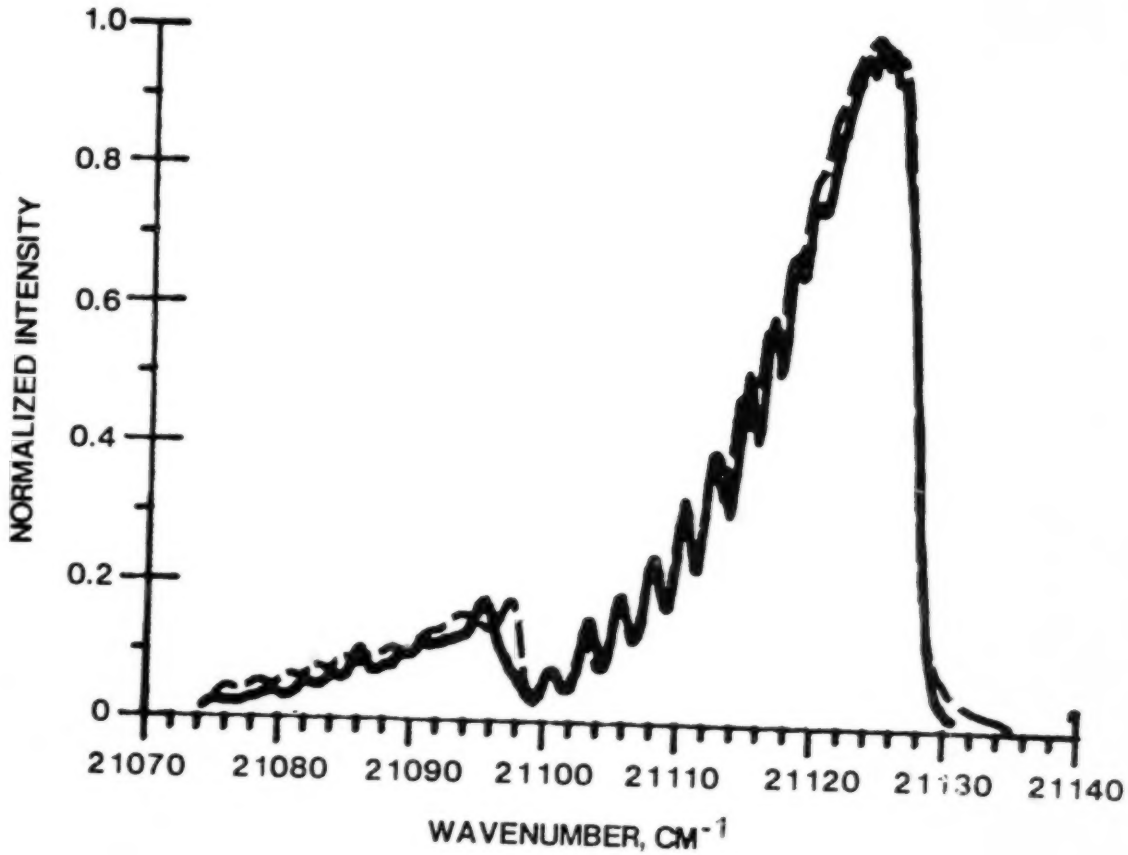
1.0
0.8
0.6
0.4
0.2
0
NORMALIZED INTENSITY
21070
21080
21090
21100
21110
21120
21130
21140
WAVENUMBER, CM-1

78-03-165-1

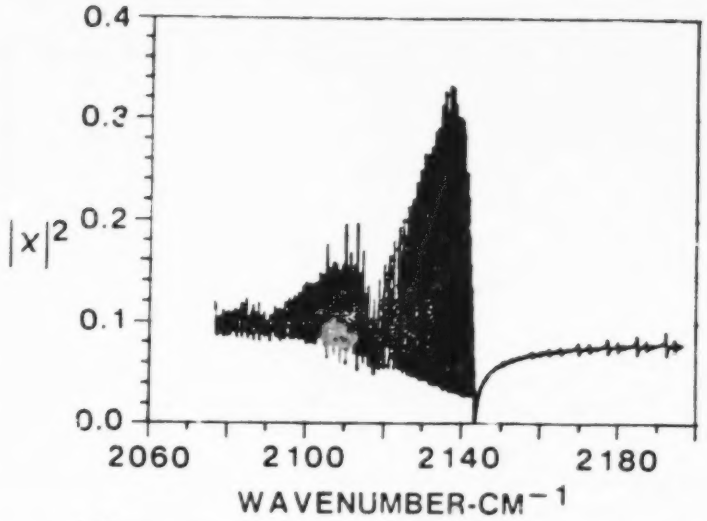
0.4
0.3
0.2
0.1
0.0
$|X|^2$
2060
2100
2140
2180
WAVENUMBER-CM^{-1}

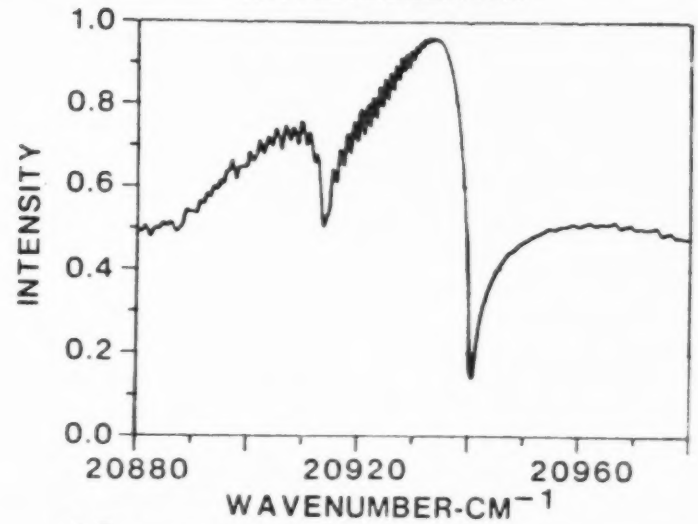
1.0
0.8
0.6
0.4
0.2
0.0
INTENSITY
20880
20920
20960
WAVENUMBER-CM^{-1}

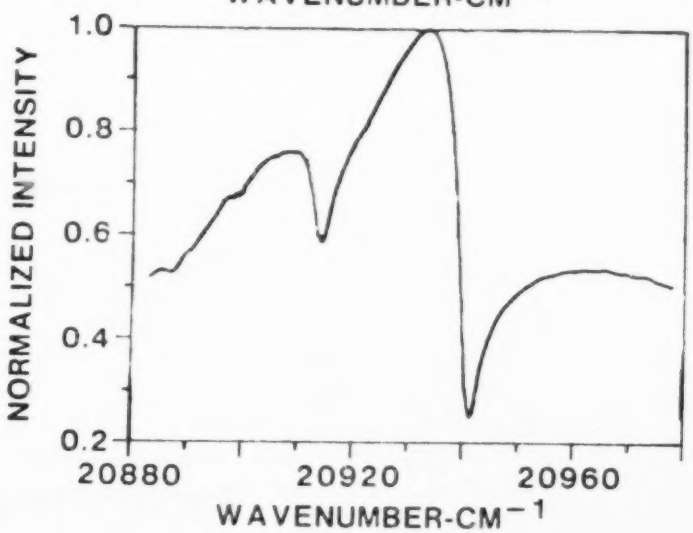
1.0
0.8
0.6
0.4
0.2
NORMALIZED INTENSITY
20880
20920
20960
WAVENUMBER-CM^{-1}

78-02-202-1

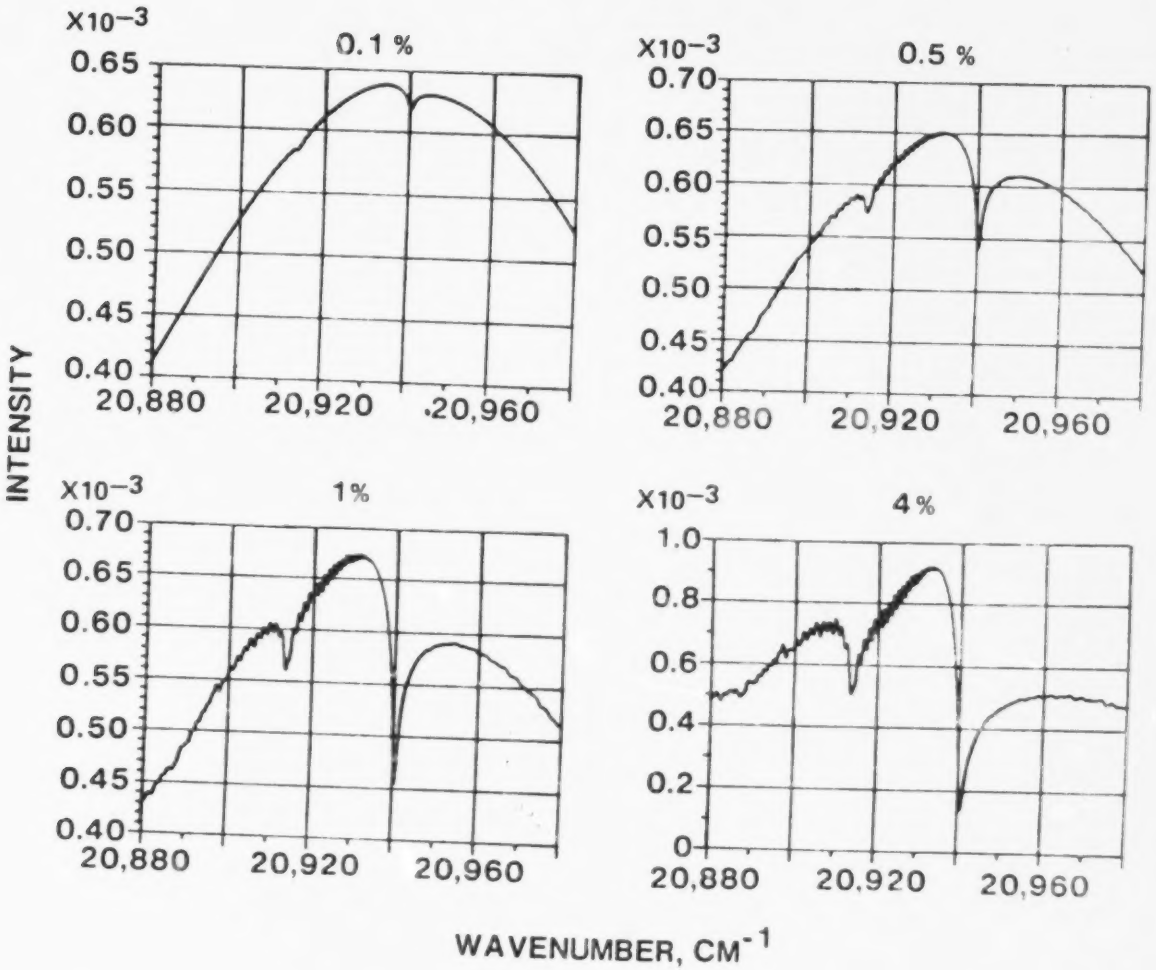
INTENSITY
X10−3
0.1 %
0.65
0.60
0.55
0.50
0.45
0.40
20,880
20,920
20,960
X10−3
0.5 %
0.70
0.65
0.60
0.55
0.50
0.45
0.40
20,880
20,920
20,960
X10−3
1%
0.70
0.65
0.60
0.55
0.50
0.45
0.40
20,880
20,920
20,960
X10−3
4%
1.0
0.8
0.6
0.4
0.2
0
20,880
20,920
20,960
WAVENUMBER, CM-1

78-03-97-01

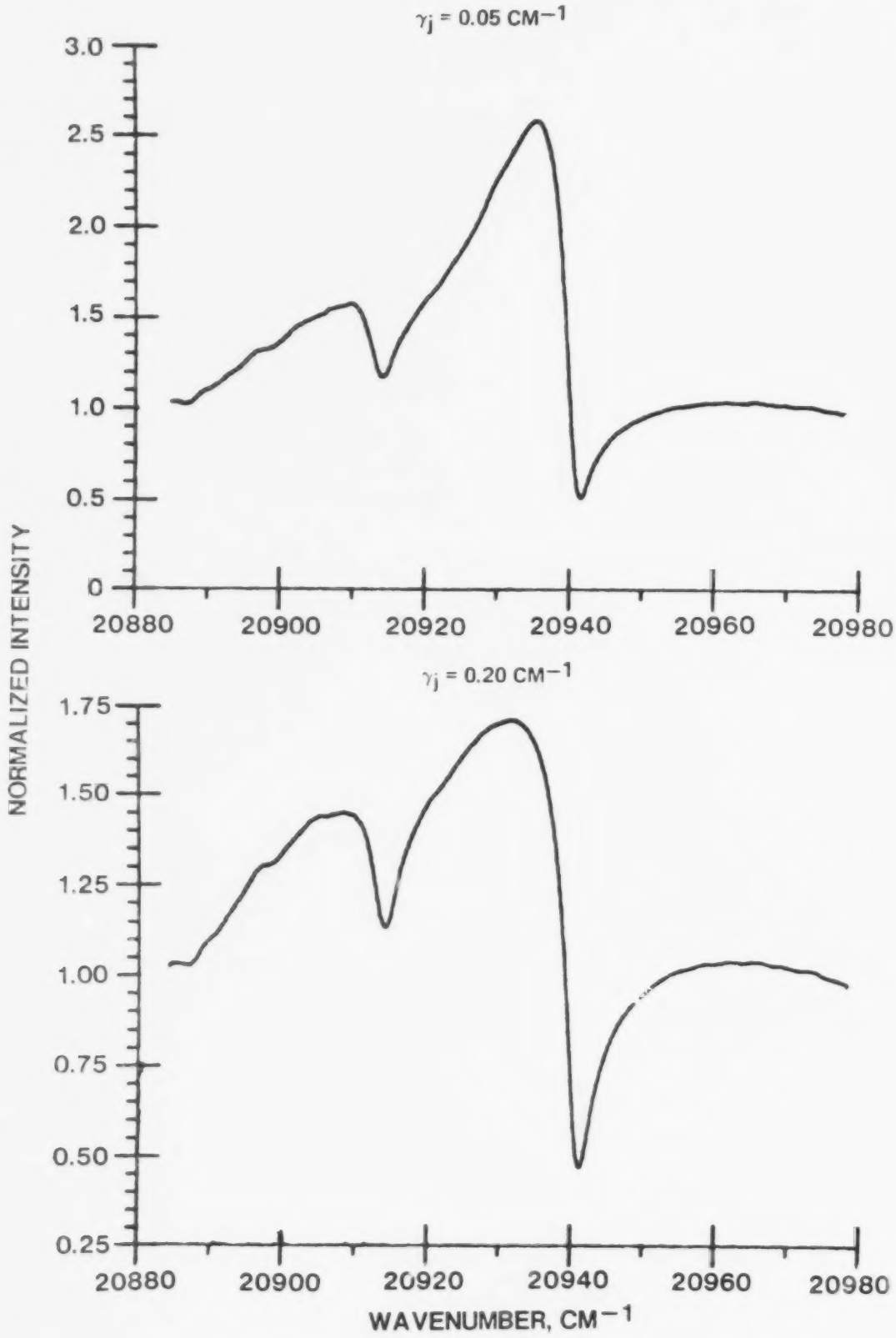
γ_j = 0.05 CM^{-1}
3.0
2.5
2.0
1.5
1.0
0.5
0
20880
20900
20920
20940
20960
20980
γ_j = 0.20 CM^{-1}
1.75
1.50
1.25
1.00
0.75
0.50
0.25
20880
20900
20920
20940
20960
20980
NORMALIZED INTENSITY
WAVENUMBER, CM^{-1}

.78-03-169-1

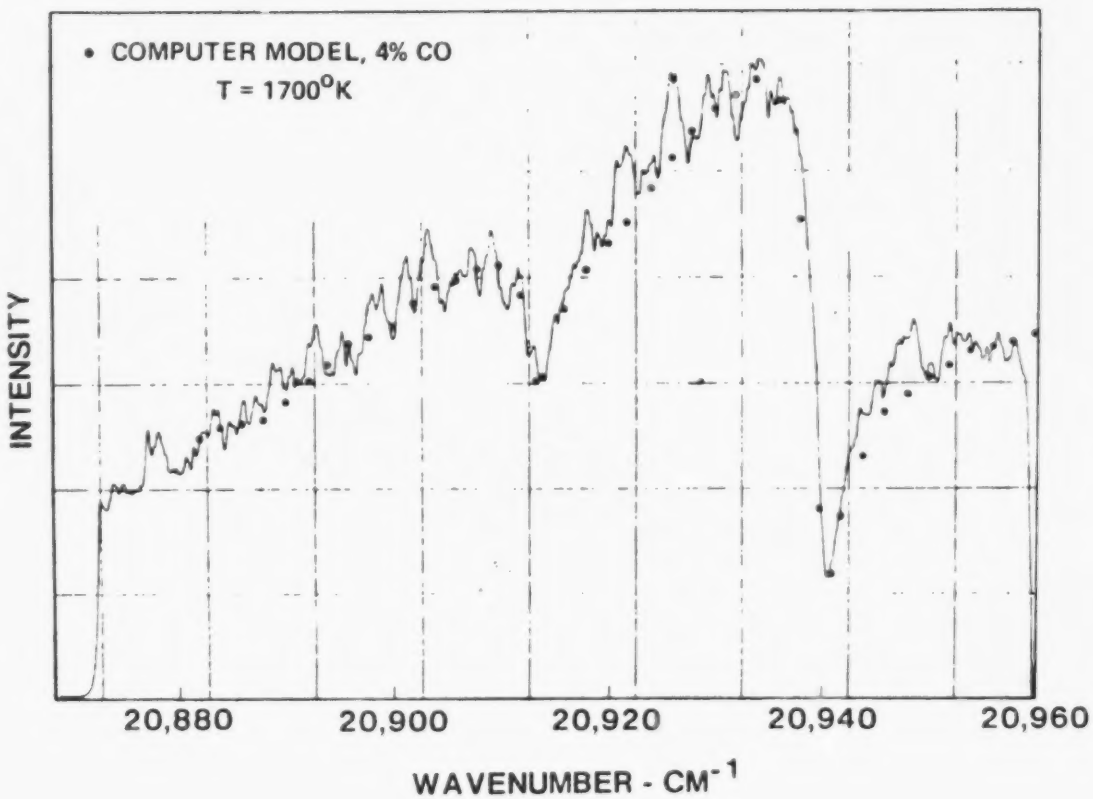
• COMPUTER MODEL, 4% CO
T = 1700°K
INTENSITY
20,880
20,900
20,920
20,940
20,960
WAVENUMBER - CM⁻¹